MAGNETOSPHERIC AND PLASMA SCIENCE WITH CASSINI-HUYGENS

M. BLANC[1], S. BOLTON[2], J. BRADLEY[2], M. BURTON[2], T.E. CRAVENS[3], I. DANDOURAS[4], M.K. DOUGHERTY[5], M.C. FESTOU[1], J. FEYNMAN[2], R.E. JOHNSON[6], T.G. GOMBOSI[7], W.S. KURTH[16], P.C. LIEWER[2], B.H. MAUK[8], S. MAURICE[1], D. MITCHELL[8], F.M. NEUBAUER[9], J.D. RICHARDSON[10], D.E. SHEMANSKY[11], E.C. SITTLER[12], B.T. TSURUTANI[2], Ph. ZARKA[13], L.W. ESPOSITO[14], E. GRÜN[15], D.A. GURNETT[16], A.J. KLIORE[2], S.M. KRIMIGIS[8], D. SOUTHWOOD[5], J.H. WAITE[17] and D.T. YOUNG[7]

[1]*Observatoire Midi-Pyrénées, Toulouse, France;* [2]*Jet Propulsion Laboratory, Pasadena, California;* [3]*University of Kansas, Lawrence, Kansas;* [4]*CESR, Toulouse, France;* [5]*The Blackett Laboratory, Imperial College, London, U.K.;* [6]*University of Virginia, Charlottesville, Virginia;* [7]*Department of Atmospheric, Oceanic and Space Sciences, University of Michigan, Ann Arbor, Michigan;* [8]*Applied Physics Laboratory, The Johns Hopkins University, Laurel, Maryland;* [9]*Institute for Geophysics and Meteorology, Köln University, Köln, Germany;* [10]*Center for Space Research, MIT, Cambridge, Massachusetts;* [11]*Department of Aerospace Engineering, University of Southern California, Los Angeles, California;* [12]*Goddard Space Flight Center, Greenbelt, Maryland;* [13]*DESPA, Observatoire de Paris-Meudon, Meudon, France;* [14]*Laboratory for Atmospheric and Space Physics, University of Colorado, Boulder, Colorado;* [15]*Max-Planck-Institut für Kernphysik, Heidelberg, Germany;* [16]*Department of Physics and Astronomy, University of Iowa, Iowa City, Iowa;* [17]*Southwest Research Institute, San Antonio, Texas*

Received 27 December 1999; Accepted in final form 13 February 2001

Abstract. Magnetospheric and plasma science studies at Saturn offer a unique opportunity to explore in-depth two types of magnetospheres. These are an 'induced' magnetosphere generated by the interaction of Titan with the surrounding plasma flow and Saturn's 'intrinsic' magnetosphere, the magnetic cavity Saturn's planetary magnetic field creates inside the solar wind flow. These two objects will be explored using the most advanced and diverse package of instruments for the analysis of plasmas, energetic particles and fields ever flown to a planet. These instruments will make it possible to address and solve a series of key scientific questions concerning the interaction of these two magnetospheres with their environment.

The flow of magnetospheric plasma around the obstacle, caused by Titan's atmosphere/ionosphere, produces an elongated cavity and wake, which we call an 'induced magnetosphere'. The Mach number characteristics of this interaction make it unique in the solar system. We first describe Titan's ionosphere, which is the obstacle to the external plasma flow. We then study Titan's induced magnetosphere, its structure, dynamics and variability, and discuss the possible existence of a small intrinsic magnetic field of Titan.

Saturn's magnetosphere, which is dynamically and chemically coupled to all other components of Saturn's environment in addition to Titan, is then described. We start with a summary of the morphology of magnetospheric plasma and fields. Then we discuss what we know of the magnetospheric interactions in each region. Beginning with the innermost regions and moving outwards, we first describe the region of the main rings and their connection to the low-latitude ionosphere. Next the icy satellites, which develop specific magnetospheric interactions, are imbedded in a relatively dense neutral gas cloud which also overlaps the spatial extent of the diffuse E ring. This region constitutes a

Space Science Reviews **104:** 253–346, 2002.

very interesting case of direct and mutual coupling between dust, neutral gas and plasma populations. Beyond about twelve Saturn radii is the outer magnetosphere, where the dynamics is dominated by its coupling with the solar wind and a large hydrogen torus. It is a region of intense coupling between the magnetosphere and Saturn's upper atmosphere, and the source of Saturn's auroral emissions, including the kilometric radiation. For each of these regions we identify the key scientific questions and propose an investigation strategy to address them.

Finally, we show how the unique characteristics of the CASSINI spacecraft, instruments and mission profile make it possible to address, and hopefully solve, many of these questions. While the CASSINI orbital tour gives access to most, if not all, of the regions that need to be explored, the unique capabilities of the MAPS instrument suite make it possible to define an efficient strategy in which *in situ* measurements and remote sensing observations complement each other.

Saturn's magnetosphere will be extensively studied from the microphysical to the global scale over the four years of the mission. All phases present in this unique environment – extended solid surfaces, dust and gas clouds, plasma and energetic particles – are coupled in an intricate way, very much as they are in planetary formation environments. This is one of the most interesting aspects of Magnetospheric and Plasma Science studies at Saturn. It provides us with a unique opportunity to conduct an *in situ* investigation of a dynamical system that is in some ways analogous to the dusty plasma environments in which planetary systems form.

Table of Contents

1. Introduction

Cassini, the second orbiter mission to a giant planet, will be a unique opportunity to conduct an in-depth study of a planetary magnetosphere other than Earth's and Jupiter's. For this purpose the spacecraft carries a very sophisticated complement of plasma and field instruments. During its four-year exploration of the Saturnian system along an orbital tour that will provide a broad coverage in local time, latitude, and radial distances, Cassini is likely to lead to a very comprehensive description of Saturn's magnetosphere, and should solve some of the most intriguing questions that this very special magnetospheric system poses.

Our actual knowledge of Saturn's magnetosphere is based on a very limited set of observations. First of all are the plasma, particles and fields measurements obtained along the Pioneer 11 and Voyager 1 and 2 trajectories (see Figures 11 and 12 in the text). In addition to *in situ* measurements, these fly-bys also provided a limited access to the ionosphere profiles of Saturn through radio occultation data. The PWS instrument was able to provide remote sensing data on Saturn's radio emissions, essentially Saturn's Kilometric Radiation (SKR). The crossing of Titans's wake by Voyager 1 returned to the Earth the only existing data on Titan's interaction with the magnetosphere, while the subsequent radio occultation of Titan's ionosphere made it possible to place at least an upper limit on its peak electron density. In addition to the spacecraft fly-by data, remote sensing measurements from Earth, its orbit, or by other interplanetary probes provided additional information on Saturn's gas clouds, aurora and radio emissions following the Voyager era.

From this limited source of information, one can characterize Saturn's magnetosphere by comparison to the family of planetary magnetospheres already explored in some detail, essentially the magnetospheres of the Earth and of the giant planets, to determine in what sense it shares common characters with them, and in what respect it is unique. To this end, let us explore the specific features of planetary magnetospheres.

i) An 'intrinsic magnetosphere' is generated by the interaction of the planetary intrinsic magnetic field with a plasma flow (generally the solar wind, or a stellar or planetary wind). The result of the interaction is to confine the planetary field inside a cavity, the magnetosphere, separated from the external flow by a sharp boundary, the magnetopause.

Saturn has an intrinsic magnetic field, which is compared in Table I (from Bagenal (1992)) to those of the other planets: its surface equatorial intensity of 0.21 Gauss is roughly comparable to those of the other planets, and only Jupiter stands out with a significantly larger value, reaching 14 Gauss at its maximum. Saturn is unique in that its dipole axis is nearly aligned with its rotation axis. Consequently the rotational modulation of its magnetic field should be small, essentially reflecting the effects of the non-dipole moments of the field. These effects are probably significant, however, since a planetary spin modulation is observed on

TABLE I
Comparison of planetary magnetic fields

	Earth	Jupiter[a]	Saturn[a]	Uranus[a]	Neptune[a]
Radius, R_{Planet} (km)	6 373	71 398	60 330	25 559	24 764
Spin Period (Hours)	24	9.9	10;7	17.2	16.1
Magnetic Moment/M_{Earth} 1[b]	1	600	50	25	
Surface Magnetic Field (Gauss)	0.31	4.28	0.22	0.23	0.14
Dipole Equator, B_0					
Minimum	0.24	3.2	0.18	0.08	0.1
Maximum	0.68	14.3	0.84	0.96	0.9
Dipole Tilt and Sense	$+11.3°$	$-9.6°$	$-0.0°$	$-59°$	$-47°$
Distance (A.U.)	1[d]	5.2	9.5	19	30
Solar Wind Density (cm^{-3})	10	0.4	0.1	0.003	0.005
R_{CF}	8 R_E	30 R_J	14 R_S	18 R_U	18 R_N
Size of Magnetosphere	11 R_E	50–100 R_J	16–22 R_S	18 R_U	23–26 R_N

[a]Magnetic field characteristics from Acuna & Ness (1976), Connerney *et al.* (1982, 1987, 1991).
[b]$M_{Earth} = 7.906 \times 10^{25}$ Gauss $cm^3 = 7.906 \times 10^{15}$ Tesla m^3.
[c]Note: Earth has a magnetic field of opposite polarity to those of the giant planets.
[d]1 AU $= 1.5 \times 10^8$ km.

radio emissions and trapped particle fluxes. The magnetopause shapes of the Earth, Jupiter and Saturn have been modeled by Maurice and Engle (1995), taking into account the contribution of the internal plasma pressure on the pressure balance with the solar wind (Figure 2). They appear very similar when their sub–solar magnetopause distances are scaled to the same length, except that the calculated jovian magnetopause is significantly 'blunter' than the Earth's, because of the effect of a plasma disk and associated current disk. Saturn's magnetopause appears intermediate, revealing a significant internal plasma pressure.

ii) Planetary magnetospheres trap plasma and energetic charged particles of internal and solar wind origins on their closed magnetic field lines.

As an illustration, Figure 3 shows the populations of trapped ions in the intermediate energy range, from about 30 keV to a few MeV, in the different planetary magnetospheres. Data on the Earth's magnetosphere come from the ISEE spacecraft, and data on the giant planets from the Voyager LECP instrument. Locations of the upstream planetary shock (labeled S) and of the magnetopause (labeled M) are indicated, showing the exact extent of the planetary magnetopause in each panel. One can see the solar wind ion population at very low energies on the two sides of each magnetosphere, and characteristic enhanced ion fluxes inside the magnetospheric cavities. The radial positions of the satellites are also indicated. The ion fluxes in this specific energy range are weaker at Saturn than at Earth and Jupiter, but significantly stronger than at Uranus and Neptune. The bulk of the solar

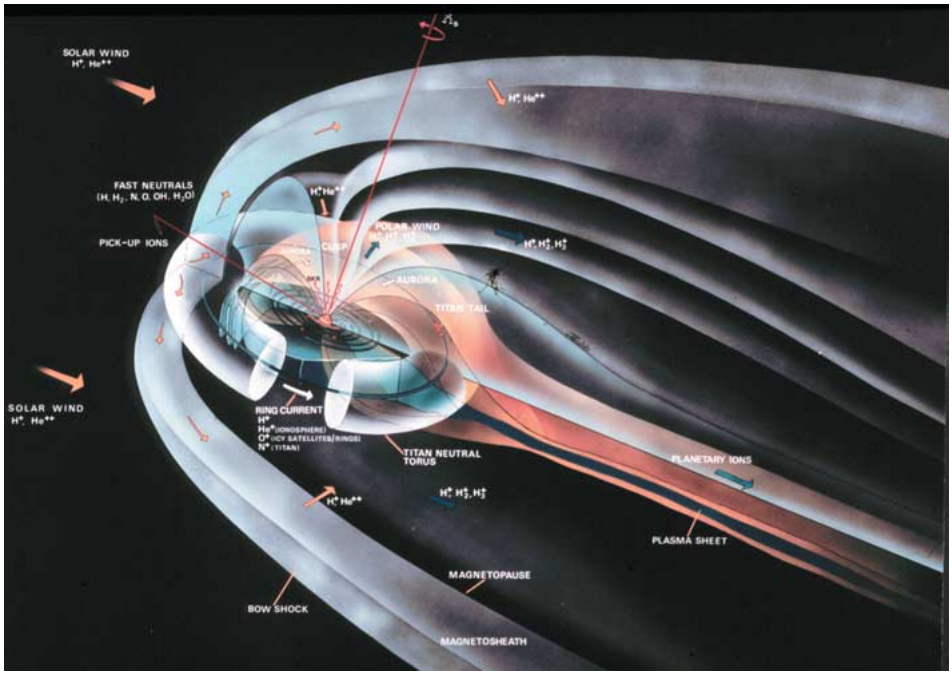

Figure 1. 'Artist's view' of Saturn's magnetosphere, showing the diversity of processes and interactions taking place within the magnetospheric cavity. Courtesy of D. Mc Comas, Los Alamos National Laboratory.

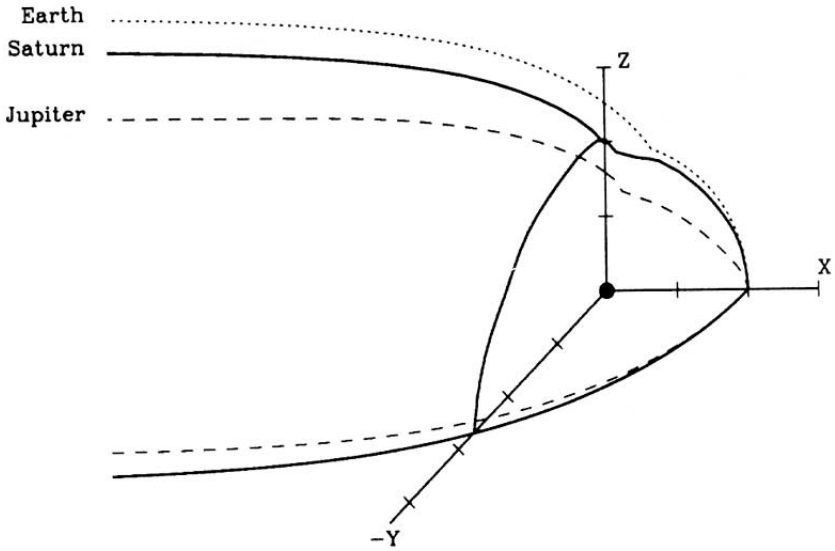

Figure 2. When scaled to the same subsolar magnetospause distance to the planet's center, the differences in the geometries of the magnetopauses of the Earth, Jupiter and Saturn, as calculated by Maurice and Engle (1995), become apparent. Saturn's magnetopause shape is closer to the Earth's, and the jovian magnetopause stands out as much 'blunter' than the other two, as a direct result of the presence of its intense equatorial current ring.

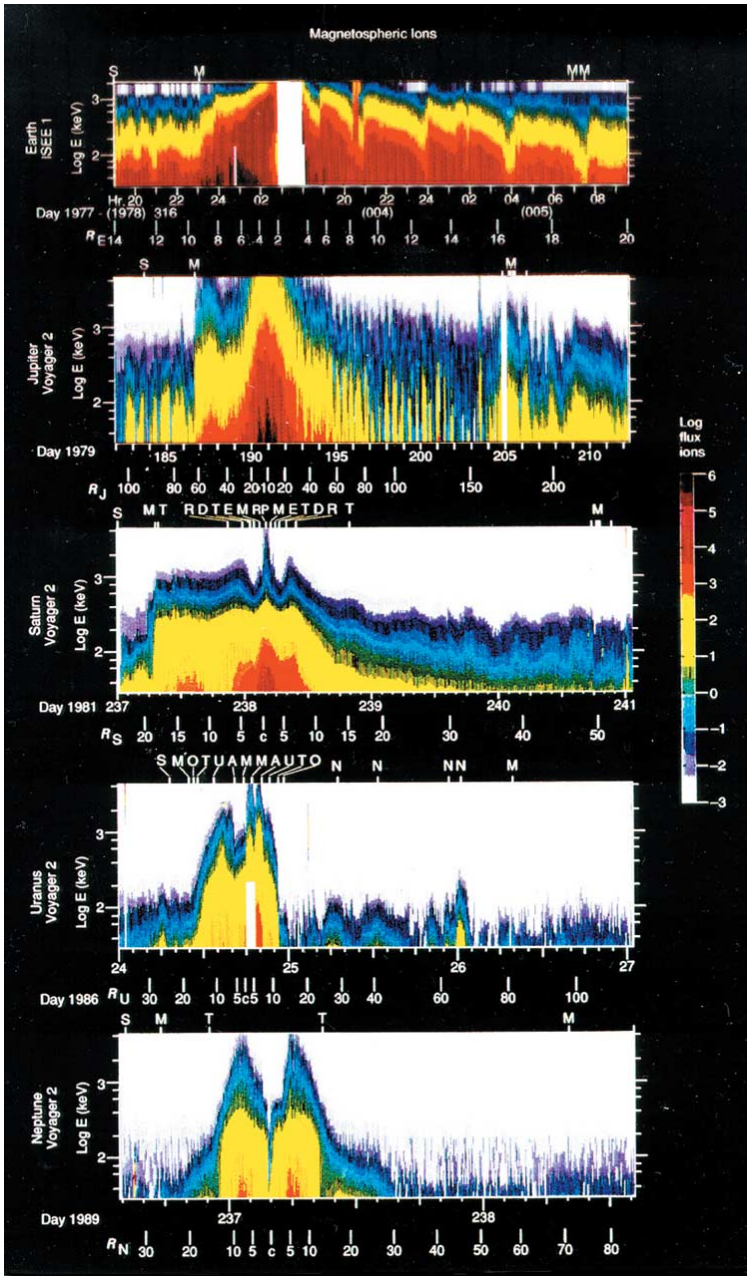

Figure 3. Radial distribution of fluxes of ions of intermediate energies (30 keV to a few MeV), in cgs units, in the magnetospheres of the Earth (from ISEE measurements) and of the giant planets (as measured by the LECP instrument on board Voyager during the planetary fly-bys). The locations of the planetary upstream shock (S), of the magnetopause crossings (M) and of the radial positions of the main satellites are also indicated.

TABLE II
Plasma characteristics of planetary magnetospheres

	Earth	Jupiter	Saturn	Uranus	Neptune
Maximum Density (cm^{-3})	1–4000	>3000	−100	3	2
Primary Sources	O^+, H^+	O^{n+}, S^{n+}	O^+, $H2O^+$ H^+	H^+	N^+, H^+
	Ionosphere	Io	Dione, Tethys	H cloud	Triton
Secondary Sources	H^+	H^+	N^+, H^+	H^+	H^+
	Solar wind[a]	Ionosphere	Titan	Solar wind	Solar wind
Source Strength (ions/s)	2×10^{26}	$>10^{28}$	10^{26}	10^{25}	10^{25}
(kg/s)	5	700	2	0.02	0.2
Lifetime	Days[b]	10–100	30 days	1–30	∼ 1 day
	hours	days	- years	days	
Energic Neutral Atom Fluxes[d]	∼ 100	∼ 440	∼ 240	<12	<4

[a]Chappell *et al.* (1987).
[b]Filling time for plasmasphere.
[c]Convective time outside plasmapause.
[d]In units of $(d/Rp)^{-2}$ cm^{-2} s^{-1} keV^{-1}, after Krimigis *et al.* (this issue).

wind ions and of the cold plasma, located below 30 keV, is missing in this diagram, but it has been partly observed by other detectors at lower energies. A summary of these observations is given in Table II, again taken from Bagenal (1992). Just as we found at higher energies, Saturn's absolute plasma densities, on the order of a few 100 particles/cm^3 at most, are intermediate between the significantly higher values found at Earth and Jupiter and the much smaller densities of the plasma populations of Uranus and Neptune.

iii) Planetary ionospheres, which are tenuous plasma domains generated by photon and energetic particle irradiation of the upper atmospheres of planets, are an important element of magnetospheric systems. In addition to their own interest, they are important plasma sources, and regulate magnetospheric dynamics by their electrical properties.

Planetary atmospheres contain regions or layers of partially ionized plasma called ionospheres. All bodies in the solar system which possess significant atmospheres also possess ionospheres (see Nagy and Cravens, 1998; Schunk and Nagy, 2000). The main ionization sources are photo ionization by extreme ultraviolet (EUV) solar photons and electron-impact ionization by electrons with energies that exceed the neutral atom or molecule's ionization potential. The electrons can be photoelectrons or energetic electrons originating in a planetary magnetosphere or in the solar wind. Each ionosphere provides a distinct plasma source of specific composition to its magnetosphere. Ionospheres have been detected both on Saturn and on its moon Titan, whose atmosphere is dense enough to support a collisional

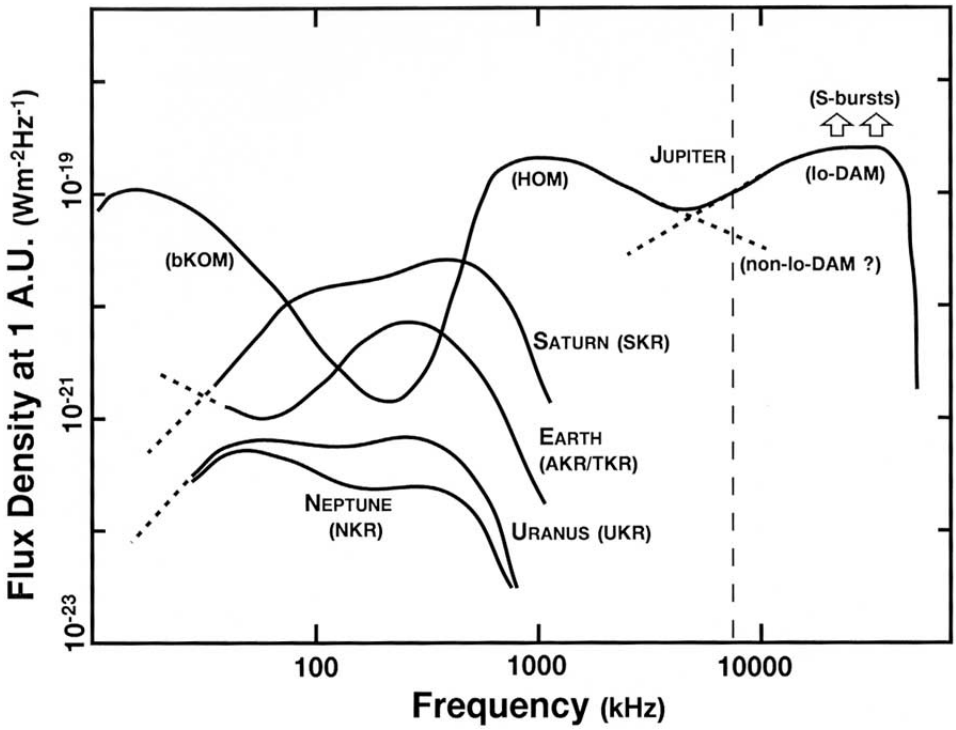

Figure 4. Comparative spectra of the five auroral radio emissions, as observed from low latitudes. Average emission levels are sketched, normalized to a distance of 1 AU from the source. They are based on 2–6 days of Voyager/PRA measurements for each spectrum, recorded from a 100–500 planetary radii range, with LH and RH polarizations mixed together. Peak flux densities are about 10 times higher than the displayed levels. The displayed curves may vary with time and observer location (from Zarka (1998)).

ionospheric layer. It has been suggested that ionospheric-type plasma also exists in the tenuous atmosphere associated with the rings system. With three different ionospheres inside its magnetospheric cavity, Saturn is a unique environment from the point of view of ionospheric physics.

iv) The electrodynamical coupling of a planetary ionosphere with the outer magnetosphere and its boundaries with the solar wind is at the origin of a broad variety of dynamical phenomena, including the generation of electrostatic potential differences, electric current flows and charged particle acceleration along magnetic field lines. These phenomena in turn produce a broad spectrum of so-called auroral emissions, which are a common feature of planetary magnetospheres.

Auroral emissions from Saturn have been observed in the radio, IR, visible and UV wavelength ranges. Saturn's auroral radio emissions are much less intricate than Jupiter's: they simply consist of one northern and one southern kilometer X mode source (SKR), with respectively right-hand and left-hand circular polarizations. As shown in Figure 4 (Zarka, 1998), where the average spectra of the auroral

radio emissions of five magnetized planets (including the Io-Jupiter emission) are compared, the SKR spectrum covers a frequency range similar to that of the Earth, Uranus and Neptune radio emissions. The broad spectral range of Jovian radio emissions reflects the higher amplitude of the Jovian surface field, which results in a higher electron cyclotron frequency near the planet. The SKR average intensity is 5–10 times higher than that of the Earth's auroral radio emissions, and second only to that of Jovian radio emissions, which are driven by a much larger solar wind input.

Saturn's aurora (in the UV, visible and IR) appears to be less intense, as the Saturnian magnetosphere is both more distant and less active than the Jovian one. The few observations available from Voyager UVS and more recently from the Hubble Space Telescope indicate that the Saturnian aurora appears to be about one order of magnitude fainter than the jovian aurora. It emits mainly in the far UV, in the Lyman-α line of atomic hydrogen and in the Lyman and Werner bands of H_2. It seems to be organized in two ovals at about 80° latitude, dominated by bright 'hot spots' on the morning side.

v) Planetary magnetospheres develop complex electrodynamic interactions with their planet's satellites when they are located inside the magnetospheric cavity. The nature of these interactions depends on the magnetic and electrical properties of the satellites, on the presence, density and composition of a satellite atmosphere/ionosphere and on the properties of the incident flow of magnetospheric plasmas and charged particles.

Saturn's magnetosphere displays two different types of satellite interactions, with the icy satellites and with Titan, to which one should add its interactions with rings and dust particulates. For the purpose of comparison, Table III summarizes our knowledge of the characteristics of satellite interactions for Jupiter and Saturn. It shows the characteristic magnitudes of the incident flow, conveniently expressed in terms of Alfvenic (M_A) and sonic (M_S) Mach numbers, and the nature of the obstacle. The interactions with the icy satellites, as well as the jovian satellite interactions, are sub-Alfvenic and supersonic. The interaction with Titan is subsonic and super-Alfvenic (we call it 'transonic' in the remainder of the text), and the obstacle is the atmosphere and the ionosphere of this satellite. For these reasons Titan's magnetospheric interaction is a unique case, which produces a true 'induced magnetosphere' in the magnetospheric flow (and at times in the magnetosheath or even the solar wind flow).

vi) Magnetospheric plasmas are fed by a broad variety of plasma sources, which differ in each particular magnetosphere.

At Earth, for instance, only two sources exist: the solar wind and the terrestrial ionosphere. At Jupiter, the significant sources of plasma which Galileo has found to be associated with Ganymede, Europa, and even Callisto are probably indicative of what we might expect for the icy satellites at Saturn. But these are dwarfed by Io, which is most likely the dominant jovian plasma source. The jovian ionosphere, however, may also be an important plasma source (Nagy *et al.*, 1986). Saturn

TABLE III
Known characteristics of satellite/magnetosphere interactions at Jupiter and Saturn

	M_S	M_A	Nature of the obstacle	
			Atmosphere. Ionosphere/solid surface	Magnetized or not
Jovian satellites[3]				
Io	1.65	0.30	Yes[1]/yes	?
Ganymede	2.4	0.48	No/yes	Yes[4]
Europa	1.75	0.39	Yes[2]/yes	Probably not
Callisto	2.4	0.94	No/yes	No
Kronian satellites				
Titan	0.57	1.9	Yes/solid +lakes or oceans?	no
Tethys	1.24	0.25	No/yes	unknown
Dione	1.31	0.46	No/yes	unknown
Rhea	1.29	0.56	No/yes	unknown
Enceladus	2.4	0.14	No/yes	unknown

[1]See Saur *et al.* (1999).
[2]See Kliore *et al.* (1997), Saur *et al.* (1998).
[3]The figures for the galilean satellites are taken from Neubauer (1998).
[4]For the discovery of Ganymede's magnetic field, see Kivelson *et al.* (1996), Gurnett *et al.* (1996).

probably displays the largest diversity of sources: in addition to the solar wind and the planetary ionosphere, there are two other dominant plasma sources in the vicinity of the equatorial plane, which are directly related to the satellite interactions we just described. The first, in the external magnetosphere, is Titan which probably provides mainly H^+ and N^+ ions; the second, in the inner magnetosphere, is constituted by the neutral gas torus produced from sputtering of the surfaces of icy satellites and rings. It mainly provides ions of the dissociation products of water molecules. As Table II shows, these satellite sources alone are comparable in intensity to the total source of ions at Earth, but much smaller than the Io source at Jupiter.

vii) Each magnetospheric ion species is connected to its sources and sinks by transport processes acting on different scales. These may also differ strongly from one magnetosphere to another and need to be specifically identified.

Large-scale plasma circulation in planetary magnetospheres is generally described to first order as the superposition of the planetary corotation flow and of large-scale flow vortices, usually called 'magnetospheric convection', driven by the interaction of the outer magnetosphere with the solar wind. We know solar-wind-driven convection is important at Earth, and planetary corotation dominates the dynamics of the jovian magnetosphere. The case of Saturn is probably intermedi-

ate, but very little is known about it, except that corotation dominates up to at least 6 Saturn radii from the planet center along the Voyager fly-by trajectories. In addition, small-scale motions and plasma instabilities may also significantly contribute to the redistribution of the different ion species throughout the magnetosphere: the characteristics of plasma transport at Saturn are basically unknown to-day, and should be a subject of intense research during the CASSINI years.

Saturn's magnetosphere looks intermediate between the terrestrial and the jovian magnetospheres from the point of view of its plasma and field characteristics: its magnetic field topology or the absolute amount of trapped plasma are more similar to the Earth's; its plasma circulation regime is probably similar to the jovian one. So what is really unique about Saturn's magnetosphere is the variety of its interaction processes with the other components of Saturn's environment. Saturn offers two magnetospheres in one, an 'induced magnetosphere' at Titan and an 'intrinsic magnetosphere' around Saturn itself, which we shall describe in this article. Figure 5 gives a schematic representation of the different components of the Saturn environment which interact with these magnetospheres, and indicates the section of this article dealing with them:

(a) Section 2 of this article will be entirely devoted to the description of Titan's magnetospheric interactions: we first describe Titan's ionosphere (section 2.1), which constitutes with its atmosphere an obstacle to the flow of the magnetospheric plasma (or at times of the solar wind or magnetosheath). We then study in section 2.2 Titan's induced magnetosphere itself.

(b) Saturn's magnetosphere itself is described in Section 3. We first start with a summary of the morphology of magnetospheric plasma and fields. Then we describe the interaction processes in each region, beginning with the innermost regions and moving outwards. We first describe the region of the main rings and their connection to the low-latitude ionosphere. Next the icy satellites, which develop specific magnetospheric interactions, are imbedded in a relatively dense neutral gas cloud which also overlaps the spatial extent of the diffuse E ring. This region constitutes a very interesting case of direct and mutual coupling between dust, neutral gas and plasma populations. Beyond about twelve Saturn radii is the outer magnetosphere, where the dynamics is dominated by its coupling with the solar wind and a large hydrogen torus. It is a region of intense coupling between the magnetosphere and Saturn's upper atmosphere, and the source of Saturn's auroral emissions, including the kilometric radiation. For each of these regions we identify the key scientific questions and propose an investigation strategy to address them.

Finally, we show in Section 4 how the unique characteristics of the CASSINI spacecraft, instruments and mission profile make it possible to address, and hopefully solve, many of these questions. While the CASSINI orbital tour gives access to most, if not all, of the regions that need to be explored, the unique capabilities of the MAPS instrument suite make it possible to define an efficient strategy in which *in situ* measurements and remote sensing observations complement each other.

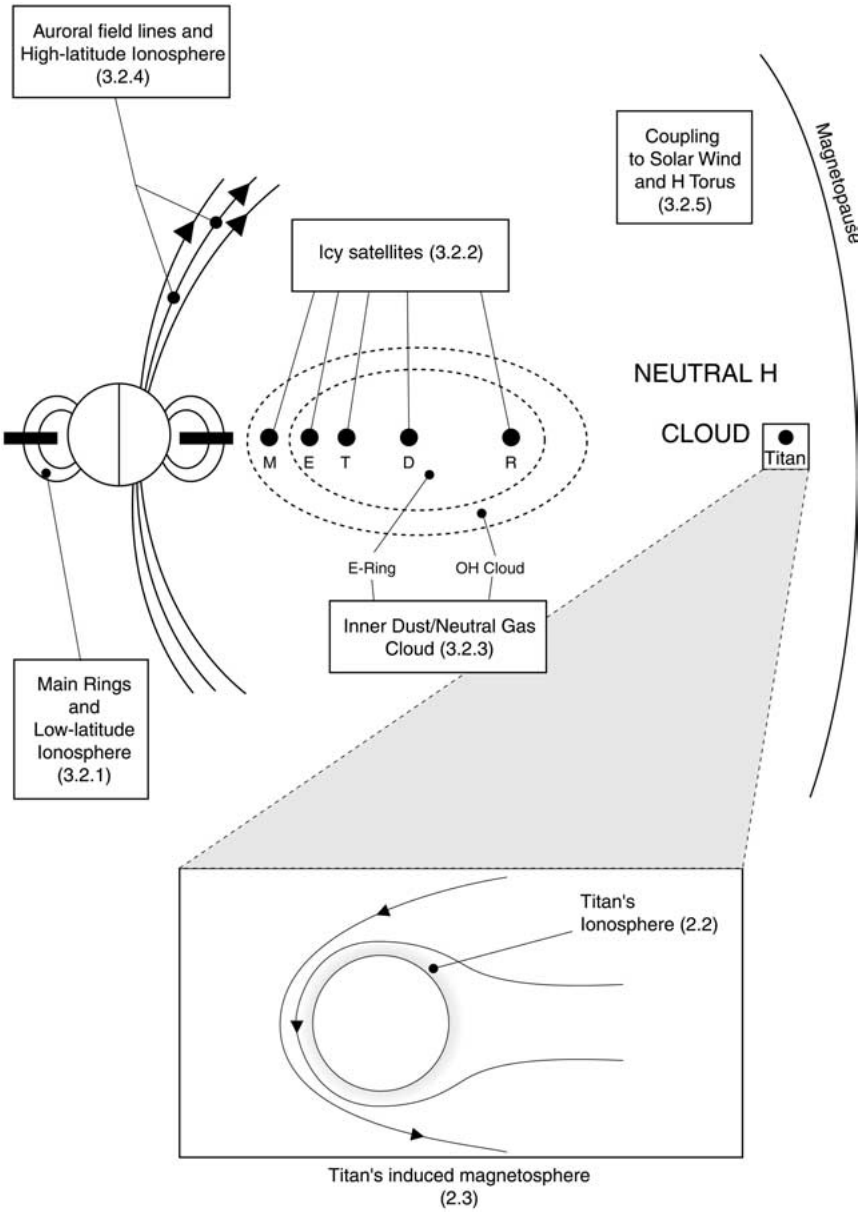

Figure 5. This schematic representation of Saturn's intrinsic magnetosphere (top) and of Titan's induced magnetosphere (bottom) shows the different regions described in detail in this paper. Saturn's magnetosphere interacts with all other components of the Saturnian environment. From the inner regions outwards, it interacts with the main rings and Saturn's low latitude ionosphere (see section 3.2.1), with the icy satellites (section 3.2.2), with the inner gas torus and the E ring (section 3.2.3), with Saturn's upper atmosphere and ionosphere along auroral field lines (section 3.2.4) and finally, in the outer magnetosphere, with the solar wind and extended hydrogen torus (section 3.2.5). Our discussion of Titan-related science will focus on Titan's ionosphere (section 2.2) and Titan's interactions with the surrounding plasma flows (section 2.3).

2. Titan's Plasma and Magnetospheric Interactions

2.1. Uniqueness of the problem

Titan's interaction with its plasma environment is the only case in the solar system where a satellite with a substantial atmosphere (Hunten *et al.*, 1984) characterized by an exobase well above the planetary surface interacts with the magnetospheric plasma. The plasma interaction is mostly of the atmospheric type (Neubauer *et al.*, 1984), although a magnetic field of internal origin may play an important albeit secondary role as will be argued later. The three-dimensional picture of the plasma flow and its associated magnetic field in Titan's vicinity is determined by the properties of the atmosphere, which at least at high altitudes is strongly influenced by the flow, and by the characteristics of the incident flow, which carries mass, momentum and energy into Titan's surroundings. The energy input is enhanced by hot electrons flowing into the interaction volume along the field lines, particularly in the magnetosphere, and by solar UV photons. This interaction determines the loss of mass from Titan and constitutes an important source of magnetospheric plasma in the outer magnetosphere of Saturn. It also fixes the outer boundary condition of the atmosphere of Titan and contributes to the mass budget of this interesting atmosphere. In addition to its role for the Titan-Saturn system as a whole, it is also unique as a special case of a plasma interacting with an atmosphere. Because of its large scale height the atmosphere is an obstacle to the incident plasma flow, which is intermediate between the 'hard' target Venus and the very 'soft' target of a comet with substantial gas production. Titan is also unique, because it may be engulfed in the magnetospheric plasma with the Alfvén velocity and the speed of sound approximately equal to the flow velocity (see Table III) or in the magnetosheath of Saturn or even the solar wind, when Titan is near 12:00 in Saturn local time. A further unique aspect is the fact that the gyroradii of newly created heavy pick-up ions are larger than the satellite's radius and are expected to lead to new flow effects in addition to substantial asymmetries. The carefully designed Titan tour and measurement programs will shed important light on many questions associated with these issues. The *in situ* measurements are done along specifically designed flyby trajectories, therefore theoretical modeling is needed to connect these observations. The models have to be three-dimensional, multi-fluid or even kinetic with sufficient resolution in configuration space and velocity space. The *in situ* measurements will be complemented by remote sensing of the upper atmosphere, e.g. by UV-observations, radio occultation studies of the ionosphere etc.

2.2. Titan's ionosphere

2.2.1. *Present Knowledge and Open Questions*

Titan's atmosphere is dominated by molecular nitrogen (N_2) although a considerable abundance of methane (CH_4) is present (see review by Hunten, 1984). Many other species are present in lower abundances including ethane (C_2H_6), propane

(C_3H_8), acetylene (C_2H_2), and hydrogen cyanide (HCN). In the upper atmosphere, where the ionosphere forms, molecular nitrogen is the most abundant neutral below an altitude of about 1700 km but methane becomes the dominant neutral constituent above this altitude. Molecular hydrogen (H_2) and atomic species such as N and H become dominant species further out in the exosphere. The only observational evidence of the existence of Titan's ionosphere is the detection of the ionospheric peak region near the terminator by the radio occultation experiment onboard Voyager, with a peak electron density of 2400 cm^{-3} at an altitude of 1175 km (Bird *et al.*, 1997). So our knowledge of Titan's ionosphere nearly entirely rests upon theory and models.

At Titan, both photoionization by solar EUV radiation and electron impact ionization associated with magnetospheric electrons are thought to contribute to the creation of the ionosphere (cf., Cravens *et al.*, 1992). Gan *et al.* (1992) used a two-stream electron transport code and Galand *et al.* (1999) used a multistream code to study how magnetospheric electrons, or atmospheric photoelectrons, interact with Titan's ionosphere and atmosphere. The relative proportion of the two ionization mechanisms (EUV or magnetospheric electrons) at a particular location on Titan and at a particular time is a function of altitude, latitude and longitude, and also depends on the orbital position of Titan.

Many ion species are produced in Titan's upper atmosphere due to the complexity of the neutral composition. The dominant ion species produced include N_2^+, N^+, CH_4^+, and CH_3^+. In the main ionospheric region (altitudes less than about 1700 km) where the neutral density is high enough for chemistry to take place, the N_2^+, CH_4^+, and CH_3^+ ions originally produced are quickly converted by ion-neutral chemical reactions to a variety of other ion species, including such hydrocarbon species as $C_2H_5^+$ and CH_5^+ and nitrile species such as $HCNH^+$ (Fox and Yelle, 1997; Keller *et al.*, 1998). CH_3^+ is also produced by the reaction of N_2^+ ions with CH_4. For example, $C_2H_5^+$ ions are produced from CH_3^+ ions via reaction with methane, and $C_2H_5^+$ in turn reacts with hydrogen cyanide (HCN) producing $HCNH^+$. This ion species can further react with C_4H_2 (or other species) producing even heavier hydrocarbon species or it can dissociatively recombine. The molecular ion species produced in various ways then recombine with the thermal ionospheric electrons via dissociative recombination reactions.

Other loss processes have also been suggested for HCNH+ (Fox and Yelle, 1997). The full ion chemistry scheme for Titan's ionosphere is quite complex and is not yet well understood. Several photochemical or one-dimensional models of Titan's density structure have been constructed to study these chemical processes and the linkages to neutral photochemistry (see Table IV). The energetics of Titan's ionosphere was modeled both by Gan *et al.* (1992), who focused on suprathermal electrons and on electron energetics, and by Roboz and Nagy (1994) who studied the ion and electron energetics at Titan. Temperatures within the ionosphere range from below 1000 K to above 10^4 K. An example of predicted ion density structure in Titan's ionosphere is shown in Figure 6.

TABLE IV
Recent Titan ionosphere models

Model reference	Type
Banaszkiewicz *et al.* (1999)	coupled upper atmosphere and ionosphere photochemical model
Keller *et al.* (1992; 1998)	photochemical model with detailed and updated hydrocarbon chemistry
Fox and Yelle (1997)	coupled upper atmosphere and ionosphere photochemical model
Gan *et al.* (1992)	2-stream electron transport and ionospheric electron energetics
Galand *et al.* (1999)	multi-stream electron transport photochemical ionosphere.
Ip (1990)	one-dimensional MHD model of ram side
Keller and Cravens (1994)	1D hydrodynamic ionospheric wake
Keller *et al.* (1994)	1D ram side multi-species MHD
Cravens *et al.* (1998)	2D ram side 3-species MHD
Roboz and Nagy (1994)	energetics (electrons and ions)

At higher altitudes (above about 1700 km) where the neutral density is rather low, dynamical processes associated with rapid flow driven by the external plasma interaction start to become more important than chemical processes in controlling the ionospheric plasma distribution. The one-dimensional MHD models of Ip (1990) and Keller *et al.* (1994) demonstrated that the ionosphere of Titan is likely to be magnetized on the ram side due to the interaction of Saturn's magnetospheric plasma with the ionosphere. The field structure and plasma behavior in the wake will be quite different and Keller and Cravens (1994) used a 'polar wind' type ionospheric outflow model to study this. 2-D and 3-D models are now also available, but they naturally focus on Titan's magnetospheric interaction and will be described in Section 2.3.

2.2.2. *Key Questions and MAPS Investigation Strategy*

Considering the lack of observational data on Titan's ionosphere, measurements from all the MAPS instruments, as well as from other Orbiter and Probe instruments, will be needed in addition to modeling work to discover and understand the ionosphere of Titan and its coupling to the neutral atmosphere and magnetosphere. The key questions to address are indeed very basic:

(1) What is the average morphology of Titan's ionosphere and how is it determined by its coupling with Titan's neutral atmosphere and with magnetospheric particles and fields?
(2) What is the variability of this ionosphere, and to what extent is it controlled by magnetospheric effects (importance and variability of energetic charged

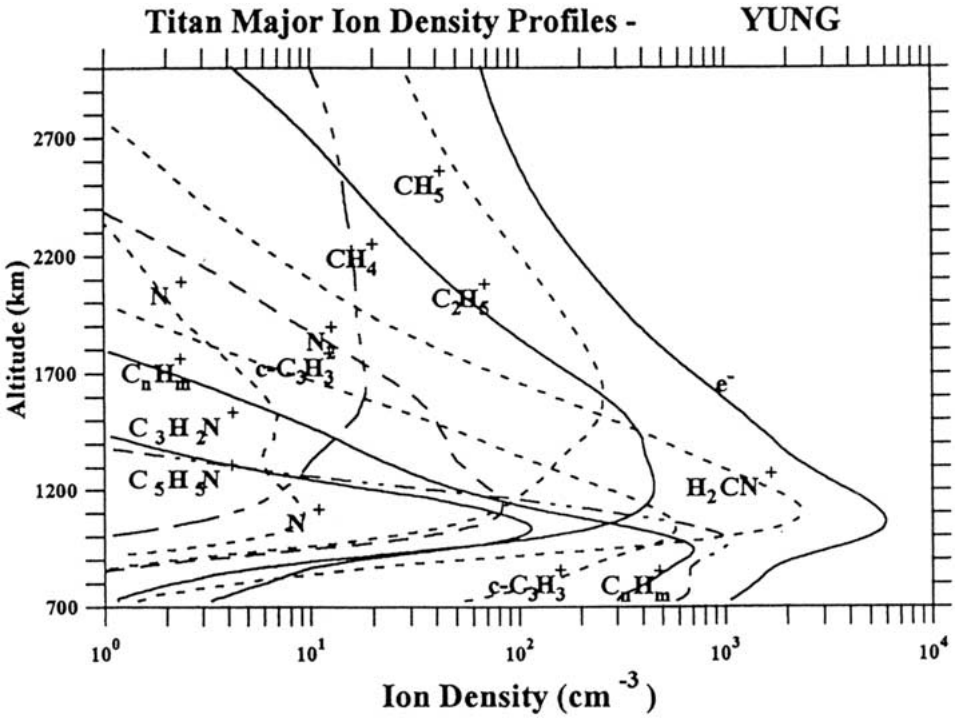

Figure 6. Ion density profiles for Titan's ionosphere from a photochemical model. From Keller *et al.* (1998).

particles as plasma sources, of its magnetization by the surrounding plasma flow, etc.)?

(3) How important are the different escape processes from Titan's upper atmosphere and ionosphere, in the neutral or ionized phases, in the balance of magnetospheric plasma sources and for the long-term evolution of Titan's upper atmosphere?

The ion neutral mass spectrometer (INMS) will measure both neutral density profiles in the upper atmosphere and ion density profiles in the ionosphere for species with mass numbers ranging from 1 amu up to 99 amu. This mass information will allow the chemical pathways controlling the ionosphere to be deduced. The vertical and horizontal structure of the ionosphere and upper atmosphere will also be determined by INMS. RPWS will determine the plasma density near and in the Titan ionosphere by measuring the upper hybrid resonance band. More importantly, RPWS includes a Langmuir probe added specifically to measure the electron density and temperature in Titan's ionosphere. In addition to these very important parameters, however, modeling of the current-voltage relationship should provide information on the ion temperature, given the composition measured by INMS and/or CAPS, and a measure of the solar UV flux. The radio science experiment (RSS) will provide electron density profiles. CAPS will measure the distribution

functions of electrons and ions with energies up to 20 keV. The MIMI experiment will measure fluxes of energetic ions, electrons, and neutrals. These experiments will provide important information on energy inputs (and ionization sources) into Titan associated with magnetospheric particle populations. They will also provide information on the plasma velocities in and near Titan's ionosphere. The UVIS experiment, by providing information on ultraviolet emissions from the upper atmosphere, will also tell us about both solar inputs and magnetospheric particle inputs into the upper atmosphere and ionosphere. The magnetometer experiment (MAG) will tell us the magnetic field topology around Titan and in its ionosphere. This topology, which largely controls the ionospheric dynamics and the energy inputs from the magnetosphere since the magnetic field guides magnetospheric electron motions, is the result of Titan's interaction with the magnetosphere.

2.3. TITAN'S INTERACTION WITH THE MAGNETOSPHERE

2.3.1. *Observational Knowledge*

All our observational knowledge of Titan's interaction with the magnetosphere is limited to the data obtained by Voyager 1 on November 12, 1980, which were published in special issues of Science (10 April 1981) and Journal of Geophysical Research (1 March 1982). The detailed reports on the observations made by the magnetic field experiment (Ness *et al.*, 1982), the plasma wave instrument (Gurnett *et al.*, 1982), the PLS plasma analyzer (Hartle *et al.*, 1982) and the LECP charged particle detector (Mc Lennan *et al.*, 1982) were summarized by Neubauer *et al.* (1984).

Let us give a brief overview of this unique data set, centered on the identifications of the main particles and fields signatures observed during the Titan fly-by. The Titan encounter occurred at 13.30 Saturn local time, along a trajectory which had a low inclination (8°) to Titan's orbital plane, crossing it from north to south at a point very close to the closest approach, which occurred at a distance of 6959 km from Titan's center (see Figure 1 of Neubauer *et al.* for the exact encounter geometry). The upstream magnetospheric flow conditions, as derived from the plasma data, corresponded to an Alfven Mach number of 1.9, and a sonic Mach number of 0.57, resulting in a fast Mach number of 0.55. For this 'transonic' situation, no upstream shock was expected in Saturn's plasma flow. Voyager passed through the wake of Titan in Saturn's magnetospheric plasma flow. This wake appeared to be shifted by 20° towards Saturn from the direction expected for exact corotating flow. As a result, the point of closest approach was very near the center of the wake, and the trajectory was not far from perpendicular to the wake axis, thus making the interpretation easier. Figure 7 shows a sketch of the different signatures observed, extrapolated from the V1 trajectory in a plane including this trajectory and perpendicular to Titan's orbital plane, which is actually nearly orthogonal to the wake axis.

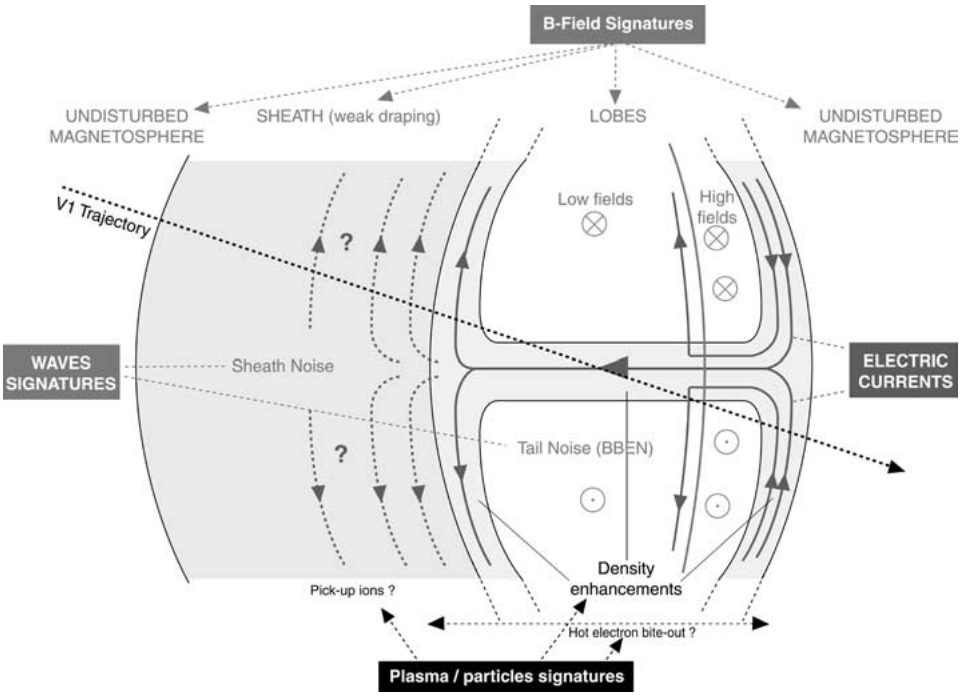

Figure 7. 2-D interpretation of plasma, particles, B-field and waves signatures observed by Voyager 1 during its encounter with Titan's wake.

The magnetic field signature clearly showed an induced magnetotail configuration, with two lobes of opposite polarities closely matching the size of the Titan obstacle itself (fields towards Titan in the northern lobe, away from Titan in the southern lobe). They were separated by a sharp current sheet flowing away from Saturn near Titan's orbital plane, and apparently closing through two sets of current sheets to the north and south of Titan's orbital plane. This magnetic signature is consistent with the draping of Saturn's magnetospheric field lines around the Titan obstacle. The two tail lobes were separated from each other and from the external plasma flow by regions of enhanced total plasma density (hatched areas in the figure) compared to the densities in the lobes and in the undisturbed magnetosphere.

A bite-out of the electron spectrum above 700 eV was observed in the PLS data over a region just slightly broader than the lobes, consistent with the absorbing or decelerating effect of Titan's upper atmosphere on these hot electrons.

Another spectacular feature of the data was a strong asymmetry between the Saturn-facing and the anti-Saturn facing sides of this induced tail. On the Saturn-facing side, the lobe magnetic field appeared more intense, and the lobe appeared separated from the external flow by a sharp boundary carrying a narrow and localized electric current sheet. The picture is very different on the anti-Saturn facing

TABLE V
Titan/Magnetosphere interaction models

Model reference	Type
Cravens *et al.* (1998)	2-D multi-fluid MHD
Ledvina and Cravens (1998)	3-D MHD
Kabin *et al.* (1999)	3-D MHD
Brecht *et al.* (1999)	Kinetic model (see Figure 2.3)

side: lobe fields appeared weaker, and they were separated from the undisturbed magnetospheric flow by a much broader boundary. This smooth transition actually extends over a width comparable to that of the tail itself, forming a sheath on only one side of Titan's wake, which apparently includes the region of distributed currents closing the cross-tail currents to the north of the spacecraft.

The electromagnetic emissions detected by PWS supported the identification of these different plasma domains. The lobes were associated with a 'tail noise' very similar in morphology to the characteristic Broad Band Electrostatic Noise (BBEN) observed in the Earth's magnetotail. Emissions in the sheath were dominated by a 'sheath noise', a low frequency electrostatic noise which has been interpreted as generated by fresh H^+ pick-up ions extracted from Titan's exosphere on its anti-Saturn side.

Finally, the analysis of PLS ion data appeared at least consistent with the expected geometry of the magnetospheric flow around the Titan obstacle. While H^+, as previously indicated, seemed to be dominant outside Titan's wake, a reduction in plasma flow speed was observed close to the tail boundary, consistent with mass loading of the flow by the addition of the heavier ions, such as N_2^+, H_2CN^+ and N^+, extracted from Titan's ionosphere.

The schematic representation of the V1 encounter with Titan shown in Figure 7 rests upon implicit assumptions such as the symmetry of the wake about Titan's orbital plane (which is basically orthogonal to the incident magnetospheric magnetic field). As for the interpretation in terms of draped field lines and the possible presence of pick-up ions in the sheath, it corresponds to a 'reasonable' 3-D extrapolation guided by our a priori physical understanding of Titan's magnetospheric interaction, complemented by what we learnt from the few presently available numerical simulations.

2.3.2. *The Contributions of Numerical Models*

Numerical simulation studies of the Titan-magnetosphere interaction (see Table V) are still oversimplified, because of limitations in spatial resolution, limited consideration of the multi-ion chemistry and dynamics, and lack of consideration of the non-stationary features, which are essential to study electromagnetic induction

effects. But they are very useful for a first-order understanding and description of the Titan interaction, and as planning tools for the preparation of CASSINI observations. 3-D magnetohydrodynamic models have been developed by Ledvina and Cravens (1998) and by Kabin *et al.* (1999). A more detailed and multi-fluid model was developed in 2-D by Cravens *et al.* (1998), and in 3-D by Nagy *et al.* (2001). The 3-D models, for instance, reproduce many expected features, such as the region of magnetic pile-up on the upstream side, the draping of field lines and the formation of Alfven wings, and the formation of an induced tail downstream. They also display significant differences, which to a large extent may be explained by the different numerical schemes and boundary conditions used. The first attempt at developing a kinetic model has been made by Brecht *et al.* (1999). Figure 8 shows, in the ideal plane of equatorial corotational flow, the calculated positions of the different ions in this model. Incident N^+ ions are shown in the left-hand column. The positions of the pick-up ions, H^+, N^+ and $C_2H_5^+$ are shown on the right-hand side, in panels (A), (B) and (C) respectively, for a case corresponding to 18.00 LT. The observed asymmetry between the two sides of the wake produced by finite gyroradius effects, which is evidently beyond the scope of ideal MHD models, is clearly seen in the figure.

2.3.3. *Key Problems and MAPS Investigation Strategy*

Even if we combine V1 encounter data and presently available simulation studies, we are left with enormous gaps in our understanding of Titan's interaction with the Saturnian magnetosphere. CASSINI studies will have to address three major problems.

i) Determine the 'average' properties of Titan's plasma environment and magnetospheric interaction.

We have summarized in Figure 9 what we can say to-day about Titan's plasma environment. It schematically shows the interaction, for the case when Titan is in Saturn's magnetosphere, in two orthogonal planes containing the direction of the incident flow vector: the 'vertical' plane containing the incident magnetic field, which is approximately perpendicular to Saturn's equatorial plane, and the 'horizontal' plane perpendicular to it, which is close to the equatorial plane for a purely corotational flow. As the plasma runs into Titan's atmosphere, it is loaded with mass by pick-up ions created from atmospheric neutrals by photoionization and electron collisional ionization. Thus the initial momentum is distributed over an increasing mass, corresponding to a deceleration of the incident plasma and an associated draping of the magnetic field lines frozen into the plasma. The mass-loaded plasma leaving Titan on the wake side thus forms an ion tail as indicated.

Mass is also lost via a neutral particle flux due to elastic collisions between fast ions and atmospheric neutrals (atmospheric sputtering) and via charge-exchange reactions, in addition to the classical atmospheric loss mechanisms. If the ionization rate is large enough and/or the momentum flux of the incoming flow is low enough, an ionopause will form separating an outer region threaded by Saturn's

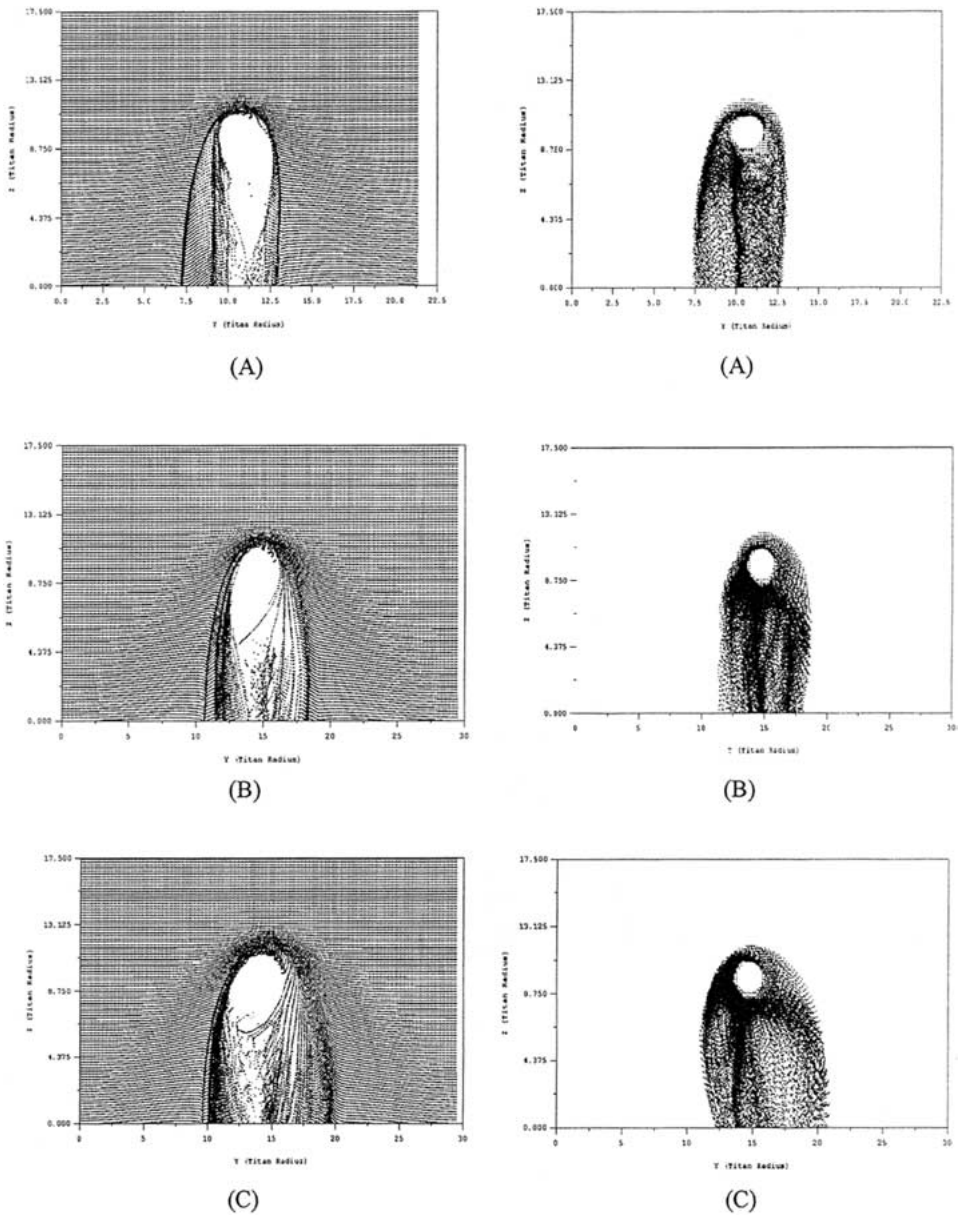

Figure 8. The ion positions calculated in the numerical kinetic model of Titan's magnetospheric interaction developed by Brecht *et al.* (1999) are shown in the equatorial plane of the ideal corotation flow, which comes from above, with the unperturbed magnetic field perpendicular to the plane of the figure. The left-hand column shows the positions of original incident N^+ ions, while the right-hand side panels show the positions of pick-up ions, H^+, N^+ and $C_2H_5^+$ in panels (A), (B) and (C) respectively.

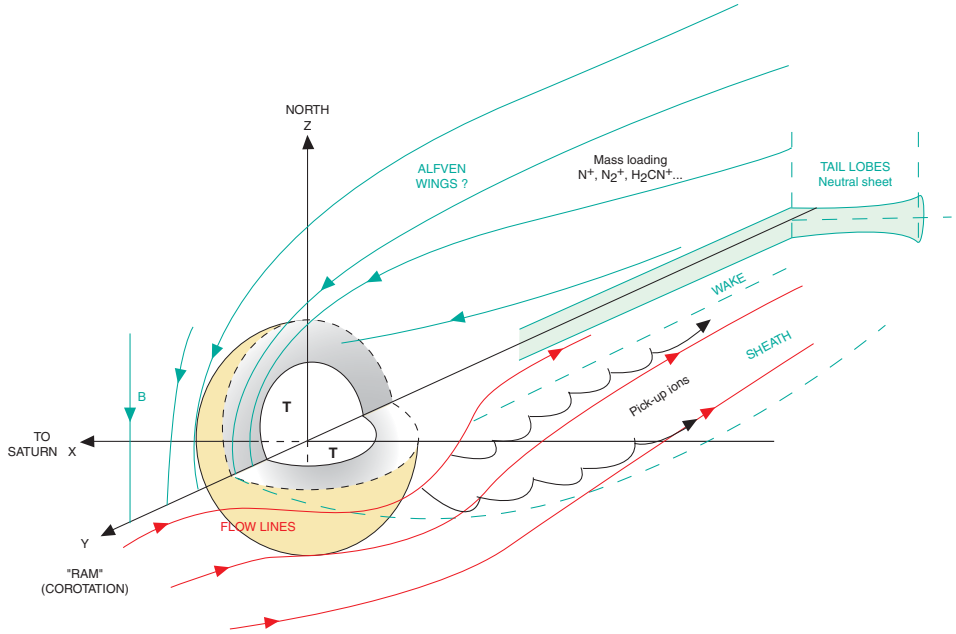

Figure 9. A sketch of the interaction between Titan and the magnetospheric plasma flow is presented in two orthogonal planes containing the incident flow vector $\underline{v}_o$: the plane containing the undisturbed magnetic field, and the plane perpendicular to it. The figure shows a magnetic field line as it is convected through Titan's atmosphere, as well as horizontal flow lines around the obstacle and the region of pick-up ions on the anti-Saturn side. Mass loading slows down the plasma and leads to the draping with the formation of Titan's tail and the tail current sheet. Ions are lost through the ion-tail. Some of the ion species are indicated.

magnetospheric field lines and an inner region, which is free from Saturnian magnetic fields but may contain magnetic fields of internal origin. If these conditions are not fulfilled, no ionopause forms and the magnetic field of Saturn will penetrate the atmosphere. The ionopause also represents a sheet of concentrated plasma currents.

In the 'horizontal' plane, the figure visualizes plasma flow lines which are diverted around the obstacle before continuing into the induced tail and around the flanks. On the side of the obstacle opposite to Saturn, ions picked-up from Titan's extended exosphere are accelerated out of the exosphere by the large-scale electric field associated with the flow and then dragged downstream, whereas similar ions on the Saturn-facing side will tend to be precipitated into Titan's atmosphere by the same electric field.

Further downstream, there is also a tail current sheet, as observed by Voyager 1, separating the northern and southern parts of the tail with essentially opposite magnetic field directions. In addition the tail will contain a north-south trending boundary between field lines draped over different hemispheres of Titan, as the incoming field lines separate at the stagnation point. If the plasma conditions are

very different on the two sides, this boundary may be easily identifiable, leading to a four-lobe induced tail as it seems to have been the case at the time of the V1 encounter (see Figure 7): because of variations in the relative directions of the magnetospheric plasma flow and of incoming solar photons (separated by an angle α) the north-south boundary may be very pronounced at times. An additional boundary is the outer boundary of the magnetotail, which may be referred to as the tail magnetopause.

Other chemical boundaries may also exist. A bow shock was absent at the Voyager 1 encounter but should obviously be looked for at each encounter, because variations in the outer magnetosphere due to magnetospheric dynamics may lead to occasional favorable conditions. As is clear from the discussion, the complicated geometry destroys many symmetries found e.g. at Venus, where our angle α is generally close to zero.

Three-dimensional observations of magnetic fields, plasma properties with chemical resolution, energetic particles, neutral particles and plasma waves are needed to disentangle the picture, ideally for all possible incident flow conditions. However, a sufficient number of carefully selected flyby trajectories is sufficient to describe the interaction, where they should be grouped by approximately equal incident flow conditions. Special emphasis must be given to the description of the various boundaries and current sheets alluded to above. To evaluate the mass losses through the ion tail, good coverage of the plasma flow on the wake side is necessary as a function of chemical species. For studies of the ionopause and the surrounding regions, flyby orbits with very low altitudes at closest approach are important like the nominal 950 km minimum altitude orbits of the Cassini mission.

The interaction picture will be different if the magnetosphere is sufficiently compressed for Titan to be located in the magnetosheath or the solar wind. In the latter case a pronounced bow shock is expected.

ii) Study the variability of Titan's plasma environment.

Titan is subjected to a strongly varying incident plasma flow due to variations of the solar wind and the Saturnian local time at Titan varying through 24 hours during the orbital period of 15 days. The analysis of the flow picture around Titan will lead to erroneous results, if this is not taken into account.

For a stable solar wind with an average momentum flux, the magnetopause will be at a stable location outside the orbit of Titan. Even then conditions at Titan vary mostly because of the variation of the angle α between the direction of corotational flow and incoming solar photons (Wolf and Neubauer, 1982). The situation is shown schematically in Figure 10. It shows that magnetospheric flow and ionizing photons from the sun provide the strongest ionization source in the upstream region of the flow around 18:00 LT, where LT denotes local time. The ionopause is expected to be best developed at this local time. Solar photons do not contribute to the ionization in the upstream stagnation region around 6:00 LT. The upstream ionopause may disappear in this case. Apart from the variation of α, magnetospheric plasma conditions will be dominated by Saturn's inner tail plasma

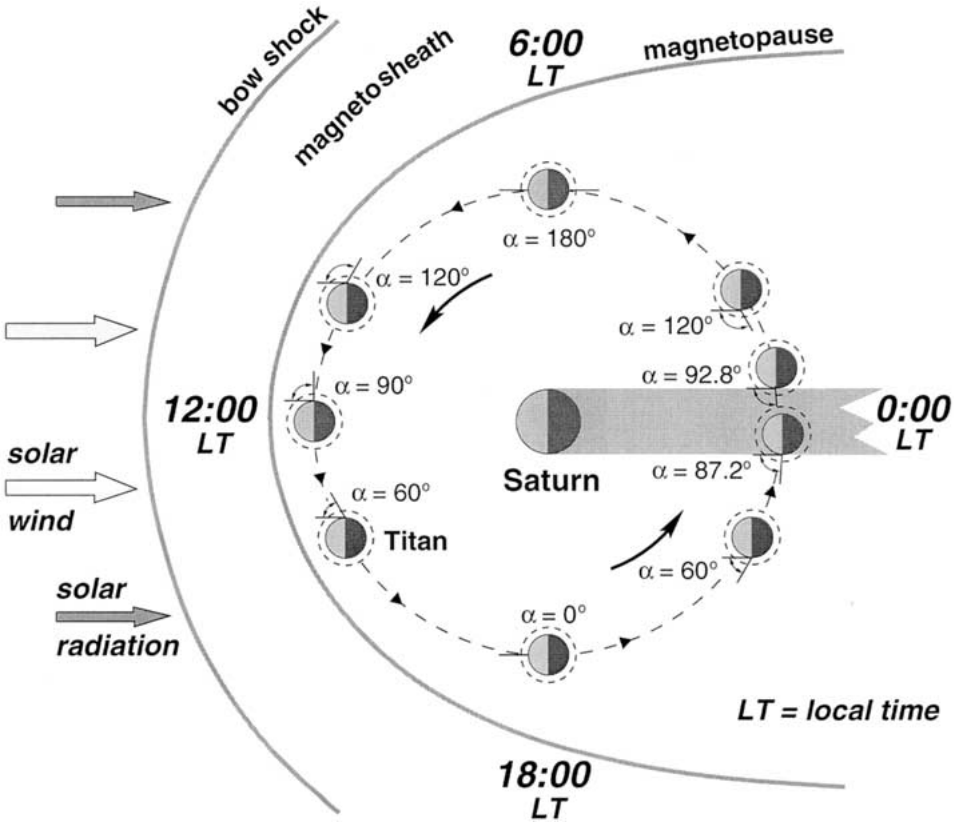

Figure 10. Titan's varying position during its orbital motion around Saturn. The angle α between solar photon radiation and the magnetospheric flow direction varies through 360°. Sketches of the magnetopause and the bow shock are also shown. Around the equinoxes there will be times when the sun is eclipsed by Saturn seen from Titan. This situation is also shown.

population and magnetic field configuration around 24:00 LT. Here substorm-like phenomena may play a role. If now the variation of the solar wind is taken into account, the magnetopause configuration will change with the possibility of Titan being located in Saturn's magnetosheath or even the solar wind. Obviously this will occur most easily near 12:00 LT.

Another interesting situation arises, when the sun is eclipsed by Saturn as seen by an observer on Titan. The sudden cut-off of sunlight will make interesting experiments possible with the upper atmosphere of Titan. This situation will occur near the equinoxes, e.g. at the end of 2008 or in 2009 just after the primary mission of Cassini.

Through the study of the variability of Titan's ionosphere and magnetospheric interaction, it will be possible to partly disentangle the effects of the different parameters which play a role in the interaction of a non-magnetized atmospheric/ionospheric obstacle with an external plasma flow. For instance, by varying solar il-

lumination and consequently the density of the ionospheric layers, we shall learn about the role played specifically by the ionosphere as a planetary obstacle to the external flow. Variations in the characteristics of this external flow (Mach numbers, composition, temperature etc.) similarly have a strong effect on the geometry of the different interaction regions. The repeated study of Titan's magnetospheric interaction during the CASSINI tour will make it possible, in principle, to explore rather extensively the parameter space of this very particular type of interaction between a flow and an obstacle. But for this exploration to be comprehensive enough, there is a need for a very good coverage of Titan fly-bys by the MAPS instruments throughout the mission.

iii) Contribute to the investigations of Titan's interior.

Magnetic fields due to currents in Titan's interior influence the interaction in various ways and can be diagnosed most easily by flybys at very low altitude. They can be used to probe Titan's interior. In principle, dynamo magnetic fields or magnetic fields due to remanent magnetization could produce permanent fields in the frame fixed to Titan. An upper limit to a permanent dipole has been derived after the Voyager I encounter. Other interpretations are possible, although the 'noise' due to dynamic magnetic field variations in the outer magnetosphere makes a too detailed interpretation difficult. This is apart from the consideration that contemporary models of Titan's interior do not allow large remanent magnetization because of the 'icy' outer shells.

After the discovery of a dynamo at the somewhat larger Jovian satellite Ganymede, one might be tempted to also expect at least a weak dynamo at Titan. However, Titan is not in a strong orbital resonance with the central planet as Ganymede is, and this resonance is suspected to play an important role in creating/maintaining a dynamo. Also, the evolution of Titan is likely to have been quite different from that of Ganymede.

There are probably better chances to observe an internal magnetic field due to electromagnetic induction in an electrolytically conducting ocean inside Titan. The inducing magnetic field could be the Saturnian magnetic field, which could periodically penetrate the Titanian atmosphere and ionosphere around 6:00 LT. This could also happen during the eclipses mentioned above. Again magnetic field measurements during very close encounters (950 km altitude for Cassini) are very important at the appropriate local times, as are MAPS measurements in general, in order to best understand the local plasma environment which will aid in identification of how any internal magnetic field is generated.

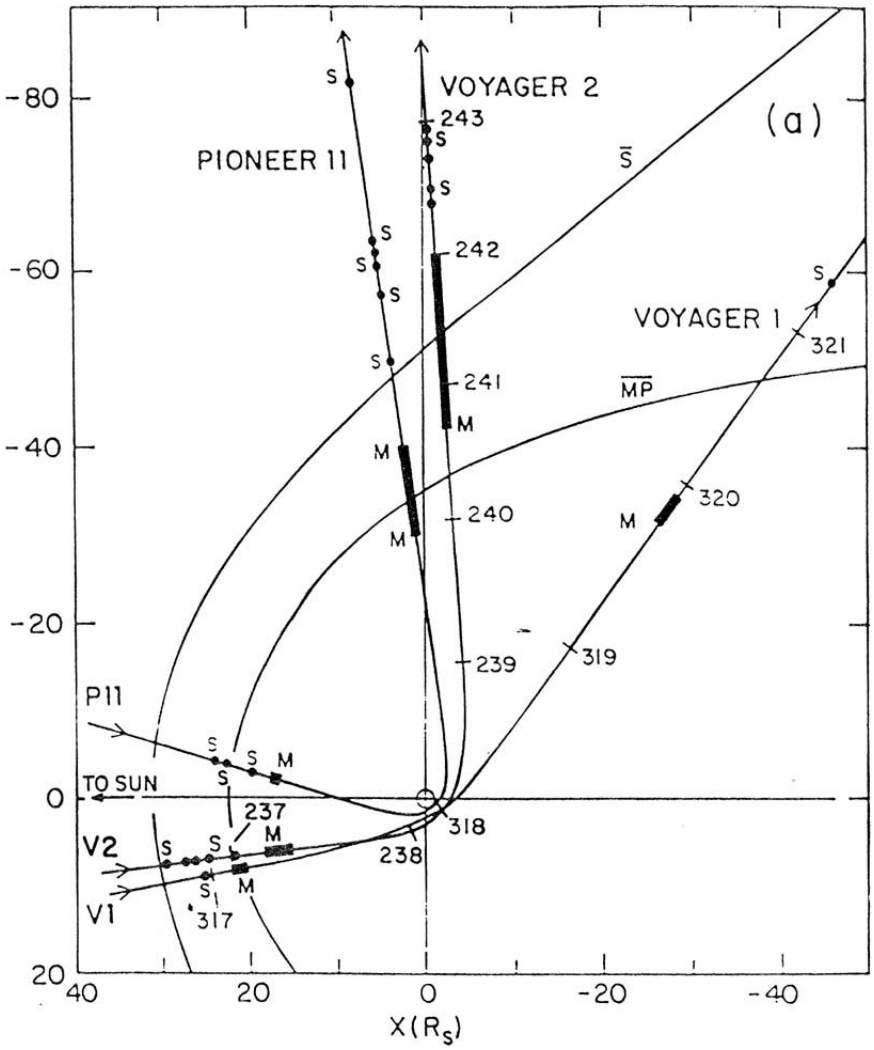

Figure 11. Trajectories of the Pioneer 11, Voyager 1 and Voyager 2 s/c, projected onto Saturn's equatorial plane. The average locations of the magnetopause (MP) and shock (S) are indicated, as well as their specific crossings during these three fly-bys. One can notice that only the noon and early morning sectors were explored.

3. Saturn's Plasma and Magnetospheric Interactions

3.1. Large-scale structure and dynamics of plasmas and fields

In order to set the stage for the discussion of the diversity of magnetospheric interactions operating in Saturn's magnetosphere, it is necessary to first give a brief overview of what we know of the large-scale distribution of its plasmas and fields.

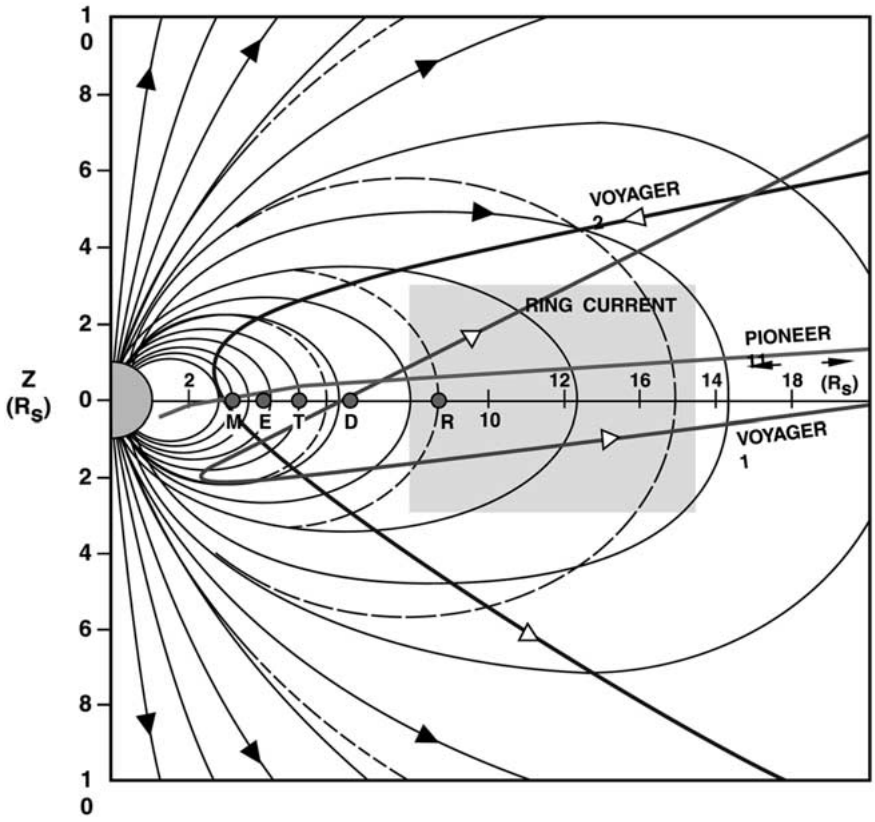

Figure 12. Trajectory of the three planetary fly-bys in a latitude/radial distance reference frame reduced to a Saturn meridian plane. The dashed lines show the magnetic field lines of the best fit dipole, the full lines those of a more realistic magnetic field model including the effect of the Saturn ring current, located inside the grey box in the center of the figure. Satellite locations are also indicated.

The three planetary fly-bys provided us with a preliminary description of the magnetic field configuration, the main plasma domains and plasma wave emissions. Figure 11 shows their trajectories projected onto Saturn's equatorial plane and Figure 12 shows the same trajectories in a Saturn latitude/radial distance coordinate system, represented in a Saturn meridian plane and overlaid with modeled magnetic field lines and ring current. As the figures show, these three fly-bys provided a very limited local time coverage of Saturn's magnetosphere, basically limited to the noon and early morning sectors, but some coverage in latitude. These observations have sometimes been extended in space coverage by a variety of empirical or physical models.

3.1.1. *Magnetic Field Configuration*

As for all planetary magnetospheres, the magnetic field at Saturn can be described as the sum of the internal contribution to the planetary field, produced by the planet-

ary dynamo, and additional contributions from the ring current, magnetopause and magnetotail currents. Smaller and more localized contributions are also expected from currents flowing along magnetic field lines between the equatorial magnetosphere and the ionospheric hemispheres of Saturn, and from currents generated by the interactions with the satellites, rings and neutral gas and dust clouds.

The ring current carried by charged particles trapped in Saturn's magnetic field has been detected extending from 8 R_S to 15.5 R_S near Saturn's equatorial plane (Figure 12). The magnetopause has a subsolar point distance of about 23 R_S from Saturn's center. The magnetotail has not been directly explored, and is only described by predictive models, such as the one of Behannon *et al.* (1981) shown in Figure 13. The tail should extend first symmetrically about Saturn's equatorial plane, and then along the Sun-Saturn axis beyond a hinge point estimated to be located in the midnight meridian at about 30 R_S from Saturn in the anti-solar direction.

More detailed descriptions of Saturn's magnetic field and associated boundaries are given in appendix A.

3.1.2. *Plasma Domains*

Saturn's plasma domains were first discovered by Pioneer (Frank *et al.*, 1980), and later analyzed in detail by the three charged particle investigations carried by Voyager: PLS, LECP and CRS.

The plasma science instrument (PLS) provided most of our current knowledge of the thermal plasma at Saturn up to about 6 keV (Bridge *et al.*, 1981, 1982; Lazarus and Mc Nutt, 1983; Sittler *et al.*, 1983; Richardson, 1986). Higher-energy particles were measured by the low-energy charged particle (LECP) experiment (Krimigis *et al.*, 1981, 1982, 1983). The cosmic ray subsystem (CRS) covered energies greater than 1 MeV (Vogt *et al.*, 1981, 1982). Altogether, the three instruments left a gap in energy coverage between about 6 and 22 keV which won't be covered before CASSINI returns data from Saturn.

Let us summarize what we know of the electron and ion populations, their energy spectra and their fluid parameters.

Electron populations

A comprehensive analysis of electron observations, merging the information from the three investigations, has been performed by Maurice *et al.* (1996). Through a careful re-analysis and intercalibration of all available data, they have been able to produce composite energy spectra with a 15-min. time resolution all the way along the V1 and V2 trajectories. For each spectrum, using a logarithmic interpolation across the PLS-LECP energy gap, the authors systematically computed three moments of the electron distribution function, assumed to be isotropic: the electron density n_e, the electron pressure P_e, and the total electron return current density to the spacecraft, F_e, which is simply the intensity spectrum integrated in energy.

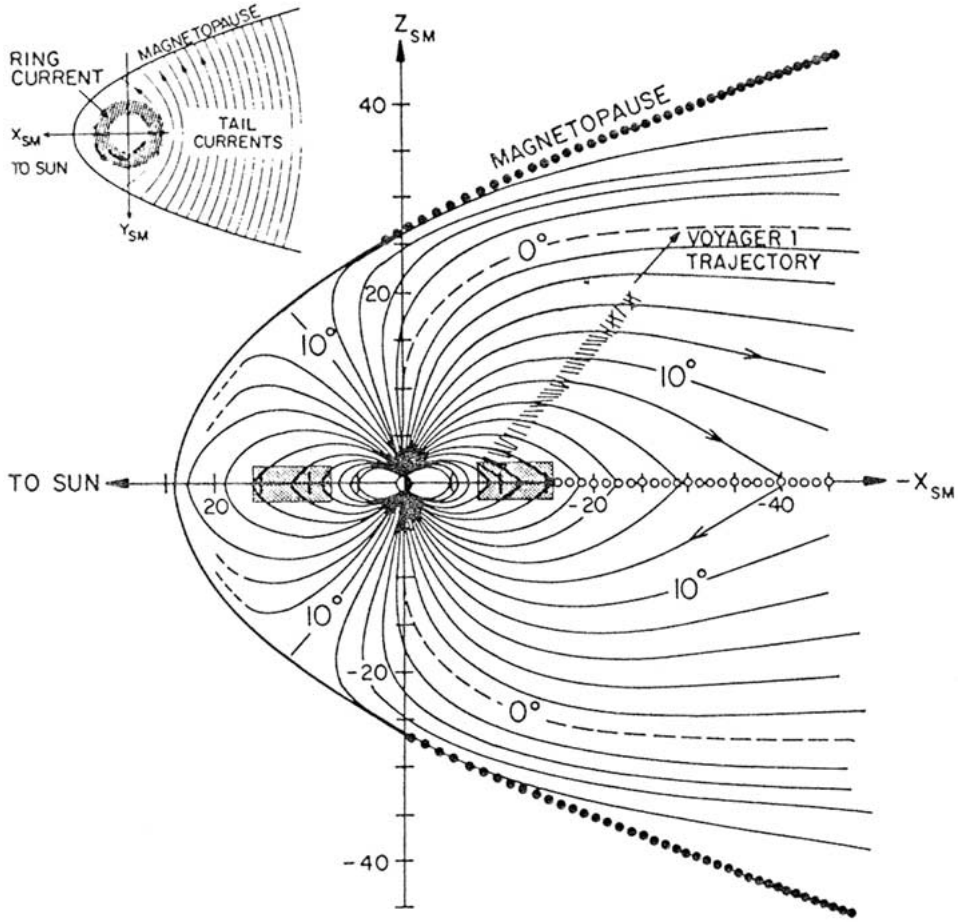

Figure 13. Representation of magnetic field lines in the noon-midnight meridian plane in the Saturn magnetotail model of Behannon *et al.* (1983), for the case when the sun is in Saturn's equatorial plane.

Figure 14 shows the moments calculated in this way along the Voyager 2 spacecraft trajectory, together with the latitude of the spacecraft (lower panel) and the electron beta of the plasma (third panel). Open circles show the value of beta extrapolated to the magnetic equator assuming a constant pressure of the warm/hot electrons along field lines. The regions where beta reaches 1 nearly coincide with Connerney *et al.*'s (1981) model ring current. Densities and pressures regularly increase inward, until the orbit of Dione, and then decrease inward of it. A similar curve for Voyager 1 (see Figure 8 of Maurice *et al.*) shows that electron densities can reach higher values, up to 10 cm^{-3}, near the equatorial plane.

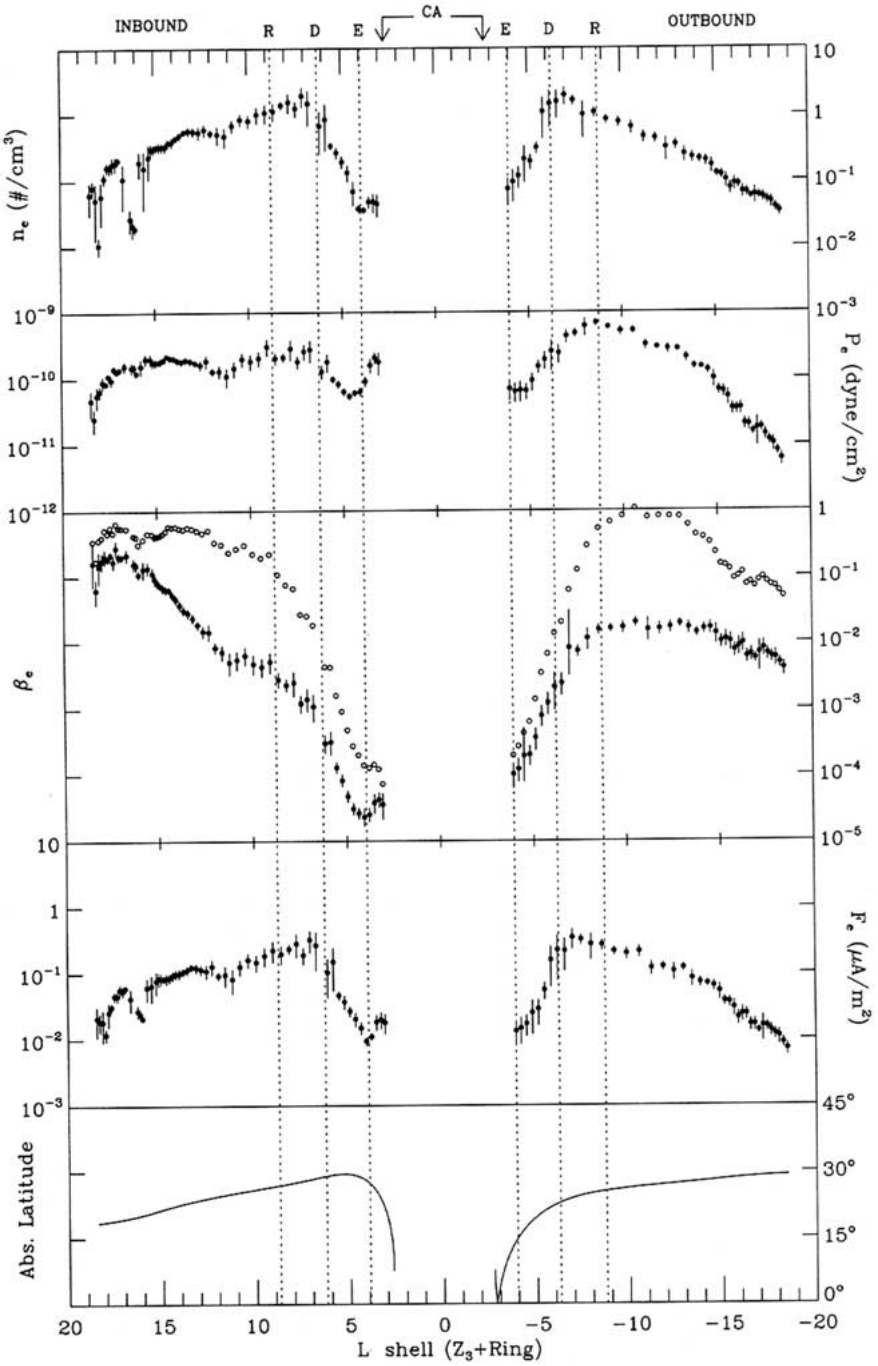

Figure 14. Voyager 2 electron density (n_e), electron pressure (P_e), electron beta (β_e), and electron return current density (F_e) plotted as a function of L shell with their 1-sigma uncertainty (solid circles). Open circles are used for the beta values extrapolated to the magnetic equator of each field line. The absolute value of the spacecraft latitude is shown in the bottom panel.

Ion populations

The Voyager PLS instrument had no direct capability to discriminate the different ion species. However, as long as the Mach numbers of the different ion species remained sufficiently greater than 1, each species gave a different and separable peak in the PLS energy spectra, from which one could determine the density (from the peak total intensity) and the temperature (from the peak width), whereas the comparison of the three Faraday cup records gave access to the ion drift velocity vector (e.g., Lazarus and Mc Nutt, 1983; Richardson, 1986). The analysis revealed the presence of two different mass components in the Voyager spectra, a light-ion component at mass 1 corresponding to protons, and a heavier ion component near 16 amu. It could not be determined, however, if this peak was composed of O^+, OH^+, H_2O^+ or a combination of them since the peak was broad enough to cover all these possibilities, or even N^+ at 14 amu. So this peak was arbitrarily treated as a single ion species, denoted 'O^+' for simplicity. A detailed review of thermal plasma at Saturn has been published by Richardson (1998). Here we shall simply show one illustrative example of the original analysis of Richardson (1986): Figure 15 shows the ion drift velocity, reduced (from top to bottom) in terms of azimuthal, radial and vertical components in a reference frame linked to Saturn's equatorial plane, and the temperatures and densities of the two ion species (bottom two panels), plotted as a function of L shell. The dotted lines on the drift panels show the corresponding components of the local corotation velocity. The striking feature emerging from these data is that the thermal plasma corotates with the planet only in the inner magnetosphere (inside $L = 5.5$ for Voyager 1 as seen in Figure 15, or inside $L = 8.5$ for Voyager 2). But it systematically moves more slowly than corotation outside these limits, reaching at times as low as 50% of the corotation speed. There is also an increase in the departure from corotation just outside the orbits of Dione and Rhea. In addition to these azimuthal flows, radial flows of significant magnitudes are also seen in the outer magnetosphere.

Using the distributions of ion densities, ion and electron temperatures along the spacecraft trajectories, Richardson and Sittler (1990) extrapolated the density distribution of each charged species to a full magnetic meridional plane by using the equation of pressure balance along field lines, for a range of L values extending to $L = 12$. The resulting density model is shown in Figure 16, in terms of iso-contours of proton, 'oxygen', and electron densities. One sees that the ion species are concentrated toward the equatorial plane, as a result of the effect of the centrifugal force acting on the plasma trapped in each magnetic flux tube. This effect is negligible for electrons, significant for the light ion and dominant for the heavier ion. In addition, the three species are coupled along each field line by a charge-separation electric field which restores quasi-neutrality. This field results in a lesser confinement of the heavier ion, which is partly pulled away from the equator by the electric field which couples it to the electron gas, while the light ion tends to 'float' away from the equator where its density has a local minimum, as one can see in the 'proton' panel. This model was extrapolated further outward

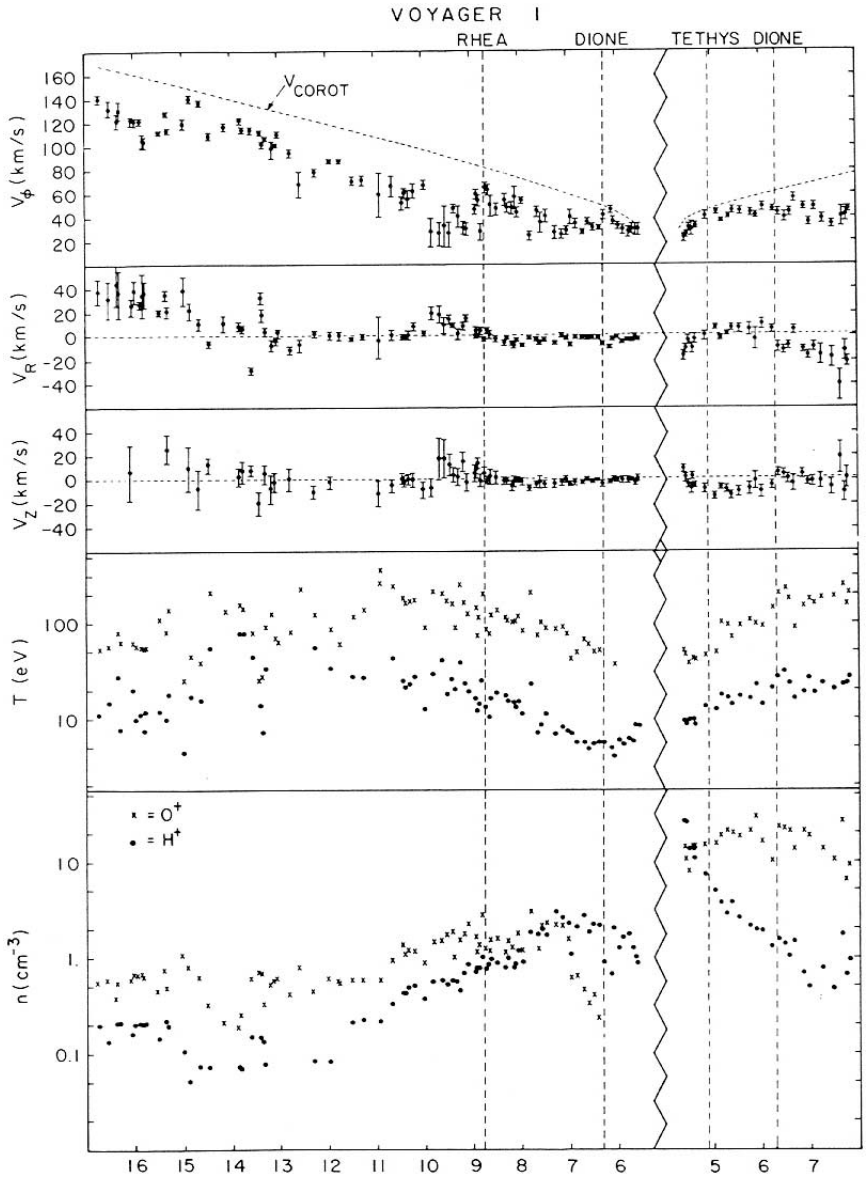

Figure 15. Thermal ion moment profiles along the Voyager 1 trajectory deduced from the PLS data by Richardson (1986), assuming the presence of two ion masses: the three components of ion drift in the Saturn-centered cylindrical coordinate set are shown at the top, and the density and temperature of the two mass components at the bottom.

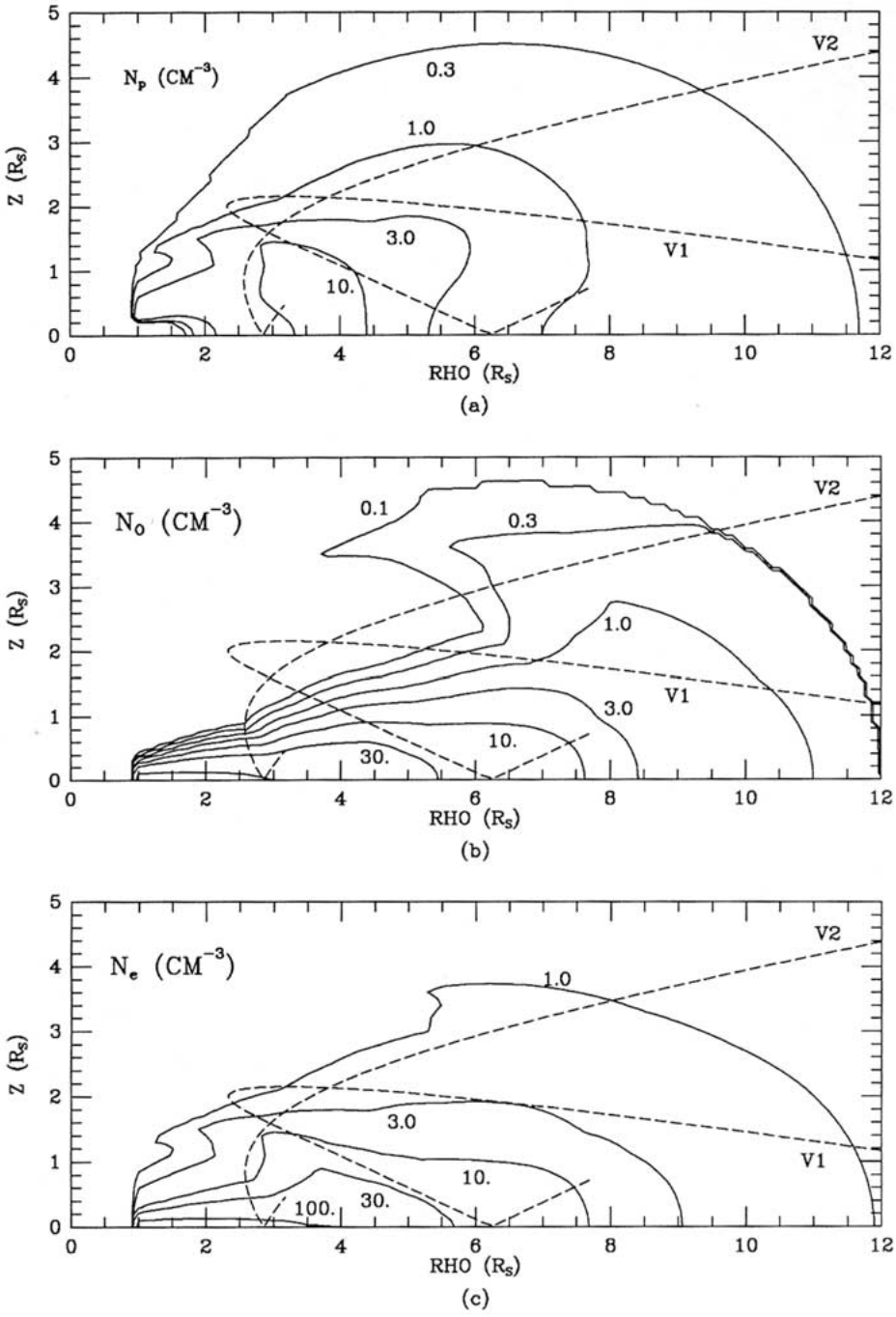

Figure 16. Isocontours of thermal H^+, O^+ and electron densities in Saturn's meridian plane in the model of Richardson and Sittler (1990), deduced from PLS data.

to L = 20 by Richardson (1995). These two studies used simplifying assumptions of constant temperatures and temperature anisotropies along field lines. A self-consistent calculation of the exact distribution of each species along field lines, allowing for distribution functions of arbitrary shapes and for temperature anisotropy variations, was later developed by Maurice *et al.* (1997) and applied to the special cases of Jupiter and Saturn.

Plasmas and fields in the outer magnetosphere

The region outside about 15 R_s in the equatorial plane and centered on Titan's orbit appears to display a broad variety of dynamic phenomena and irregular structures. This is very probably because it is under the combined influence of the solar wind and its variability, the magnetic tail, Titan and its neutral torus. Let us describe the irregular structure of plasmas and fields in this domain.

Observations of regions of detached plasma were made by two of the three spacecraft flybys of Saturn. These signatures on the dayside inbound passes of the Voyager 1 and 2 spacecraft occurred whilst the magnetosphere was in an expanded and rather disturbed state as a result of relatively quiet solar wind conditions. The Pioneer 11 inbound pass occurred during a period when the solar wind was itself very disturbed, resulting in a very compressed and rather quiet magnetosphere.

The detached plasma regions are of higher density than the surrounding medium and of a much colder temperature. There are also corresponding signatures in the magnetic field, where a sharp dropout in the north-south component is mirrored by a corresponding dropout in the field magnitude (Dougherty, private communication). Such signatures are to be expected from simple pressure balance arguments. This cold detached plasma is observed in the hot outer magnetosphere in the rather turbulent region between the last magnetopause entry into the magnetosphere and the outer edge of the equatorial plasma sheet.

Four of these signatures observed during the Voyager 1 encounter in the vicinity of Titan have been interpreted as the spacecraft having crossed through remnants of the plasma plume of Titan (Eviatar *et al.*, 1982). The observations were consistent with a gradual aging of the plume as well as dispersal of the plume in response to changing solar wind conditions. Closer in to the planet but still beyond the outer edge of the plasma sheet the plasma signatures have been described as detached plasma flux tubes which have broken off from the edge of the plasma sheet by the centrifugally driven instability (Goertz, 1983). For the Voyager 2 fly-by, Titan was in the magnetosheath during the inbound pass, yet numerous cold plasma enhancements, also associated with magnetic field drop-outs, were observed between entry into the magnetosphere and the outer edge of the plasma sheet.

Similar signatures of detached plasma flux tubes have also been observed in Jupiter's dayside magnetosphere, again just beyond the outer edge of the plasma sheet (Southwood *et al.*, 1995). Once detached from the planetary field the only forces imposed on the bubble will be those imposed by the external field. The magnetic pressure force compresses the bubble transverse to the external field but

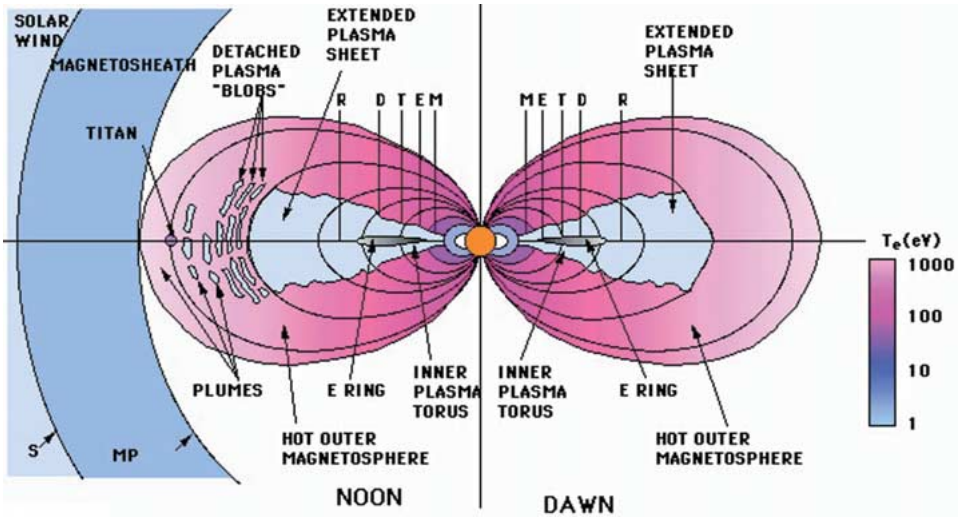

Figure 17. Schematic representation of the plasma populations of Saturn's magnetosphere, as it has been proposed for the noon and dawn sectors explored by Voyager by Sittler *et al.* (1983). Typical electron energies are indicated using the color code indicated on the right-hand side.

exerts no force along the field direction and so the bubble expands in that direction. Dispersal of the plasma within the flux tube is likely as they evolve and observations which the Cassini orbiter will make at Saturn are crucial for allowing a better understanding of these flux tubes and their evolution at different local times and radial distances. Such phenomena are important since they are likely to represent evidence of dynamical processes occurring in fast rotating magnetospheres and may represent an important mechanism for loss of material from such magnetospheres.

A summary picture of plasma regimes and flows

From the set of available observations, a summary picture of magnetospheric plasmas in the middle and low latitude magnetosphere has been proposed by Sittler *et al.* (1983), as shown in Figure 17, adapted from their study. Due to the local time coverage of the inbound and outbound Voyager fly-bys, it can be established only for the noon sector (left-hand side of the figure) and for the dawn sector (right-hand side). The region of closed field lines of the magnetosphere can be divided radially into relatively homogeneous plasma domains. Going from the planet radially outward, the regions of dense plasma correspond to the inner plasma torus, certainly coupled to the rings and icy satellites as their main source, and then to the extended plasma sheet, extending basically from 8 to 12–15 R_S. Both temperatures and flow speeds of the ions increase outwards, with a trend which closely corresponds to corotation and pick-up ion energies up to about 6 R_S, and then progressively departs from exact corotation to display a significant sub-corotation. This region of relatively cool and dense plasma is embedded into a hotter and more

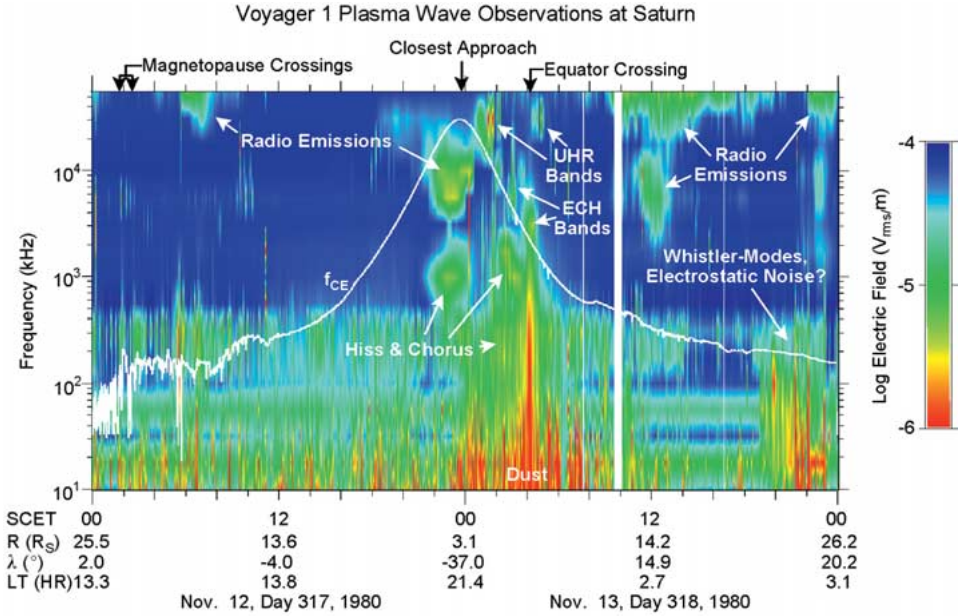

Figure 18. Summary plot of plasma and radio wave observations by the PWS instrument from the Voyager 1 flyby (Gurnett *et al.*, 1981a). This figure represents the 16-channel spectrum analyzer data in the form of a frequency-time spectrogram with the intensities of waves indicated by the color bar at the right plotted as a function of frequency and time.

tenuous plasma in the outer magnetosphere, which is not centrifugally confined to the vicinity of the equatorial plane as the cold plasma is. Between the outer edge of the extended plasma sheet and the magnetopause on the dayside, a very irregular plasma structure has been detected by Voyager, which may be partly composed of plasmas from Titan and of plasma 'blobs' centrifugally detached from the plasma sheet. The structure of this region is probably highly variable with solar wind conditions.

3.1.3. *Plasma Waves*

Saturn's plasma wave spectrum shows strong similarities to those of other planetary magnetospheres (Kurth and Gurnett, 1991). The observations from the Voyager 1 flyby (Gurnett *et al.*, 1981a) are summarized in Figure 18. This figure represents the 16-channel spectrum analyzer data in the form of a frequency-time spectrogram with the intensities of waves indicated by the color bar at the right plotted as a function of frequency and time. We've used a fitting algorithm to interpolate wave intensities between the coarsely-spaced spectrum analyzer channels; some features which appear to be rather broadbanded in this presentation are narrowbanded in fact. The observations are generally well-ordered by the electron cyclotron frequency f_{CE} derived from the measured magnetic field and this characteristic frequency is provided as a white line overlaying the spectrogram. At the very

highest frequencies the low-frequency extent of the Saturn kilometric radiation, which will be discussed extensively in section 3.2.4., can be observed. One set of radio emissions which is not related to the kilometric radiation, however, occurs near closest approach at frequencies below f_{CE} but above the local electron plasma frequency (Gurnett *et al.*, 1981b). These are narrowband radio emissions in the frequency range of a few to 10 kHz based on high resolution wideband observations. That they are found in Figure 18 at frequencies below f_{CE} means that they are propagating in the left-hand ordinary mode. Gurnett *et al.* (1981b) suggest that the frequency spacing between the narrowband lines implies that there may be some connection between the icy satellites and the generation mechanism of these waves.

Just above f_{CE} on the outbound portion of the trajectory inside of about 8 R_S Voyager observes electron cyclotron harmonic emissions, called ECH in the remainder of the text (Kurth *et al.*, 1983). The primary band observed is the so-called $3f_{CE}/2$ band just above the electron cyclotron frequency and below its harmonic. Also seen, however, is the upper hybrid resonance band which is a special case of the ECH bands between the harmonics of f_{CE} near the upper hybrid resonance frequency. Below f_{CE}, especially near closest approach and near the equator crossing, are bands of whistler-mode hiss and chorus. A relatively intense feature right at the equator is likely to comprise both whistler-mode hiss and the response of the instrument to dust impacts (Barbosa and Kurth, 1993; Tsintikidis *et al.*, 1985). Finally, the broadband emissions near the end of the plot in Figure 18 could be some combination of whistler mode or electrostatic waves (such as broadband electrostatic noise) associated with the near-tail region.

The ECH bands at Earth are occasionally observed at intensities of a few mV/m and are capable of pitch-angle scattering electrons of a few hundred eV to a few keV. However, the observed ECH bands at Saturn are quite weak, only about 30 μV/m and are unlikely to be an important loss mechanism for low-energy electrons. Similarly, Scarf *et al.* (1984) have calculated that the whistler-mode emissions near 1 kHz resonate with electrons near 2 keV, but are considerably weaker than required to cause strong diffusion. They also report that the flux of resonant electrons observed is well below the stable trapping limit, so this is not a surprising result. The magnetic equator is a location where certainly the ECH waves and to a lesser extent the whistler-mode waves tend to be most intense at other planetary magnetospheres. Because of the aligned magnetic dipole the Voyagers only sampled the near-equatorial region near 6 and 3 R_S, so it may be that an orbiter such as Cassini might find that there are either radial or temporal variations in the intensities of these emissions, which would increase their importance as a loss process for electrons (Kurth and Gurnett, 1991).

3.1.4. *Saturn's Ionosphere*

Molecular hydrogen is the primary neutral constituent of the thermospheres of the giant planets (Jupiter, Saturn, Uranus, and Neptune), although atomic hydrogen is also present in the upper atmospheres and exospheres of these planets as well

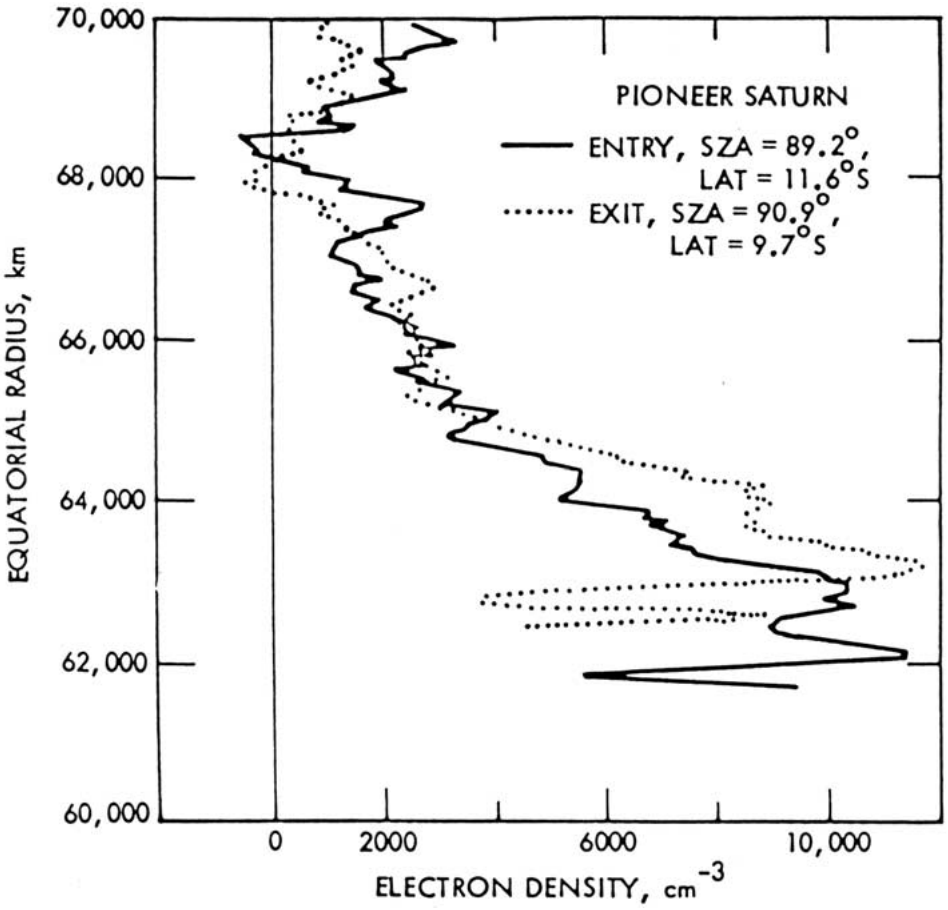

Figure 19. Electron density profile of Saturn's ionosphere deduced from Pioneer 10 radio occultation data. From Kliore *et al.* (1980).

as some methane (CH_4) in the lower thermosphere (cf., Atreya, 1986). Electron density profiles were measured in Saturn's ionosphere by the Pioneer 11 and Voyager 1 and 2 spacecraft by means of the radio occultation technique (see review by Waite and Cravens, 1987). The typical maximum electron density observed in Saturn's ionosphere was about 2×10^4 cm^{-3} (cf., Waite and Cravens, 1987). The electron density profiles measured by Pioneer are shown in Figure 19. Radio occultations of the atmosphere or ionosphere of the outer planets are possible only near the terminators, which severely limits the available local time information on these ionospheres. However Kaiser *et al.* (1984) used radio measurements of the observed low-frequency cut-off of Saturn electrostatic discharges (SED) from lightning to determine the peak ionospheric electron density and its variation with local time (see Figure 20). The peak electron density deduced in this way at local noon is 10 times higher than radio occultation values at the terminator (i.e., dusk

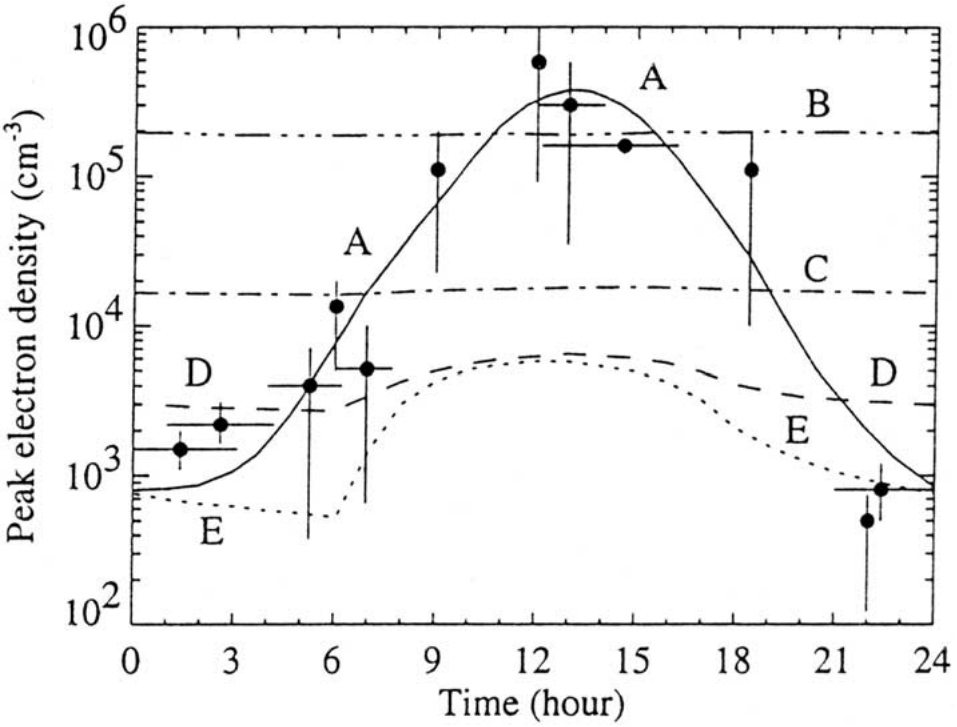

Figure 20. Peak electron density versus local time in Saturn's ionosphere. Data points are from the SED measurements of Kaiser *et al.* (1984) and the curves (A through E) are from the model of Majeed and McConnell (1996) for different water influxes and abundances of vibrationally excited H_2. Curve A is for a 'standard' model with no water influx and no vibrationally excited H_2. Model D has no vibrationally excited H_2 but does have a water influx of 5×10^7 cm^{-2} s^{-1}. Model E has no water influx but does have vibrationally excited H_2. From Majeed and McConnell (1996).

or dawn). Kaiser *et al.* also noted that some ionospheric structure appeared to be linked to the rings. Infra-red observations of H_3^+ provide another source of information on the auroral region, indicating the presence of this important ionospheric species (Geballe *et al.*, 1993).

H_2^+ is the main ion produced in all these ionospheres although some H^+ is also produced (cf., Schunk and Nagy, 2000). Photoionization by solar EUV radiation is the main ion source at low and mid-latitudes. Electron impact ionization by energetic magnetospheric electrons is thought to be the main ionization source in the auroral regions (see section 3.2.4 on auroral processes).

Just as in the E regions of the inner planets (Earth, Venus, and Mars), ion-neutral chemistry alters the ion composition. In particular, the following reaction quickly removes H_2^+:

$$H_2^+ + H_2 \longrightarrow H_3^+ + H \qquad (1)$$

TABLE VI
Main characteristics of Saturn Plasma/particles models

Model reference	Main characteristics
Maurice *et al.* (1996)	Provides composite electron energy spectra with a 15-min resolution along the V1 and V2 trajectories for the energy range 10 eV–2 MeV.
Richardson and Sittler (1990)	Meridian plane distribution of thermal O^+, H^+ and electron densities deduced from PLS Voyager up to L = 12.
Richardson (1995)	Extrapolation of the previous model to L = 20, describing irregular structures in the outer magnetosphere.

TABLE VII
Main Saturn ionosphere models

Connerney and Waite (1984)	1D chemical/vertical transport model including vibrationally excited H2 and ring water influx.
Majeed *et al.* (1991)	1D chemical/vertical transport model including vibrationally excited H2.
Majeed and McConnell (1996)	1D chemical vertical transport including vibrationally excited H2, water influx, and vertical ion drifts.

The H_3^+ ions that result from this reaction are rapidly removed by dissociative recombination, and for this reason have relatively short lifetimes. H_3^+ ions can also be removed in the lower ionosphere by reaction with CH_4, thus forming CH_5^+ions. Subsequent photochemistry leads to the formation of heavier, more complex hydrocarbon ion species. Metallic ion species also probably exist in Saturn's lower ionosphere, just as they exist in the Earth's lower ionosphere where they are produced by the meteoritic source. Ionospheric models show that the main ionospheric peak is located in a 'F_1-type' region and that the major ion species near this peak is H^+. The reason for this is that the chemical lifetime of ionospheric protons is quite long, whereas the other ion species have much shorter chemical lifetimes. The main chemical loss process for the H^+ ion is the slow radiative recombination reaction allowing the H^+ density (in what are called 'standard' models) to build up to rather large values. In fact, in order to bring calculated density values into line with the observed values, most theoretical models of Saturn's ionosphere (see Table VII) had to invoke additional loss processes for H^+ such as removal by reaction with water molecules, presumably associated with the rings (Connerney and Waite, 1984) or by reaction with vibrationally excited H_2 (Mc Elroy, 1973; Majeed and McConnell, 1991); see the review by Waite and Cravens (1987).

By analogy with the terrestrial ionosphere, Saturn's ionosphere is likely to be extremely dynamic. Both vertical and horizontal ion drifts, associated with both neutral winds and magnetospheric electric fields, are likely to be present. Very little work has been carried out in this area. Majeed and McConnell (1996) adopted reasonable values of vertical ion drifts in their ionospheric model in order to ascertain the effects on the ionospheric density profile. They also included the effects of H^+ loss by reaction with vibrationally excited H_2 or with water. Figure 20 shows some of these results. Majeed and McConnell find that the model (with a reasonable choice of parameters) can reproduce the radio occultation profiles at the terminator but not the large diurnal variation evident in the SED data. Influx of water from the rings may help to increase the rate of loss of H^+ ions, but this mechanism is not proven to actually operate.

MAPS investigation strategy for the study of Saturn's ionosphere

It is clear that Saturn's ionosphere remains very poorly understood although it may be an important source and/or sink of plasma for the magnetosphere and ring ionosphere and plays a role in magnetospheric dynamics via electrodynamic coupling effects of the ionosphere's electrical conductivity. The Cassini mission can contribute to a greater understanding of Saturn's ionosphere and its linkages to the lower atmosphere, to the magnetosphere and to the rings. To this end every opportunity will have to be used to measure electron density profiles from radio occultation. Critical information on particle fluxes (electrons, ions, neutrals, and dust, from low to high energies) into and out of the ionosphere will be obtained by a number of MAPS instruments (e.g., CAPS, MIMI). The analysis of SED's by the wave instrument (RPWS), as demonstrated by Voyager experimenters, can also be a powerful sounding technique to determine the diurnal variations of the ionospheric layers. All these observational inputs will be much needed to develop a new generation of Saturn ionospheric models and try to reconcile the large discrepancies existing to-day between models and observations.

3.2. SATURN'S MAGNETOSPHERIC INTERACTIONS

3.2.1. *Interactions of the Inner Magnetosphere with the Ionosphere, Rings and Dust*

A schematic representation of Saturn's inner magnetosphere region is shown in Figure 21. This region is characterized by the strong coupling of three components: plasma populations, ring and dust particulates, and energetic charged particles from the radiation belts.

Plasmas of 3 different origins, from Saturn's ionosphere (in blue), from the tiny rings' atmosphere (in green) and finally from the icy satellites torus (in red), are likely to exist in this region. The existence of a specific component of the plasma, narrowly confined to the vicinity of the ring plane and related to the rings' ionosphere, was first suggested by Eviatar and Richardson (1990, 1992) and later

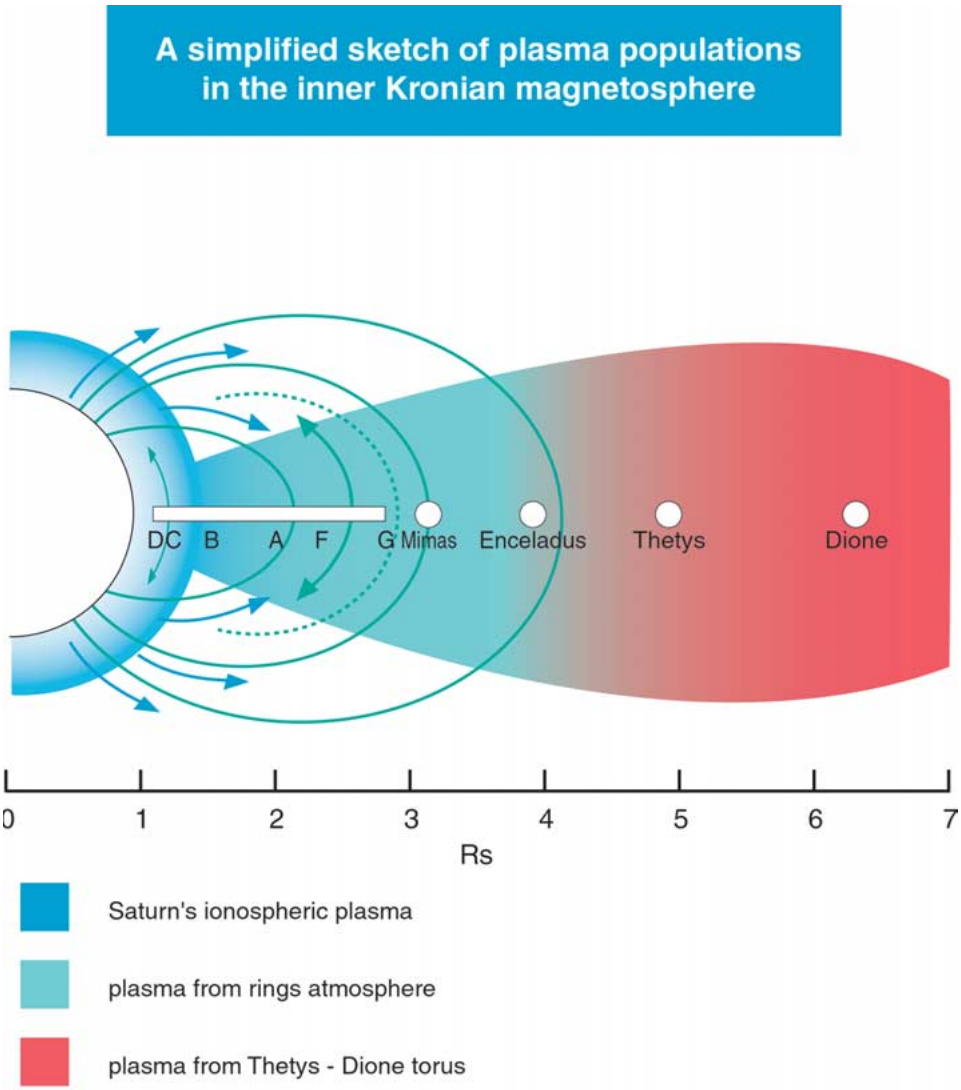

Figure 21. The innermost magnetosphere is a region of strong mixing and interactions between the different plasma sources. The Saturn ionospheric source diffuses partly upward along field lines towards the equatorial plane, where it mixes with the plasma generated in the tiny rings atmosphere (green) and the icy satellites ion torus (red). Downward diffusion of water-group ions into the upper atmosphere of Saturn may play an important role in the balance of the ionospheric plasma itself.

confirmed by the detailed analysis of PLS data in the vicinity of the ring plane crossing, near 2.85 R_s, by Gan-Baruch *et al.* (1994). It showed a relatively dense plasma, with a peak density around 100 cm^{-3}, a large anisotropy of about 5, and a strong confinement within ± 0.3 R_s about the ring plane, consistent with the observed anisotropy. This observation confirmed the existence of a ring ionosphere,

predicted by Ip (1983) to result from the ionization of the tenuous H_2O atmosphere of the rings, which was observed for the first time by Wagener and Caldwell (1986).

These three plasma populations of significantly different densities, temperatures and composition are partly superposed in the inner magnetosphere, as a result of a variety of diffusion processes: magnetic-field-aligned upward diffusion of ionospheric plasmas towards the equatorial plane, field-aligned downward diffusion of ring plasma towards the ionosphere, and probably some cross- field diffusion of the rings and icy satellites plasmas.

The second component of the region is constituted by the rings and dust particulates, which cover a broad range of sizes from 100 meter to sub-micron. The small-size component of this population is composed of dust particulates which may interact with the plasma in several ways, being subject to electrostatic charging under the effect of UV irradiation, bombardment by charged particles, and interaction with the plasma. This additional charged particle population constitutes, together with the ion and electron components, a very interesting 'dusty plasma' disk near the equatorial plane.

The third component of this region is constituted by the trapped energetic particles observed by Pioneer 11 (Simpson *et al.*, 1980) and Voyager (Krimigis *et al.*, 1983). Their strong interaction with the satellites and rings is very clearly evidenced by strong absorption features at the main satellite locations in their radial flux profile, and by a sharp inner edge right on the outer edge of the A-ring. This indicates they are absorbed by satellite surfaces and solid particles, a process in which they interact with these solid surfaces, producing energetic neutral atoms (ENA's) via sputtering, charging, and probably inducing some surface erosion and modification (see Johnson, 1990, for a comprehensive analysis of the physical processes involved).

A diversity of mechanisms, which ultimately control the coupling between plasmas, dust and energetic particles, and in part the distribution of each of these components, are at work. We shall mention a few of the most important and interesting ones.

Plasma transport

As already mentioned, plasma transport along and across field lines plays a very important role in mixing the three plasma sources present, and therefore in defining the particular plasma regime as a function of radial distance and magnetic latitude.

Cross-field plasma transport, in this region which is essentially dominated by corotation, may exist if some modes for field line interchange motions are unstable. The resulting time scale for radial diffusion has been estimated to be very long, on the order of years, but some of these interchanges have been proposed to involve dust-plasma coupling, as will be seen later. It is this diffusion process which controls the degree of mixing between ring plasma and icy satellites plasmas near the outer edge of the rings system.

Field-aligned plasma transport has been studied with a high degree of sophistication in this region, because it controls the net exchange of ionized matter between the rings and Saturn's ionosphere. A first kinetic model of plasma transport along field lines was developed by Wilson and Waite (1989). This steady-state model included gravitational, magnetic mirror, centripetal and ambipolar electric forces, as well as two plasma sources at the two ends of each modeled field line. In the equatorial plane, a warm water ion plasma simulated the rings ionosphere, whereas at the ionospheric foot of the same field line a cool hydrogen ion plasma simulated Saturn's ionosphere. The model showed that the regime of plasma exchange was not the same throughout the rings system. Near the C ring, in the innermost part, the dominant ion was found to be H^+, whereas over the outer B ring and the A ring access of ionospheric plasma to the ring plane was inhibited by the ambipolar electric field, and water ions remained dominant. The model results also showed that significant fluxes of water-derived ions, of up to 5.10^7 cm^{-2} s^{-1}, could be established and maintained through the outer edge of the B ring, thus giving some support to the hypothesis that water ions from the rings play a role in ion recombination in Saturn's ionosphere (see section 3.1.4). A later study by Wilson (1991) made it possible to calculate the diurnal variations through a time-dependent model, and used the computed plasma densities to determine the charge state of dust particles in the rings system. As the plasma and charge state distribution are basically fixed with respect to the sun, the keplerian motion of dust particles through this fixed pattern must in principle generate magnetic field-aligned motions closing through the ionosphere, as initially proposed by Ip and Mendis (1983). Wilson's calculation showed that the effect of this current system on ExB plasma drifts was negligible. Finally, a plasma transport model using the alternative technique of 16-moment equations was developed by Demars (1995) who explored a large fraction of the parameter domain for stationary conditions.

Physics of dusty plasmas

The vicinity of the plane of the main rings, as well as the volume of space occupied by the more diffuse E ring, are regions of strong coupling between plasma, dust particles and energetic charged particles. Under the effect of bombardment by these particles, of UV irradiation and of interactions with the plasma, each particle carries a net equilibrium electric charge which may be positive or negative depending on the environmental conditions. As a result, the 'gas' of dust particles becomes electrostatically coupled to the ambient plasma and forms what is currently called a 'dusty plasma', a complex system which has received increased interest over the last decade. Saturn's magnetosphere and ring/dust system certainly offer one of the most interesting opportunities to study a natural dusty plasma in space.

Dust-associated current systems. This system has, for instance, the property of being a permanent current carrier. The drift motion of a charged dust particulate is a combination of keplerian motion in Saturn's gravity field and of gyration/drift in

its corotating magnetic field. Since keplerian motion remains dominant over most of the mass spectrum of dust particles, there is a permanent relative drift among the charged dust particles in Saturn's corotating frame. This drift is eastward inside the synchronous orbit, and westward outside of it, and therefore also carries a net azimuthal current whose direction depends on dust charge, size and location. As the ambient plasma parameters and charged particle fluxes vary with radial distance and local time, this azimuthal current may also vary in local time, leading to current divergence along magnetic field lines and its closure into the ionosphere, as initially proposed by Ip and Mendis (1983). Wilson (1991), however, showed that the resulting ExB drifts induced by this ionospheric current closure are negligible.

Dust-associated waves and instabilities. The presence of this 'dusty' azimuthal current is suspected to play a role in the development of a variety of instabilities and specific mechanisms. The most spectacular one is probably the generation of 'spokes', these sporadic radially-aligned albedo features which were observed by Voyager, as shown in Figure 22. A good concise summary of the observational characteristics of spokes can be found, for instance, in Tagger *et al.* (1991). As spokes appear dark in backscattered light, but bright in forward-scattered light, they must be formed by sub micron grains electrostatically levitated over the larger ring grains. They usually have a V shape, with the apex of the V at the synchronous orbit (in the B ring at a radius of $\sim 1100\,000$ km). In the initial stage of spoke formation, one edge of the V rotates at the keplerian frequency and the other one at the planetary rotation frequency. They appear most of the time at dawn on the disk and also seem to be created at a particular longitude, which corresponds to the preferential longitude for SKR generation.

Several theories for the generation of spokes have been elaborated, all founded on the specific properties of dusty plasmas. The model of Goertz and Morfill (1984) starts from the initial idea that spokes become visible when small micron-sized dust particles are elevated above the ring plane. According to the authors, this levitation is made possible locally by the injection of an additional source of dense trapped plasma in contact with the ring plane, which may be the neutral and ionized dense cloud generated by a meteor impact on the rings (Morfill and Goerz, 1982). Then the very local plasma density enhancement produces the elevation of dust above the ring plane necessary for spoke formation, but also carries a local enhancement of azimuthal electric current due to the differential drift of plasma and dust particles, as already explained. This current, which diverges on the eastward and westward edges of the plasma cloud, closes through the ionosphere via magnetic field-aligned currents and induces a radial ExB drift, which drags the initial plasma cloud away from the synchronous orbit for the case of a negative space charge of dust particles, and towards it for the opposite case. The radial spoke structure, in this theory, is then only the visible trace of the motion of the plasma cloud, which produces elevation of dust above the ring plane along its trajectory. This theory indeed explains several of the observed characteristics of spokes, in particular their

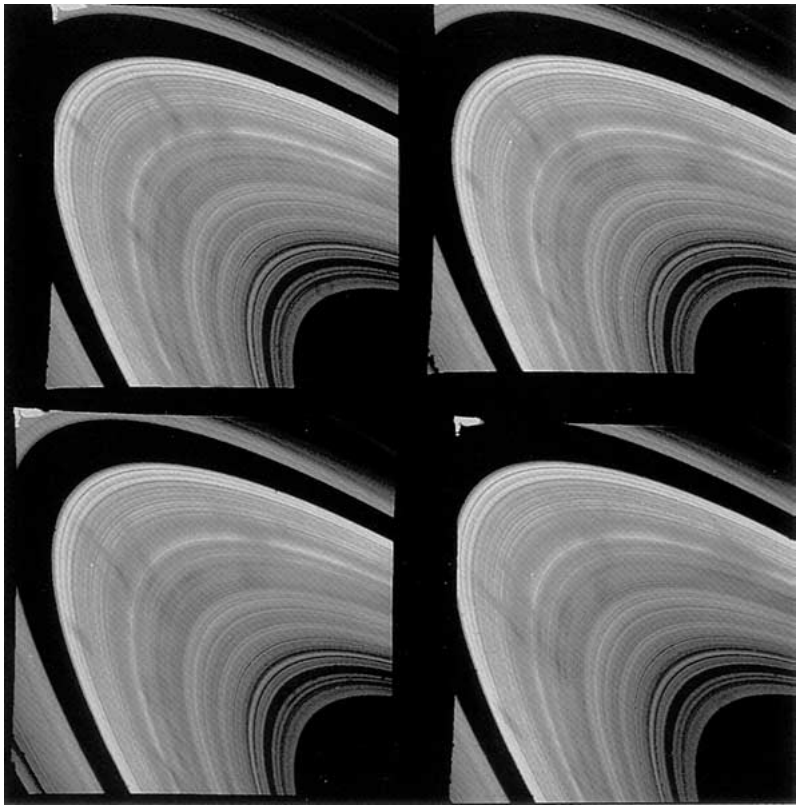

Figure 22. The spokes, a set of sporadic albedo features observed by the Voyager imaging system to be corotating with the planet, are one of the intriguing manifestations of dust-plasma-magnetic field coupling in the rings system.

preferential appearance north of the ring in the active sector, which is consistent with the idea that they must be formed on the side of the ring facing the magnetic equator for the enhanced plasma cloud to be stably trapped.

Tagger *et al.* (1991) developed a more elaborate theory, in which they relate them to the particular characteristics of magnetosonic waves in a weakly ionized disk in keplerian rotation, embedded in a vertical magnetic field. These waves have been proposed to be at the origin of radial and spiral density waves in magnetized accretion disks.

The question of the origin of spokes belongs to a more general class of phenomena involving dust-plasma coupling, which must play a diversity of roles in the system. For instance the instability mechanism invoked by Goertz and Morfill (1984) for the formation of spokes has also been proposed, with some adaptation, to be the source of radial plasma transport in Saturn's icy satellites torus (Morfill *et al.*, 1993).

Key problems and MAPS investigation strategy

Two important scientific questions emerge from the analysis of our present knowledge of the region of the magnetosphere directly connected to the rings:

(1) What is the net exchange of plasma, neutral species and dust particles between the rings, Saturn's ionosphere and its inner plasmasphere, and what effect does this exchange have on the maintenance of the ionosphere and the evolution of the rings?
(2) What are the mechanisms responsible for the formation of spokes on Saturn's main rings?

Magnetic field lines connected to the main rings will be explored by Cassini only during the Saturn Orbit Insertion (SOI) phase. As shown by Mauk *et al.* (1998) in their Figure 5, the spacecraft on its inbound and outbound legs will cross the ring plane near 2.5 R_S and then fly above the main rings at an altitude lower than 0.5 R_S. This sequence will therefore be a unique opportunity to study rings/plasmas/ionosphere coupling by means of an observational strategy combining in situ and remote sensing measurements.

In-situ measurements will use the standard MAPS instrument complement to provide the characteristics of plasmas, dust, energetic particles and possibly neutral gas at the ring plane crossings and above. As the spacecraft will fly through field lines directly connected to the rings and the ionosphere of Saturn, the angular resolution of the particle instruments (CAPS, MIMI) will make it possible to really characterize the flows of the different plasma species between these two reservoirs, as well as to measure the populations of trapped electrons and ions. This should provide an important contribution to the question of the exchange of ions between the rings and Saturn's ionosphere, and of the possible role of water-derived ions in ionospheric recombination.

Close distance remote sensing measurements will be of very special interest during SOI. While rings imaging by the different cameras on board will provide numerous constraints on the composition and size distribution of ring particles, ENA imaging by MIMI/INCA will provide a wealth of information concerning the dynamics of trapped energetic particles and their interaction with the rings (Mauk *et al.*, 1998): constraints on the radial transport rates of energetic particles, a better determination of energetic particles impact rates on the rings and their effect on sputtering and erosion, and of the importance of rings as a sink of these particles. Finally, the measured energy spectra of the ENA emissions will provide an additional type of constraint on the size distribution of ring particles.

3.2.2. *Interactions with the Icy Satellites*

Whereas Hyperion, Iapetus and Phoebe interact directly with the solar wind, the inner icy satellites of Saturn, Mimas, Enceladus, Tethys, Dione and Rhea are imbedded in the inner magnetosphere of Saturn. The interaction of the magnetosphere's fields and particles with these icy satellites, while being interesting by itself, can provide important information about their bulk and surface properties.

Present knowledge

The surfaces of these satellites are believed to be composed primarily of ice with a trace amount of O_3 being the only other identified species. Other suggested volatile constituents are CO_2 and NH_3 with dark components of the surface being possibly made of C and S chains. Models also suggest the presence of hydrated minerals like those found on the Jovian satellites (McCord *et al.*, 1999; Carlson *et al.*, 1999).

The effect of sputtering induced by energetic particle bombardment and bombardment by the ambient plasma permanently maintains tenuous atmospheres around these satellites. Because these atmospheres are expected to be optically thin they will not have ionospheres which are sufficient to prevent the flowing plasma from reaching the surface of the icy satellite. Satellite surfaces are also exposed to micrometeorite bombardment that produces a porous regolith as well as a vapor and the emission of particulates into Saturn's magnetosphere. The chemical composition of the gas and particulate phases of these tenuous icy satellite environments is evidently related to their surface composition, though not in a straightforward way. Models of the atmospheres can be constructed based on knowledge of the energetic particle population originally provided by Voyager, and will be enhanced by Cassini and by knowledge of the physics of sputtering for potential surface species.

Each satellite as a whole, with its interior, surface and atmosphere, interacts with the magnetosphere's plasmas and fields. The different mechanisms involved in this interaction are schematically shown in Figure 23. The sputtered atmosphere is represented as a blue cloud surrounding the icy satellite. The bombardment of the icy satellite by the hot plasma is shown by the red dots in the figure that also shows the formation of a plasma wake behind the icy satellite. Because the plasma is moving faster than the icy satellite the lower energy plasma ions and the hot electrons tend to preferentially bombard the trailing side of the satellite whereas the energetic heavy ions bombard more isotropically (Pospieszalska and Johnson, 1989). The energy spectrum of the sputtered particles is such that most of the sputtered molecules are on escape trajectories (Johnson, 1990). Therefore, as the ionization rate is low there also exists a toroidal neutral cloud co-orbiting with the satellite containing satellite surface species (see Johnson *et al.*, 1989) which will be discussed in the next section.

Partial conversion of this neutral cloud and atmosphere to ions proceeds through ion pickup. Fresh pickup ions can be distinguished from the ambient plasma by their characteristic cycloidal motion which has a distinct energy-angle dependence, as shown by yellow dashed lines in Figure 23. These fresh pickup ions, with their unique energy-angle signature, provide the most direct information about the atmosphere composition. Pioneer (Smith and Tsurutani, 1983) and Voyager (Barbosa, 1992) observations showed the presence of ion cyclotron waves in the vicinity of Dione's L shell and the frequency of the waves was consistent with the pickup ion being a heavy ion such as H_2O^+. These waves provide indirect evidence for the formation of pickup ions in the vicinity of Dione. The presence of ion cyclotron

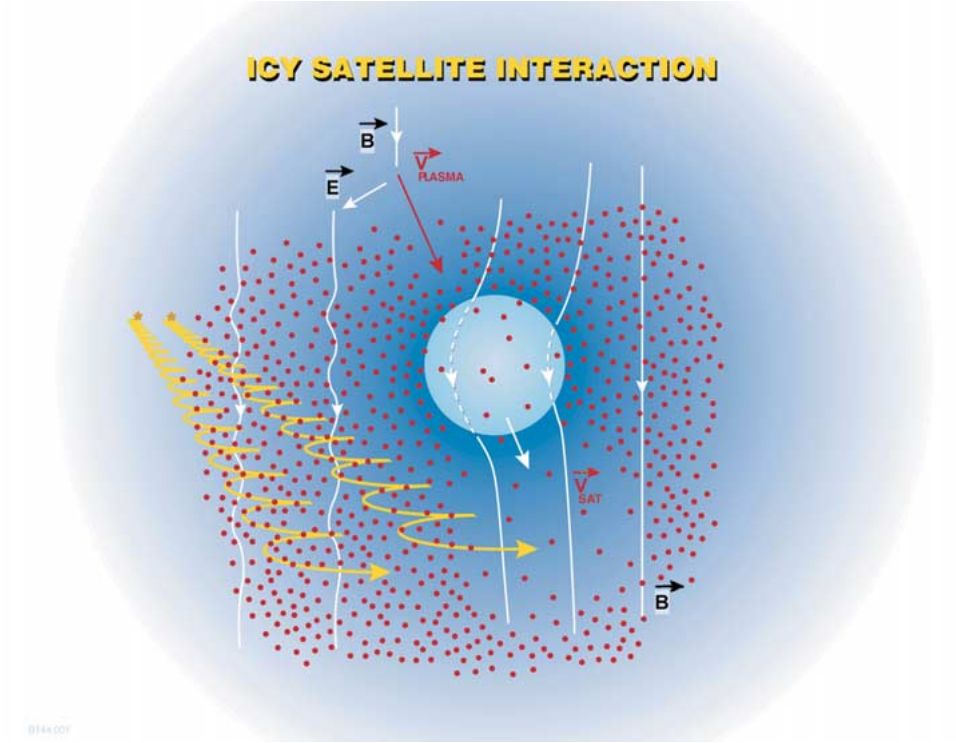

Figure 23. Sketch of the interaction between one of the inner icy satellites and Saturn's magnetosphere. The icy satellite is surrounded by a sputtered atmosphere of a dominantly H_2O composition and indicated by a blue shading. The hot plasma which is bombarding the icy satellite and contributing to the sputtered atmosphere is indicated by red dots; the formation of a plasma wake is shown on the front side of the icy satellite. The pickup ions are indicated by the yellow trajectories which are moving at right angles to the magnetic field in a cycloidal motion. The wiggles in the magnetic field lines indicate the presence of ion cyclotron waves. We also show a hanging up of magnetic field lines in the body of the icy satellite indicating a conductive core. The velocity vector of the satellite $\vec{v}_{SAT}$ and plasma $\vec{v}_{PLASMA}$ are indicated as are the magnetic field vector $\vec{B}$ and corotation electric field $\vec{E}$.

waves in the vicinity of the pickup region is schematically shown by the wiggles in the magnetic field lines in Figure 23. The pickup process should also generate an ion beam instability (Ma *et al.*, 1987) in the plasma, producing a broad spectrum of electrostatic waves which can be measured by Cassini.

If the satellite has a conductive interior then there may be a magnetic signature that could be measured by Cassini. This effect is schematically shown in Figure 23 by magnetic field lines getting hung up in the body of the satellite, complicating the interaction. Although we think this unlikely due to the small size of these satellites Cassini would be able to measure an internal field, if present and for close enough fly-bys, from which we could infer the presence of a dynamo operating in the core of the satellite. Since fast ions appear to dominate the sputtering process (Jurac

et al., 2001a), the field topology within the vicinity of the satellite is not expected to have a strong influence on the generation of the sputtered atmosphere.

Key problems and MAPS investigation strategy

Cassini fly-bys of the icy satellites will offer a unique opportunity to address two major scientific objectives of the mission:

(1) Can we contribute to determining the surface composition of the icy satellites during close Cassini fly-bys from CAPS and MIMI data?
(2) What are the modes of interaction between Saturn's magnetospheric plasma flow and the icy satellites, and how do they depend on the net contribution to ion pick-up, the internal structure and conductivity, and possibly the state of magnetization of these satellites?

CAPS measurements of fresh pick-up ions produced by the tenuous sputtered atmospheres will be the main contribution of MAPS to the investigation of the surface geology of icy satellites. As indicated before, the specific energy-angle dependence of their fluxes should make it possible to distinguish them from the background magnetospheric plasma (Johnson and Sittler, 1990). Determinations of isotope ratios from the mass spectra and from the molecular composition measurements will also be critical inputs for estimating surface age. Therefore, the CAPS instrument will complement the surface geology data provided by VIMS. The RPWS Langmuir Probe will also contribute to the measurement of electron density and temperature near the icy satellites.

The characterization of surface-magnetosphere interactions will involve the whole suite of MAPS instruments. The CAPS instrument will measure the ambient plasma characteristics and its interaction with the satellite, in addition to the pick-up ions. This data set will provide information about the ionization processes for pickup ions such as charge exchange and electron impact ionization. The MIMI instrument will be able to measure the very energetic ions which are believed to provide a dominant contribution to the generation of the sputtered atmospheres of the satellites; their data should also show evidence of a wake forming behind the satellite indicating the net ion bombardment of its surface. MAG will be able to measure the presence of ion cyclotron waves in the pickup region. If the satellites are conductive, it will measure the perturbations in the magnetic field produced by the systems of d.c. currents and/or MHD waves – including possible Alfven wings – generated by their interaction with the magnetospheric plasma flow. It could also potentially measure the presence of an internal magnetic field if present. The RPWS instrument will measure whistler-mode emissions, electrostatic solitary structures, ion cyclotron waves, electrostatic electron cyclotron harmonic emissions, and upper hybrid waves created via the interaction of the icy satellites with the Saturnian magnetosphere, similar to effects observed near the Galilean satellites at Jupiter. All these measurements critically depend on the fly-by geometry, which will have to be studied very carefully to meet the MAPS objectives.

3.2.3. *Interactions with the Neutral Gas and the E Ring in the Inner Plasma Torus*

As described in Section 3.1, the inner plasma torus extends out to about 8 R_S, and is continued through the extended plasma sheet out to L = ∼13 R_S . This region contains all the important plasma and neutral sources except Titan: the rings, the planet, and the inner icy satellites, whose magnetospheric interactions have just been described. It is characterized by a strong chemical and dynamical coupling between the plasma, the neutral gas and E-ring particles. Since the neutral gas, based on recent observational constraints, dominates the plasma in terms of local density, this is a very interesting and unique environment in which the variety of chemical and dynamical mechanisms involved in dust/gas/plasma coupling can be studied in depth at Saturn by a combination of *in situ* and remote sensing measurements.

Present knowledge: distribution of neutral gas and E-ring particles

Saturn's magnetosphere is now known to be dominated by neutral gas throughout the region inward from 30 R_S. The presence of atomic hydrogen in significant amounts was predicted by McDonough and Brice (1973), who argued that a large atmosphere on Titan would produce a torus of H at 20 R_S. Atomic hydrogen was subsequently observed in a rocket experiment (Weiser *et al.*, 1977), although no definition could be established on its distribution. The magnetosphere also contains large quantities of OH (Shemansky *et al.*, 1993), in addition to atomic hydrogen, and by inference atomic oxygen in comparable amounts to OH. This neutral gas torus entirely covers the region of space covered by the diffuse E ring. Let us review the observational evidence.

Atomic hydrogen. The present determination of its distribution is derived from Voyager 1 post encounter observations of H Ly-α (Shemansky and Hall, 1992). The distribution is asymmetric in local time with most of the gas concentrated inside 15 R_S in the dusk region and with concentrations up to ≈ 150 cm^{-3}. The latitudinal distribution is roughly ± 8 R_S, and extends from Saturn's atmosphere to ≈ 30 R_S. The source of the atomic hydrogen is not definitively determined. A component must be provided by Titan, but according to Shemansky and Hall (1992), most of the H atoms are on ballistic trajectories exiting Saturn's atmosphere. Based on the recent observations of OH, discussed below, H from the water products in the inner magnetosphere may also be important.

H_2O products. The observed OH is assumed to be the product of H_2O chemistry. The source may be complex with a number of components; sputtering from satellite and E ring grain surfaces by hot ions (Johnson *et al.*, 1989), E-ring particle impacts (Hamilton and Burns, 1994), as well as meteoroid bombardment (Ip, 1983) and reactions at the rings (Ip, 1984a,b, 1995). The HST observations obtained in 1992 and 1994 with the Faint Object Spectrograph provide a large number of measure-

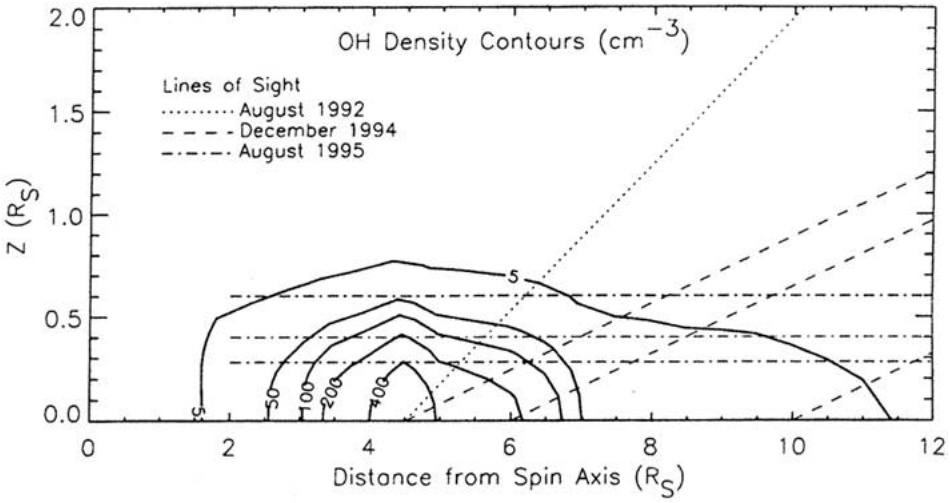

Figure 24. Iso-density contours of the OH cloud derived by Richardson *et al.* (1998) from Hubble Space Telescope Faint Object Spectrograph measurements under the assumption of axial symmetry about Saturn's rotation axis.

ments from which an assumed azimuthally symmetric cloud has been constructed (Figure 24). The trend in the distribution suggests that the abundance peaks at ~ 4.5 R_S. From the data at 1.8 R_S one can infer that there is no detectable OH above the rings because all of the observed line-of-sight abundance at 1.8 R_S can be accounted for by the gas in the region > 3 R_S. Atomic oxygen, which is much more difficult to detect, has not been observed, but it is calculated (Richardson, 1998) to be comparable in density to OH. The densities rapidly decrease inside of ~ 3 R_S and the inferred scale height of the cloud is comparable to the plasma scale height.

IUE observations by Festou and Shemansky (2000) provide a rough measure of latitudinal distribution. The Saturn system was spatially explored using the IUE long wavelength spectrograph (large slit) on 31 Oct–2 Nov. 1995. OH was positively detected along the equator between ~ 2.5 R_S and ~ 5.5 R_S. In the equatorial plane, the mean brightness (10 by 20 arcsec slit) decreases from ≈ 130 R to ≈ 60 R. There is some indication that OH emission could be weakly present at a point located ≈ 1 R_S from the ring plane and 2.5 R_S from the planet center. This is consistent with a scale height of order 0.5 to 1 R_S of the OH emission at ≈ 2.5 R_S in the equatorial plane.

E-ring Grains. The neutral gas in the inner magnetosphere is coupled not only to the plasma, but also to the population of solid particles which exist as charged grains in the E-ring and, in part, the G-ring. In fact the extent of the E-ring is determined by its interaction with the plasma, the Lorentz forces (e.g., Horanyi *et al.*, 1992), and the lifetime of the grains which is determined by sputtering by the

trapped plasma. A recent analysis (Jurac *et al.* 2001b) indicates that in the region 3–6 R_S the E-ring is the dominant source of neutrals, but only if there are many more grains than seen optically. That is, there is apparently much more surface area than observed to be tied up in small sub micron grains. Such grains are readily transported in the magnetosphere and rapidly eroded by sputtering, hence, need to be replenished rapidly. In fact it is likely that there is a continuous spectrum of neutral sizes from atoms to molecules to molecular clusters and small grains. Since the grains are known to be charged there may also be charged clusters surviving in the vicinity of Enceladus and Mimas (Johnson *et al.* 1989). This is an interesting region having very low electron temperatures and low relative collision velocities between the co-rotating plasma and the neutrals.

Contributions from modeling

Saturn's neutral gas torus results from a complex balance between source processes, chemical and photochemical reactions between neutral species and loss of these species. The main source mechanisms for neutrals, in addition to the outgassing of Titan's atmosphere, are the collisions of energetic particles, corotating plasma, and micrometeorites with the ring particles and satellites, which sputter H_2O from the surfaces, as partly described in the previous section. The ion sputtering yields depend on the flux, energy, and mass of incoming particles (Johnson, 1990). Another mechanism suggested as a source of additional neutrals is collisions of E-ring particles with each other and with satellites embedded in the ring (which extends from 3–8 R_S) (Hamilton and Burns, 1994), but the magnitude of this source is not well determined. The neutrals orbit Saturn until lost via either ionization, dissociation, or collision with a ring particle or satellite. Plasma is formed when the neutrals orbiting Saturn are ionized by UV radiation, electron impact, or charge exchange. The plasma densities again result from a balance between the formation rates and loss rates due to recombination, charge exchange, collisions with satellites and ring particles, and transport processes.

Since the observational base is limited, models of the spatial distribution of density and composition of neutral and ion species have been developed. Monte Carlo schemes have been used to calculate the neutral distributions, which depend on the ejection energy from the sputtered surface and the lifetime of the neutrals (i.e., Johnson *et al.*, 1989; Pospieszalska and Johnson, 1991; Ip, 1995; Jurac *et al.*, 2001a). These studies show the neutrals and plasma are tightly confined to Saturn's equator. Models of plasma transport and chemistry have been used to determine ion composition and transport rates (Barbosa, 1990; Shemansky and Hall, 1992; Richardson *et al.*, 1986; Richardson, 1995, 1998). Figure 25 shows a chart of the ion and neutral processes; we show only the most important reaction paths for simplicity. Where multiple paths are important, we show a very rough magnetosphere-averaged percentage for each path. The actual percentage varies with position in the magnetosphere. These reactions, transport, and the distribution of ions and neutrals in latitude are a necessary component for an accurate model of

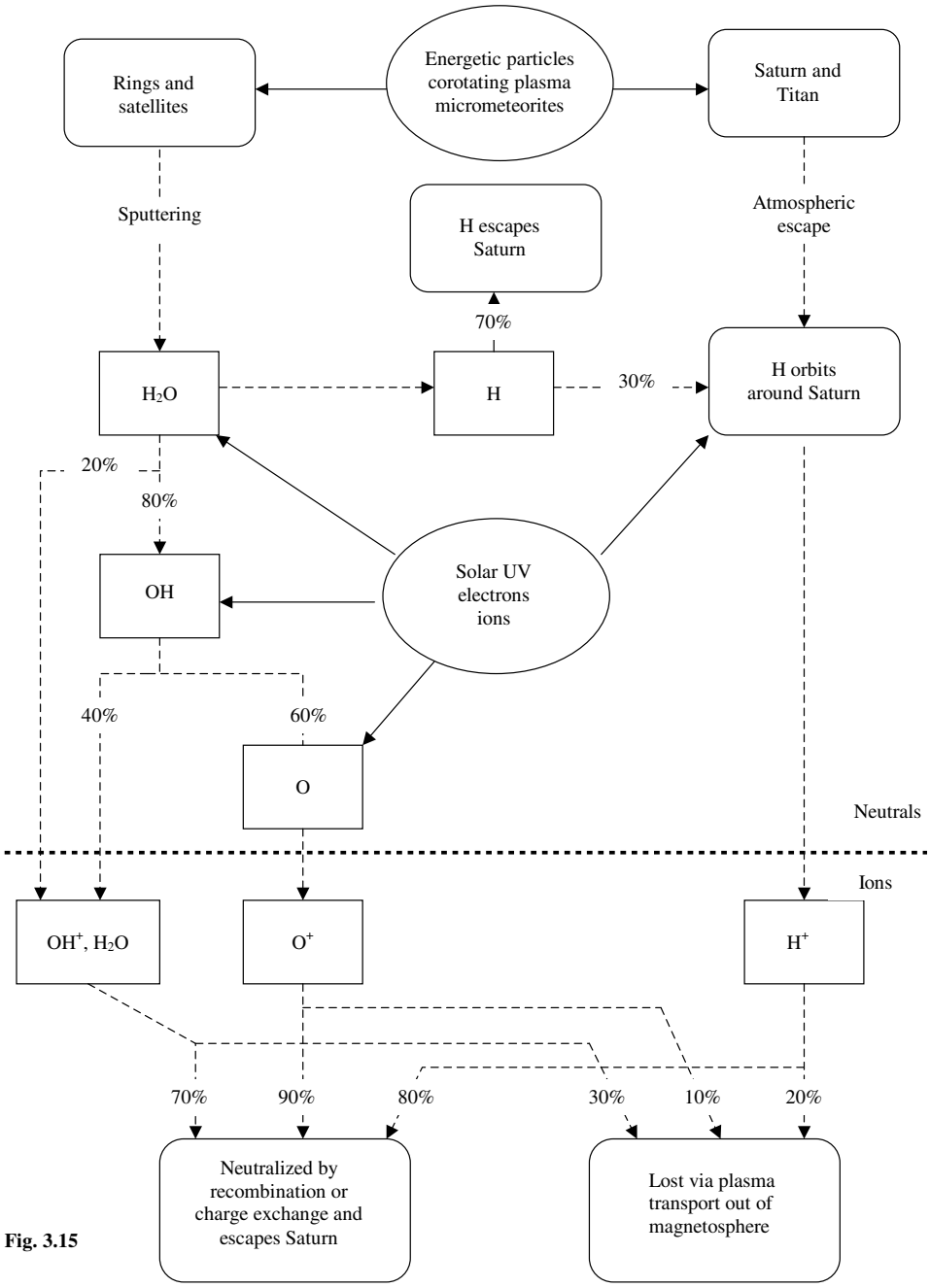

Fig. 3.15

Figure 25. Schematic representation of the main chemical paths contributing to the balance of the inner torus. The irradiation agents acting on the different objects of the Saturn system are shown in light blue boxes. The sources and sinks are shown in yellow boxes. The approximate, spatially averaged, branching ratios of the different reactions are shown along the chemical paths.

the inner magnetosphere. A recent model which includes both neutrals and plasma was able to match both the plasma and neutral observations fairly well (Richardson *et al.*, 1998). To fit both the neutral and plasma data, the total sputtered source of H_2O required from the rings and satellites is 1.4×10^{27} s^{-1}, with the source strongly peaked near 4.5 R_S, and the transport time is about 5 days at $L = 6$. Figure 26 shows the densities of the major ion and neutral species predicted by this model. The total neutral density is near 1000 cm^{-3} near 4.5 R_S. OH is the densest neutral component inside 7 R_S, outside 7 R_S H and O are most important. The ion densities increase inward with peak densities near 200 cm^{-3}, with O^+ the dominant ion followed by H^+.

Several problems remain, however, before full consistency between the presently available data and model estimates can be achieved:

(1) The neutral source required by the model is at least a factor of 4 greater than published sputtering estimates (Shi *et al.*, 1995) and more than an order of magnitude larger than obtained from a recent reanalysis of the plasma LECP data (Jurac *et al.*, 2001b). This led Jurac *et al.* (2001a) to suggest that very small ring grains in the E ring could provide a sufficient source of neutrals. More recently, using a new set of HST observations of the OH cloud, Jurac et al. (2002) showed that a vast majority of the H_2O molecules originates from Enceladus' orbit, and attributed this to the presence of an unknown population of colliding small bodies.

(2) Although the model fits the heavy ion observations very well, it predicts more protons than observed by a factor of 2–3 between 5 and 8 R_S.

(3) The model sets the ion and electron temperatures equal to those observed by Voyager. Recent work to model the temperatures shows that an electron energy source is needed to maintain the observed electron temperature and that slower transport, by about an order of magnitude, is needed to fit the observed ion temperature profile (Richardson, 1999). Part of the problem may come from the fact that the neutral model used is too simplistic and needs to be replaced with a Monte Carlo model which includes ion-neutral and neutral-neutral collisions and more accurately calculates the neutral distribution.

Key problems and MAPS investigation strategy

In view of the present very limited understanding of the magnetospheric interaction with neutral gas tori, two key questions will have to be addressed during the Cassini mission:

(1) Can we quantitatively understand the observed distribution of neutral and ion species in the inner torus from the balance of plasma generation, loss and radial transport?

(2) Does it provide constraints on poorly known quantities, such as satellite surfaces compositions, the sputtering rates from the icy satellites surfaces and from the E ring, and the key reaction rates along the chemical and photochemical paths?

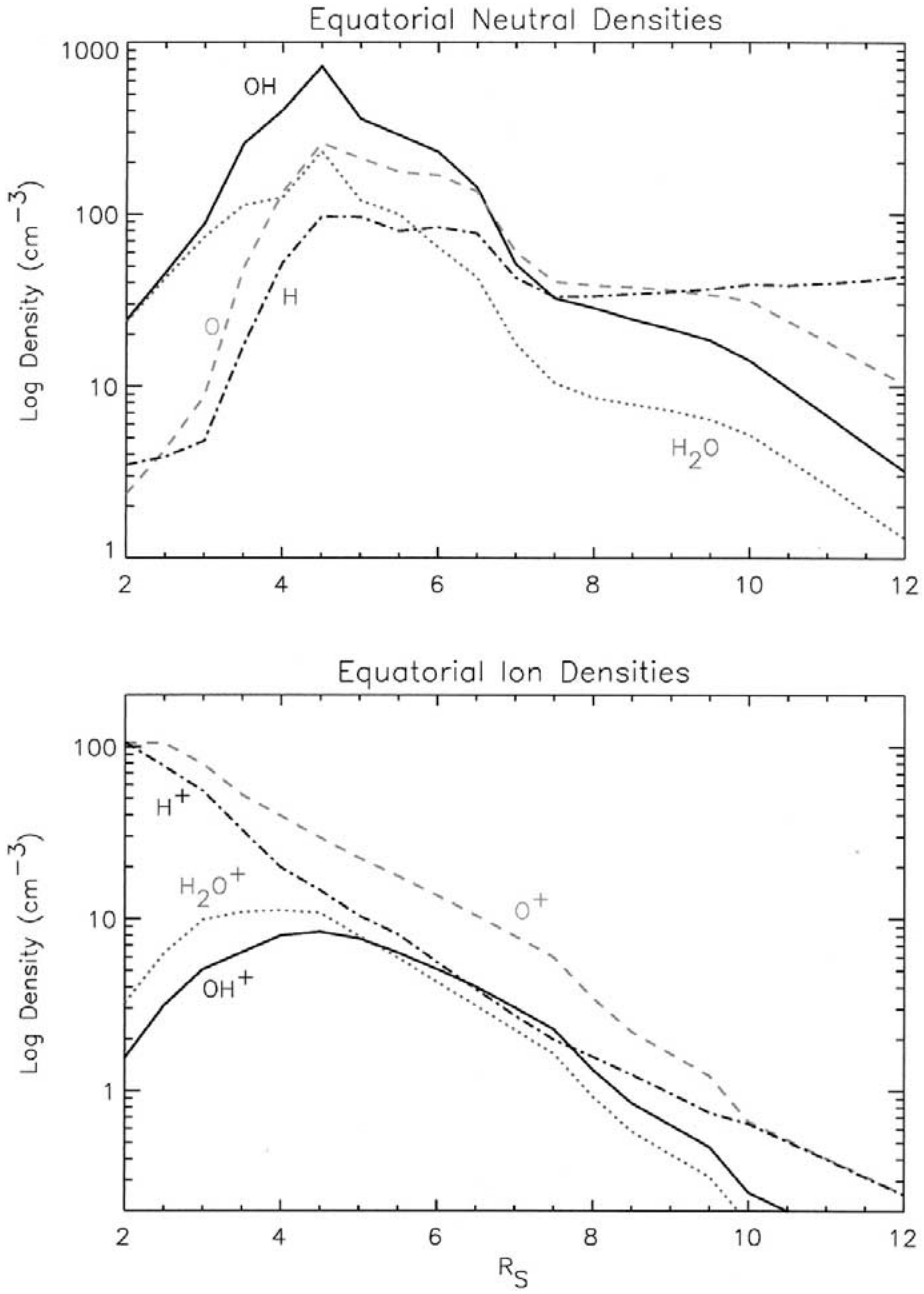

Figure 26. Radial distribution of the equilibrium neutral and ion densities calculated in the model of Richardson *et al.* (1998), using a chemical scheme similar to the one shown in Figure 25.

An efficient plan to solve these questions should include three ingredients: critical laboratory measurements, the development of an improved physical model of the dynamical and chemical coupling between solid phases (satellite surfaces and ring particles), neutral gas tori and charged particle populations, and well-planned Cassini observations:

- a program of additional measurements of key parameters (sputtering and photochemical rates, reaction coefficients, etc.) should aim at reducing remaining uncertainties;
- an improved model describing the inner torus chemistry, transport and energetics, should be progressively developed, with the capability of assimilating new data throughout the Cassini mission lifetime.
- Cassini observations should monitor neutral and ionized species, E-ring characteristics, airglow emissions, observationally-derived sputtering rates of the icy satellites, and the time dependence of all these features over the lifetime of the Cassini mission to better understand their interdependence.

UVIS does not have the appropriate channel to detect the strong OH emission band at 308 nm, but it is expected to map the distribution of the inferred large abundance of atomic oxygen. Solar flux driven fluorescence in OH does have an infrared and radio spectrum, but an investigation is needed to determine if it is possible for CIRS and/or VIMS to measure the spectrum. Combined measurements by CAPS, CDA, INMS, MAG, MIMI, and RPWS will map the distributions of neutral, charged and dust particles.

3.2.4. *Coupling of the Outer Magnetosphere to Saturn's Upper Atmosphere and Ionosphere, and Related Auroral Processes*

The regions of the upper atmosphere and ionosphere of Saturn located poleward of approximately 70° latitude, which correspond to the auroral zones and polar caps, are characterized by a strong coupling with the magnetosphere. Magnetic field lines emerging from these regions connect them directly to the outer magnetosphere, which includes the magnetotail on the nightside, and to its boundaries with the solar wind. The upper atmosphere and magnetosphere continuously exchange significant amounts of charged particles, net electric currents, angular momentum and energy along these field lines. Magnetospheric energetic particles accelerated or scattered along them precipitate into the upper atmosphere, where they generate electromagnetic 'auroral' emissions in several wavelength ranges, mostly radio (through plasma mechanisms) before their arrival into the atmosphere, and UV (through collisional and thermal excitation of neutrals) after interaction with it. Conversely, a fraction of ionospheric ions and electrons is extracted from the ionosphere by thermal and non-thermal mechanisms and constitutes one of the many sources of magnetospheric plasma. Energy deposited into the upper atmosphere via auroral particle precipitation and the joule heating of magnetospheric currents closing through the ionosphere are an important element of the energy balance of Saturn's upper atmosphere. This local energy deposition may have important

effects on the chemical composition of the upper atmosphere, and may also be partly redistributed toward adjacent latitude regions via the induced thermal neutral winds. Just like at Earth or Jupiter, auroral regions are the most important region of mass, momentum and energy coupling between the solar wind, the magnetosphere and the planet's upper atmosphere and ionosphere. Understanding their dynamical behavior is therefore critical to a quantitative description of Saturn's space environment.

Auroral emissions

Since auroral emissions are our main, though very indirect, source of information about Saturn's auroral upper atmosphere, it is a key objective to establish their morphology, identify their generation mechanisms, and understand how they are controlled by the solar wind and/or internal magnetospheric drivers.

Morphology of UV emissions. Saturn's UV auroral structures have been observed only by the Voyager 1 & 2 ultraviolet spectrometer (UVS) experiments in 1980–1981, plus a few times by IUE between 1981–1985 (in the range 115–390 nm) and by HST (FOC & WFPC2) since 1994. Voyager findings are reviewed in the Saturn book chapter by Atreya *et al.* (1984). Being slit spectrometers, Voyager/UVS and IUE did not have imaging capabilities (except through scanning). As a consequence, they could not provide an accurate mapping of the UV auroral structures, but only approximate and indirect morphological information, such as the dependence of the intensity of precipitations upon magnetic longitude (or SLS), and an estimate of the low-latitude limit of the northern and southern auroral zones. The geometry of the northern aurora was deduced from modeling of these UV observations, as two ovals at about 80° N & S latitude. HST provided a few high-resolution (∼0.1") images of auroral UV 'hot spots', on the morningside of the planet (Gérard *et al.*, 1995; Trauger *et al.*, 1998) (see Figure 27). The spectrum of UV aurora allows, in principle, a diagnostic of the nature and energy of precipitating particles. The energy of precipitating electrons is estimated to be in the 1–10 keV energy range, lower than in the case of Jupiter. An average auroral electron energy influx of 2 10^{11} W between 78° and 81.5° in each hemisphere is required to account for the UVS measurements in the Lyman and Werner H_2 bands.

Taken together, all UV observations of Saturn's aurora suggest that (i) they are weaker than at Jupiter (∼1 order of magnitude), (ii) they are subject to high short-term variability (maybe a substorm-like activity?), and possibly (iii) there may be a gradual decrease of their activity over the 80's and 90's (seasonal effects), but the sparsity of observations does not allow a definitive conclusion.

Morphology of Auroral Radio emissions. Saturn's kilometric radio emission (SKR) has been observed quasi-continuously for 6 months with Voyager 1 and 2's Planetary Radio Astronomy experiment (PRA), measuring the flux and circular polarization of incoming waves (I and V Stokes parameters) in the range 1.2–

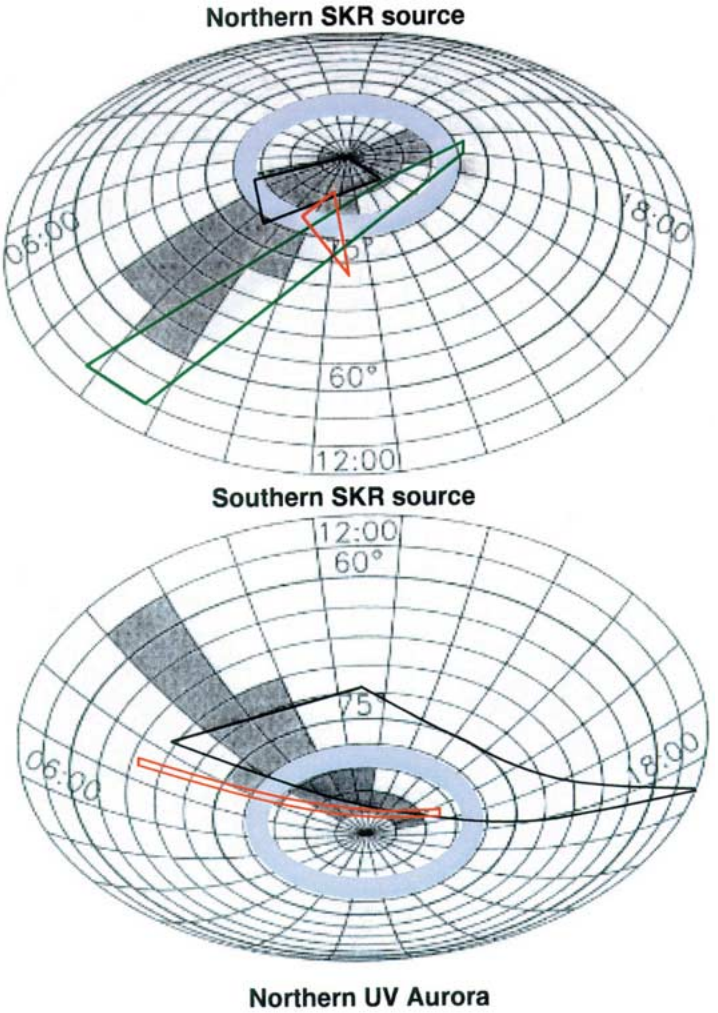

Figure 27. (a) Revised SKR source locations (Galopeau *et al.*, 1995), projected onto Saturn cloud tops (dark gray-shaded). They include high latitude regions (>80°) about noon LT and extend toward lower latitudes on the morning sector (down to 60°), and possibly in the evening sector. Northern and southern sources appear magnetically conjugate. Earlier SKR source determinations are indicated (in red & green/gray lines = (Kaiser *et al.*, 1981; Kaiser and Desch, 1982); in black lines [Lecacheux and Genova, 1983]), as well as 'Voyager' UV auroral ovals (in light blue/gray shading). (b) Hubble Space Telescope UV observations of the northern auroras confirm these results, revealing bright spots in the morning-to-noon sector (Trauger *et al.*, 1998).

1326 kHz. This constitutes our main source of information on the physical characteristics of SKR, as summarized in the Saturn book chapter by Kaiser *et al.* (1984), and in (Zarka, 1998; and references therein). Complementary information at low-frequencies ($\sim$56 kHz) was obtained by the plasma wave experiment (PWS) on-board Voyager (cf. Scarf *et al.*, 1984). SKR is also detected on a regular basis, although with very low intensity, in the data from the unified radio and plasma wave experiment (URAP) on board Ulysses, allowing for the study of its long-term variations.

SKR is very intense, reaching a flux density of 10^{-19} Wm^{-2} Hz^{-1} from 1 AU range (1–2.10^{-20} Wm^{-2} Hz^{-1} on the average – cf. Figure 28), which corresponds to a brightness temperature from over 10^{15} to 10^{19} K. It is thus of nonthermal origin. Its average spectrum covers a frequency range from $\sim$3 kHz to $>$1200 kHz, consistent with cyclotron emission from the vicinity of Saturn's poles where $|B| \sim$ 0.4 G. The spectral peak is localized between 100 and 400 kHz (depending on the LT of the observer), and the observed spectra present a slow decrease towards lower frequencies (<100 kHz) and a steep one at higher frequencies (>600–1000 kHz). The total radio power emitted on the average is $\sim 10^9$ W, while the instantaneous value can be more than 1 order of magnitude above the average one.

SKR has been found to originate from the northern and southern auroral regions of Saturn's magnetosphere. Higher frequencies and intensities are produced from the northern hemisphere, probably related to a magnetic field anomaly (discussed below). The observed SKR polarization is consistent with pure 100% circular polarization from each hemisphere (Right-Hand from the North and Left-Hand from the South), and thus corresponds to X mode emission. Stereoscopic studies using simultaneous observations by Voyager 1 and 2 (separated by $\sim$140°) showed that the SKR beaming is instantaneously narrow (at timescales <1 min.) and at large angle from the magnetic field in its source regions, but that the beam flickers in time and illuminates on the average a much broader beam $\sim 2\pi$ sr. More recent reanalysis of SKR polarization variations allowed a better description of the instantaneous beaming as a hollow cone with 60°–90° half-apex angle (the emission being beamed along the cone walls).

The high intensity of SKR requires a nonthermal, coherent generation process. The many similarities of SKR with the Auroral Kilometric Radiation of the Earth suggests that the same mechanism is operating in both cases (as well as in the other magnetized planets' auroral regions). The best candidate generation process is the cyclotron-Maser instability (CMI) through which the free energy of unstable keV electron populations is directly converted into radio waves, with an efficiency of up to 0.1–1%. In strongly magnetized plasmas ($f_{pe}/f_{ce} \ll 1$) the emission is mainly produced on the X mode near the local f_{ce}, and beamed at large angle relative to the source magnetic field. The condition $f_{pe}/f_{ce} \ll 1$ is fulfilled at Jovian high latitudes due to the high magnetic field intensity there (several Gauss). At Earth, it is fulfilled only in the so-called 'auroral plasma cavities', where the Viking spacecraft revealed filamentary, underdense regions spread along magnetic field lines, the origin of

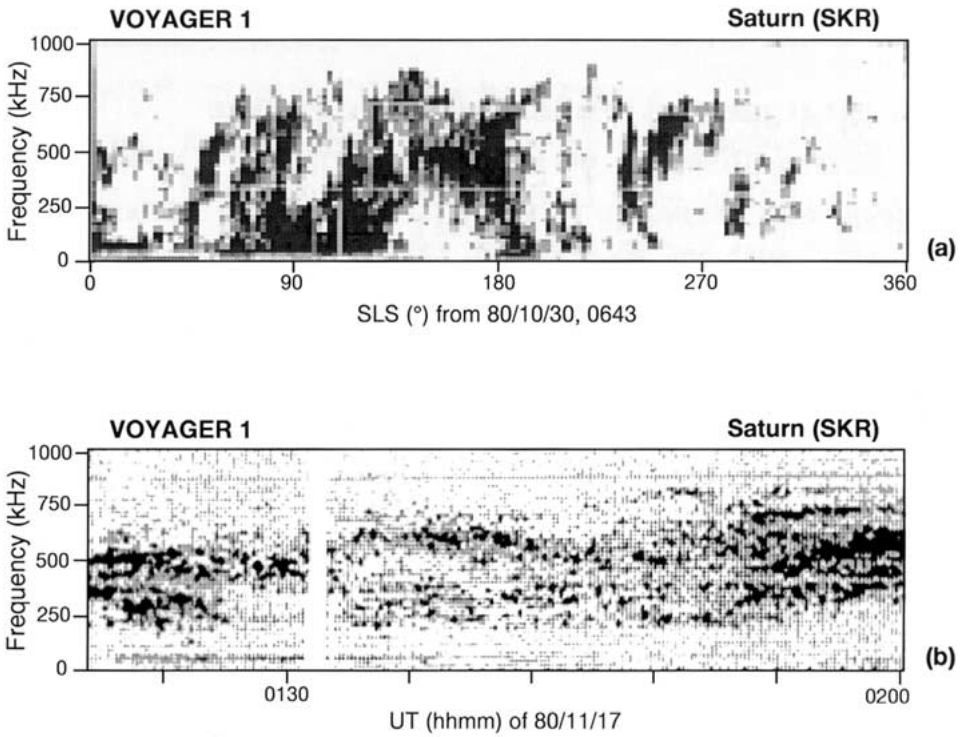

Figure 28. SKR dynamic spectra in Voyager/PRA LF range (1.2–1326 kHz). (a) One Saturnian rotation is displayed, with the abscissas labeled in longitude (SLS – increasing westward, with a rotation period of 10 h 39.4 min). Increasing darkness indicates increasing intensity. Data were recorded from close range (a few to a few tens of planetary radii). (b) SKR fine sporadic structures at Voyager/PRA best time resolution (30 ms). It consists here exclusively of spikes shorter than 6 s and narrower than 20 kHz.

which is still unclear. At Saturn, the rapid rotation confines the magnetospheric plasma in a low-latitude disk so that the condition $f_{pe}/f_{ce} \ll 1$ is fulfilled at high latitudes above the ionosphere even in the absence of any auroral cavity.

Variability and external control of auroral emissions

The SKR dynamic spectra (frequency-time images) are modulated by the planetary rotation. SKR sources appear to be fixed in LT and turned 'On' and 'Off' (or at least strongly modulated) along with the rotation of the planet. Maximum emission occurs when a so-called 'active' sector at longitude (SLS) ∼100°–130°, of yet unknown nature, passes about noon LT. Monitoring of the SKR occurrence, performed over a few years with Ulysses/URAP whose high sensitivity permits Saturn to be detected from several AU distance, revealed apparent fluctuations of Saturn's rotation rate at the 1% level (Lecacheux *et al.*, 1997) which are certainly linked to long-term variations of the SKR source locations. SKR power was found to be tightly correlated with the solar wind fluctuations, and especially with its

ram pressure, as clearly demonstrated by the extinction of SKR during Saturn immersions in the distant Jovian magnetotail. No temporal variations were unambiguously found at intermediate timescales (tens to hundreds of hours), which correspond to Saturn 'substorms', if they exist, neither was there any clear indication of a control of SKR occurrence or intensity by a satellite (e.g., Titan, Dione). At shorter timescales, smooth SKR, modulated in arc-shaped structures and narrow frequency bands (Figure 28a), is sometimes replaced by sporadic, instantaneously narrowband emissions at timescales as short as 1 second or less (Figure 28b). These fine structures are less prominent than in the terrestrial and Jovian cases, and have never been systematically studied.

The fact that both auroral UV and radio sources are fixed in LT and the tight solar wind control of SKR power strongly suggest that the main driver of auroral activity is the solar wind. The location of the most active auroral sources on the dayside of the planet suggests that the solar wind/magnetosphere interaction occurs primarily at the dayside magnetopause. For this reason Galopeau *et al.* (1995) suggested that electron acceleration may result from the parallel electric fields of surface waves generated through a Kelvin-Helmholtz instability at the dayside magnetopause, excited by the velocity shear of the solar wind flow. Signatures of these waves have been observed by Lepping *et al.* (1981).

Estimated characteristics of precipitating particles

Significant constraints on the energy of auroral particles can be deduced from model studies of auroral emissions. A theoretical model of the SKR spectrum (Galopeau *et al.*, 1989), in which a simplified description of the SKR source region was introduced, was very successful in reproducing the details of observed SKR spectra (averaged over $\sim$1 hour) within the observed ranges of the plasma disk and ionosphere scale heights, and for a perpendicular energy of auroral electrons $E_\perp$ $\sim$1–5 keV (Zarka, 1992) (Figure 29). Model calculations of the auroral UV spectrum are consistent with this determination. They indicate that the energy of electrons responsible for the observed auroral H_2 Lyman and Werner band emissions is between 1 and 10 keV, and that the Saturnian auroral UV spectrum can be reproduced through direct products of the $\bar{e} + H_2$ process only.

Locations of auroral emission sources

Early studies based on SKR occurrence, occultations, and intensity variations, have shown that SKR sources are fixed in LT, close to noon, and located at high latitudes, in the vicinity of the polar cusps of the planet (at the limit between closed and open field lines). This latitude range, about 75°–80°, was approximately correlated with that of Voyager/UVS-based determinations of the UV auroral ovals. A reanalysis of SKR polarization variations along Voyager 1 and 2 trajectories allowed determination of the SKR source location more accurately, or a more exact definition of the maximum projections of SKR sources on the planetary surface. The northern and southern sources were both found at very high latitudes ($\sim$80°, i.e. higher

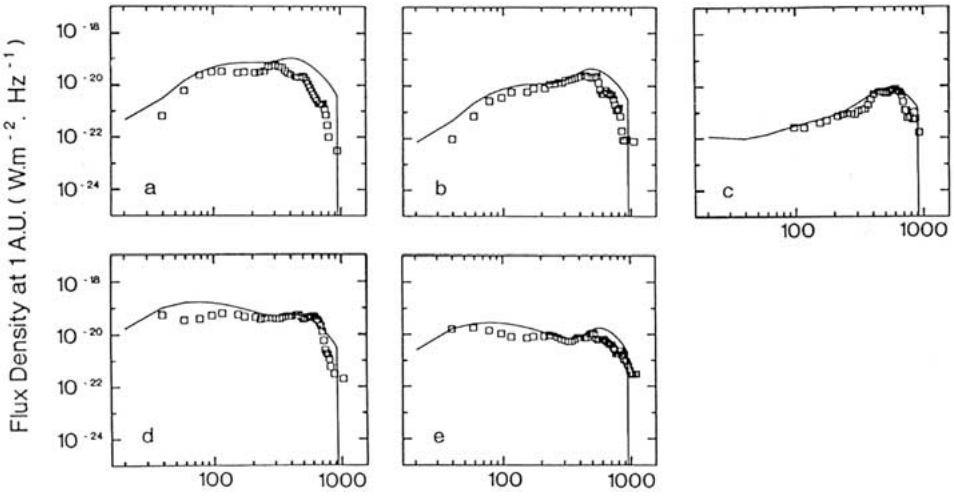

Figure 29. Observed and modeled SKR spectra. Best fit of computed cold, inhomogeneous, and saturated SKR spectra (continuous lines) are compared to spectra observed by Voyager 1/PRA 2–7 days after closest approach to Saturn (squares). Polarization is RH circular (northern X mode source). These fits are obtained by varying the magnetospheric disk and the ionospheric plasma scale heights, and the electron perpendicular energy, within limits severely constrained by Voyager observations. They permitted to precisely match the corresponding values of these parameters ($H_{disk} \sim 0.8 \pm 0.1$ R_S, $H_{ionosphere} \sim$ 600–1200 km, and E $\sim$ 1–4 keV), and to monitor their variations (Zarka, 1992; Galopeau *et al.*, 1989).

than at Jupiter and Earth) at 12–13 h LT, but with extents towards lower latitudes (60°–70°) about ∼9 h LT and marginally about 18–19 h LT (Figure 27a). These sources thus extend over L-shells of 4 to 130. Although constrained independently, the northern and southern sources appear magnetically conjugate on the average. Recent UV observations of Saturn's northern aurora by the HST, displayed in Figure 27b, revealed bright spots closely matching the above radio source locations, i.e. dominantly on the morning side with latitude extents lower than 80°. The reason why 'active' LT seems to correspond to lower latitudes is unexplained.

In view of the Cassini tour, the regions of interest for auroral studies correspond, in projection onto the planetary surface, to the 'Voyager' auroral ovals at ∼76°–82° plus the new SKR sources (at slightly higher latitude at 12 h–13 h LT, and including their lower latitude extents, especially on the morningside). In 3-D, these regions extend along magnetic field lines from the planetary surface up to ∼5 R_S, which corresponds to the lowest observed SKR frequencies. SKR (and possibly also UV) sources are active only/mainly when the 'active' longitude sector ∼100°–130°, of yet unknown nature, passes about noon LT.

Effects of auroral phenomena on Saturn's upper atmosphere

Auroral phenomena are the source of intense energy deposition into Saturn's upper atmosphere. As a result of this heat input the temperature in the upper atmosphere

reaches ∼600–800 K, much higher than the value that can be reached from solar UV heating only (∼200). An estimated heat influx of $\sim 3 \times 10^{-4}$ Wm^{-2} is required to heat the upper atmosphere to that temperature. Auroral electron precipitation is a possible heat source, as the estimated average precipitated power of 2×10^{11} W in the northern and southern auroral regions represent ∼6–9 $\times$ 10^{-4} Wm^{-2}. In the form of 1–10 keV electrons, these precipitations generate an exospheric temperature of 1600 to 650 K between 1500 km and 900 km (above the 1-bar level). Auroral energy deposition thus appears to be an important source of heating in Saturn's high latitude thermosphere, but it cannot make a significant contribution to the heating of the entire thermosphere/exosphere region (unlike at Jupiter), even if the atmospheric circulation is able to distribute this energy with 100% efficiency over the entire planet. Joule heating, related to ionospheric electric currents via the Pedersen conductivity, is another candidate heat source (as at the Earth and Jupiter) which could provide half the required flux. The transfer of energy to the thermosphere is caused in this case by ion/neutral gas friction due to the ∼10% departure from corotation of the plasma in the outer magnetosphere beyond ∼8 R_S (see Figure 15).

Auroral precipitations can also modify the composition of the auroral thermosphere, although on Saturn they do not seem to influence the global distribution of H atoms (while they cause a depletion at Jupiter). It is not clear if these modifications are of chemical or dynamical origin, as precipitations also influence the thermo-stratospheric circulation (winds, eddies, turbulence). Observations and circulation modeling favor the latter at Jupiter, where supersonic winds have been detected, and where thermospheric perturbations extend towards lower (non-auroral) latitudes. No information is yet available at Saturn.

Auroral precipitations are also responsible for the production of 'polar hazes'. They emit in the near UV (∼200 nm), but strongly absorb the FUV reflected solar flux, and thus allow the detection of auroral FUV features. The generation mechanism for the polar haze observed at Saturn, whose spatial extent and variability are not well documented yet, is not understood. It may consist of enhanced reactivity of collision-produced hydrocarbon ions, or enhanced vertical mixing (deep-atmosphere species brought to surface).

Key scientific questions and MAPS investigation strategy

In spite of the Voyager, IUE, HST and Ulysses observations, our present knowledge of Saturn's auroral zones remains poor, and the key questions regarding them are still very basic:

(1) What is the detailed spatial distribution of auroral UV, IR and radio emissions, and their temporal variability at the different scales and what does it tell us about their possible control by external (solar wind) and internal (storms and substorms) processes?
(2) What are the dominant ionosphere/magnetosphere coupling and particle acceleration mechanisms along auroral field lines?

(3) What role does the auroral upper atmosphere play in the regulation of magnetospheric plasma flows and the coupling of Saturn's environment to the solar wind?
(4) What are the effects of auroral particle, momentum and energy deposition on the energy balance, dynamics and chemical composition of Saturn's upper atmosphere?

An appropriate investigation strategy for MAPS to address these four questions must be two-fold:

– Advantage needs to be taken of the long duration of the mission to conduct a continuous monitoring (as much as possible) of the main auroral emissions, and of all airglow emissions that can provide information on the response of Saturn's upper atmosphere to auroral energy input. This monitoring will be based on the continuous survey mode of RPWS and on the best possible coverage of auroral emission features in the UV and IR ranges. Additional observations of these emissions from Earth's orbit, if carefully designed, will be an important contribution.
– Plan intense campaigns of *in situ* investigations of auroral magnetic field lines and particle acceleration regions during the very short periods of encounters with these field lines at high magnetic latitudes. As Figure 33 shows, the planned tour presently offers two such periods, and just a few orbits, one 23 to 25 months after SOI, corresponding to encounters with SKR generation regions, one 37 to 44 months after SOI during which the nightside auroral field lines will be crossed. The total observing time for these encounters will be very limited (a few hours throughout the mission), so we expect that MAPS investigations will be granted a high level of priority during these encounters, which will have to be planned just as carefully as a satellite encounter, for instance, considering the unique opportunity they offer for an *in situ* investigation of auroral processes.

The continuous remote sensing survey of auroral emissions will make it possible to cover all the relevant time scales in auroral variability, and to provide constraints on auroral emission control by the solar wind and internal magnetospheric processes. For instance the long periods of time spent by the spacecraft in the solar wind will be an ideal opportunity to study its influence. Similarly, large-scale dynamical phenomena studied in situ by the plasma and wave instruments will be correlated with auroral emission variations.

Many critical measurements can be performed during the crossing of the auroral zones and SKR generation regions, such as for instance:

– The nature and energy of precipitating particles causing UV and radio emissions.
– The search for faint UV/IR auroral emissions spots which could reveal satellite/magnetosphere electrodynamic interactions.
– Measurements of charged particle distribution functions: are they adequate for SKR generation, through CMI, and what do they imply in terms of precipitating/escaping charged particle sources and acceleration processes?

- Measurements of the level of wave electric fields in auroral regions: what constraints do they imply on SKR saturation levels? Is the level of electrostatic turbulence high?
- Measurements of radio wave polarization and beaming close to the SKR sources: is the polarization more linear than far from the source (propagation should circularize it)? Is the cone beaming angle smaller at high frequencies, as predicted by the theory?
- Are there auroral cavities (or filamentary cavities) in Saturn's auroral regions?
- Radio direction-finding results at highest SKR frequency should help to locate accurately the HF SKR sources: do they correspond to the magnetic anomaly inferred by Galopeau and Zarka (1992)?
- Is the 'active' region at 100°–130° SLS a magnetic anomaly?

3.2.5. *Coupling with the Solar Wind and the Hydrogen Torus in the Outer Magnetosphere*

As for any other magnetosphere, Saturn's magnetospheric structure, dynamics and energetics are determined by the combined effect of external forcing by the solar wind and internal forcing by planetary rotation, and the other internal sources of plasma and momentum. The Saturn case is particularly complex, because each of these factors is in a sense uniquely different. The solar wind, whose effect is particularly important in the outer magnetosphere, has quite different characteristics at Saturn than at Earth. Its density is much lower, the magnetic field magnitude is smaller, and the nominal Parker spiral gives a magnetic field that is almost completely azimuthal, with an angle of 85° of its direction to the Saturn-Sun direction. Its effect must combine with those of the internal plasma and momentum sources. In the outer magnetosphere, the dominant internal source is the neutral hydrogen torus. We focus in this section on the interactions between the solar wind, the magnetospheric plasma flow and this hydrogen torus.

The contribution of MHD simulations

With the development of advanced MHD simulation techniques, it has recently become possible to try to anticipate the dynamical behavior of Saturn's magnetospheric system under a variety of solar wind conditions. Hansen *et al.* (1999) published a series of MHD simulations on this subject. The model used a state-of-the-art numerical code that solves the ideal MHD equations. This simplified model has been successful in providing a clear picture of global dynamics for various plasma flows.

The set of basic equations, the parametric description of plasma sources and sinks and the boundary conditions used are described in Hansen *et al.* (1999). The magnetic field model used is a pure dipole aligned with the rotation axis. In order to emphasize and understand the effects specifically associated with the hydrogen torus, the only included plasma source is the one produced by this torus. The system of MHD equations has been solved for three different IMF conditions that are

representative of the many possible configurations: southward, $\mathbf{B}_{sw} = (0,0,-B)$; northward, $\mathbf{B}_{sw} = (0,0,+B)$; and Parker spiral, $\mathbf{B}_{sw} = (-0.1\ B, 0.995\ B, 0)$, where B is the magnitude of the interplanetary magnetic field (B = 0.5 nT in the simulation). Figure 30 shows the calculated steady-state distributions of mass, density and plasma flow vectors in the equatorial plane for the three values of the IMF considered. In each panel the filled circles represent the 3 R_s surface at which boundary conditions were applied, and the other circles indicate the assumed inner and outer boundaries of the neutral torus.

Southward IMF. Since Saturn's magnetic dipole has the opposite polarity from the Earth, the magnetospheric configuration for a southward IMF at Saturn is very similar to that at Earth for a northward IMF. The magnetic field lines are open to the solar wind magnetic field only over the small region occupied by the cusp and the closed magnetosphere extends approximately 125 R_S downstream, in a configuration very similar to Earth. The corotation flow of the near Saturn region interacts with the incident solar wind driven magnetospheric convection to create a stagnation region on the dawn side of the magnetosphere. The plasma resulting from the neutral torus builds up, creating a region of high density plasma near the equatorial plane with a peak value of nearly 14 times the solar wind mass density. A separatrix, located nearly along the outer boundary of the Titan torus in the dusk to midnight quadrant, separates circulating corotation flow from solar wind dominated flow. The structure of the flow and the location of the separatrix for this case seem to match the picture of Jupiter's magnetosphere given by Vasyliunas (1983), although he gives a location for the x- and o-lines which do not exist for this steady state configuration. The density maximum in the noon-midnight meridian plane extends from roughly L = 10 to L = 25 and has a half thickness of 7 R_s, corresponding reasonably well to the extended plasma sheet measured by Voyager, although slightly larger and with a slightly higher density than measured.

Northward IMF. As expected, the magnetic field configuration for this case is also very similar to the corresponding case for Earth (e.g., southward B_z). There is a clear x-line located at 20 R_s that represents reconnection of the open magnetospheric field lines on the day side while at the same time a large region of the polar cap is open to the solar wind. The plasma density and velocity field for this case are quite different from the previous southward IMF case. There are now two stagnation regions, one to the dawn side and one to the dusk side. In each of these regions the flow is slowed and plasma density from the torus is allowed to build up. The locations of the peaks in density are nearly symmetric. On the dusk side the density peaks at 3.8 times the upstream density while on the dawn side the peak value is 2.5 times the density in the incident solar wind. The extended plasma torus can still be seen for this case, although the densities are lower and the half height is smaller. For this case, the separatrix between corotation flow and anti-solar flow is much more pronounced than for the southward IMF case. The separatrix is very

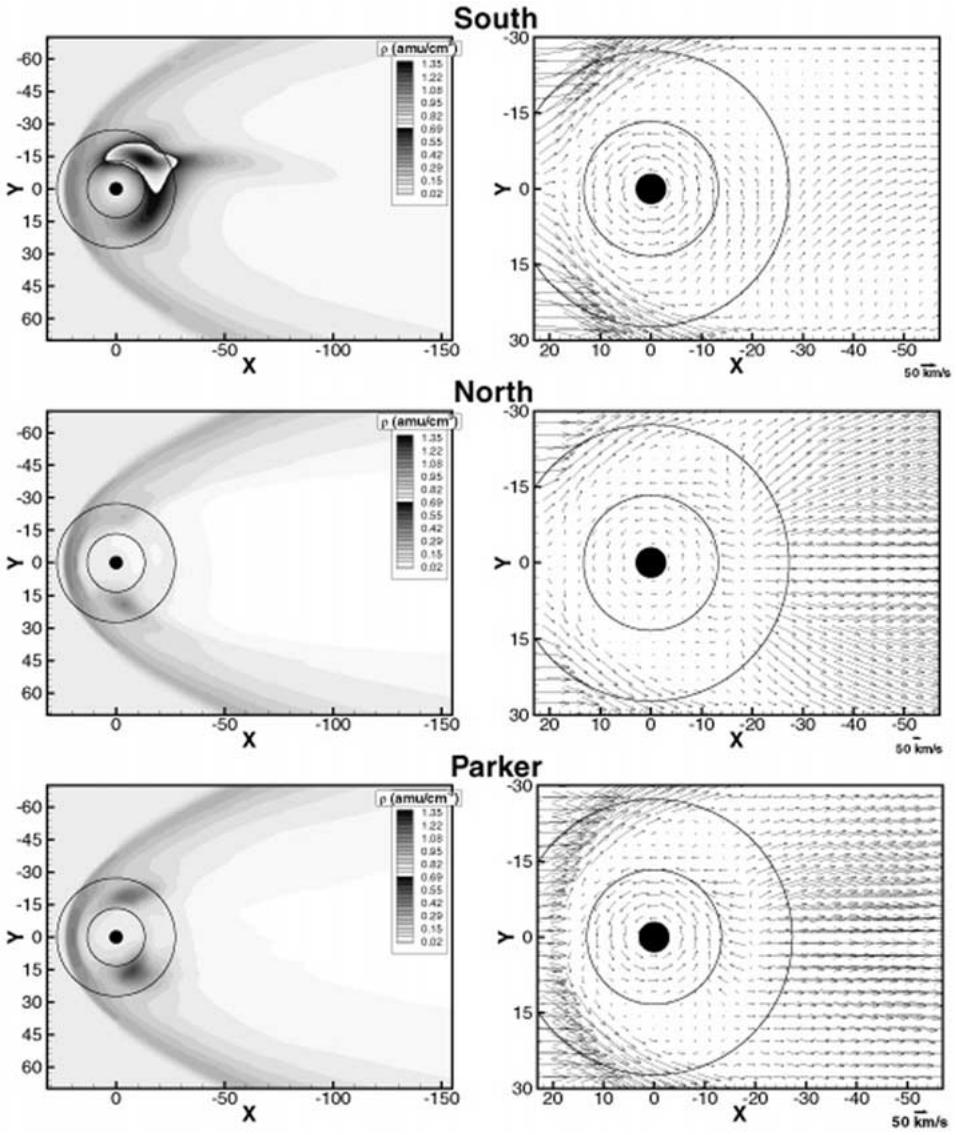

Figure 30. Calculated distributions of the plasma densities (left panels) and of the equatorial projections of the velocity field (right panels) in Saturn's equatorial plane, as determined in the ideal MD simulation of Hansen *et al.* (1999) for three different IMF conditions: southward IMF (top), northward IMF (middle) and Parker spiral (bottom panels).

nearly a line located approximately 19 R_s down the tail, and falls very close to the x-line associated with the magnetic field reconnection.

IMF along the Parker Spiral. A Parker spiral IMF at the radius of Saturn is almost entirely azimuthal. This fact, combined with the planetary rotation, eliminates any of the near symmetries that existed for the previous IMF configurations, and so field lines and stream traces are not confined to planes. Even though this case is much more complicated, the magnetic field structure is very similar to that of the Earth for a Parker spiral IMF. The interaction region between solar wind driven magnetospheric convection and the corotation flow for this case is quite similar to that for the northward IMF case. There are again two stagnation regions, one on the dawn side and one on the dusk side of the magnetosphere with the dusk side having the higher mass density. The peak values are 4.7 and 5.6 times the upstream density. The extended plasma torus can again be seen for this case. The densities are intermediate between the first two cases and the size is also somewhere between the two. As in the northward IMF case, the separatrix is very nearly a line located approximately 20 R_s down the tail, and corresponds closely to the x-line associated with the magnetic field reconnection.

Figure 30 clearly shows the differences in magnetospheric structure for different IMF configurations. As is expected, the magnetic field structure seems very similar to the Earth while the velocity and plasma density fields are quite distinct from Earth and vary with IMF orientation. The flow structure for southward IMF follows the diagram given by Vasyliunas (1983) for Jupiter, but even for this case, the steady state structure does not match his picture exactly. For the other IMF orientations, a completely different and more complicated structure exists. In essentially all cases, corotation is seen to dominate out to at least 12 R_S from Saturn.

Key scientific questions and MAPS investigation strategy

The results of this simulation give us a first idea as to the large-scale distributions of plasmas and flows in the outer magnetosphere, and on their variability under changing solar wind conditions. They suggest that with the combined use of such simulations and the analysis of Cassini observations it will be possible to address the key questions concerning the dynamical behavior of the outer magnetosphere:

(1) What is the importance of ion pick-up from the hydrogen torus as an internal source of magnetospheric plasma, and how does it operate at the microscopic and macroscopic scales?

(2) How does ion pick-up compete with the other sources of plasma and momentum, namely the solar wind, Saturn's ionosphere and planetary rotation, to determine the overall configuration of plasma distribution, composition and flow in the outer magnetosphere? How does this configuration vary with changing solar wind conditions?

To help us address these questions, observations should ideally provide:

– the large-scale distribution of the bulk parameters of the different components of the plasma in terms of moments of the electron gas and of the different ion species, derived from the particle instruments (CAPS and MIMI);
– direct measurements, or at least some constraints, on the main plasma sources: ionosphere and neutral gas tori (see previous sections);
– monitoring of the auroral upper atmosphere's UV, radio and other emissions, to provide indications on the amount of energy deposited into the atmosphere and on its variability;

Detailed information on the ion mass distribution and chemical composition as a function of energy, and on the velocity-space distribution functions of the electrons and of the main ion species, as well as spectrograms of the local plasma wave modes, will also have to be acquired regularly to study the non-MHD aspects of the plasma dynamics.

The large fraction of time spent in the magnetosheath or in the free solar wind must be used to monitor their plasma flow characteristics. As seen from the MHD simulation (Figure 30), it will be very important to describe how the magnetosheath plasma flow connects to the internal magnetospheric flow through the magnetopause. In addition, a systematic monitoring of the variability of the free solar wind and of the response of auroral emissions to its variation will be an important ingredient in evaluating the degree of control of the solar wind on the auroral ionosphere. This can be done by combining *in situ* measurements of the solar wind with remote sensing of the auroral emissions and ionospheric densities.

Combining *in situ* and remote sensing measurements will indeed be one of the key elements of the MAPS investigation strategy, making it possible to permanently place the detailed analysis of local plasma and field characteristics in the broader context of the observation of the large-scale features of the main plasma reservoirs. The other key element is the implementation of a MAPS survey mode, providing continuous monitoring of the plasma and field characteristics throughout the tour at an appropriate temporal (and therefore also spatial) sampling rate. Continuity of data acquisition through the implementation of this mode is certainly one of the most important requirements of magnetospheric and plasma science.

4. Magnetosphere and Plasma Science with the CASSINI Instruments and Orbital Tour

Some of the outstanding scientific questions about Saturn's magnetosphere and its coupling to the Saturn system have been introduced and discussed in the previous section. The CASSINI-HUYGENS mission offers two major key advantages to solve these questions, and certainly to open a large number of new ones, which we just cannot anticipate with our limited knowledge of the Saturnian system today: we expect to make real discoveries ! The first advantage is the CASSINI orbital tour, which will effectively cross most or all of the magnetospheric regions of

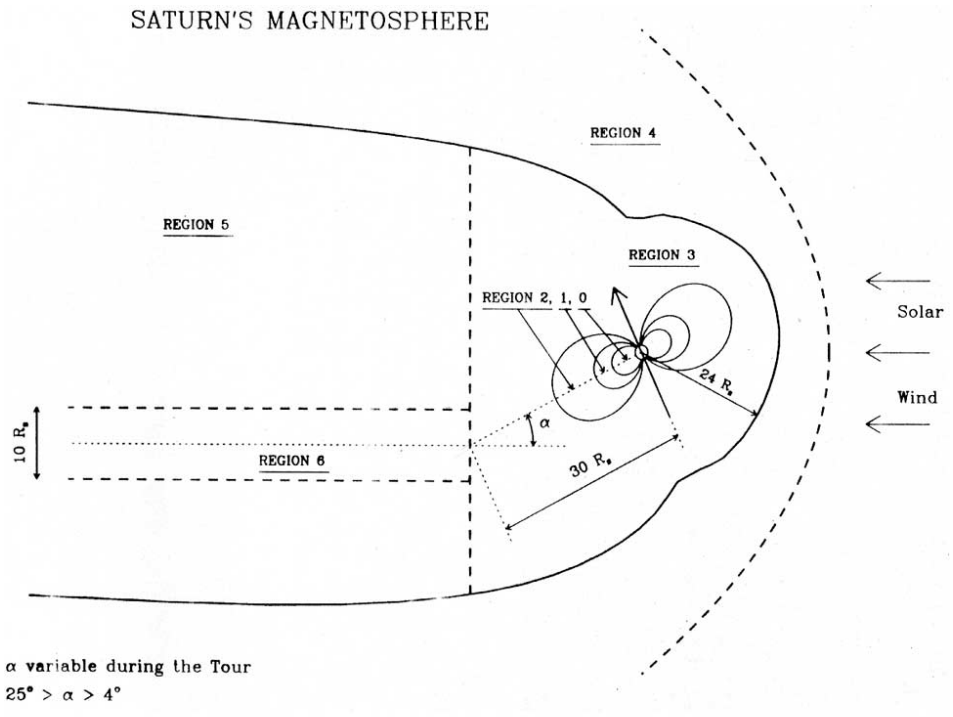

Figure 31. Schematic representation of the different domains of the magnetosphere used by the MAPS working group to evaluate the tours. An ideal tour should explore all regions, and offer a significant coverage in local time and latitude in each of them. The percentage of time spent in each of these domains by the presently selected tour, T 18.5, is shown in Table VIII.

interest, as we shall show in section 4.1. The second one is the CASSINI instrument complement. Just in terms of Magnetospheric and Plasma Science (MAPS), this is the most advanced instrument set ever flown to a planetary magnetosphere: we provide an overview of its characteristics in section 4.2, and show how the set of measurements performed by the different MAPS instruments, operating in a combination of in situ and remote sensing observing modes, can successfully address most of the key scientific questions we have identified.

4.1. Exploration of Saturn's magnetospheric regions by the Cassini orbital tour

The geographical coverage of the different regions of the magnetosphere by the tour is the first key ingredient of a MAPS strategy. Figure 31 displays a schematic break-down of the Saturnian magnetosphere into regions, and Table VIII indicates the name of each region, its geometric definition, and the percentage of time spent by the CASSINI spacecraft in the different domains along the presently selected nominal tour, tour T 18.5 (Wolf *et al.*, this issue). A first comment is that only 53%

TABLE VIII
Definition of the different magnetospheric regions used in the Tour evaluation

Code	Name	Residence time	Nominal tour	Definition
INSIDE	MAGNETOSPHERE		53%	
R-0	Innermost	Magnetosphere	1%	$L < 5$
R-1	Inner	Magnetosphere	2%	$5 < L < 8$
R-2	Middle	Magnetosphere	6%	$8 < L < 15$
R-3	Outer	Magnetosphere	35%	$L > 15$, $X > -30\ R_S$
R-5	Tail	Lobes	6%	$L > 15$, $X < -30\ R_S$, $\lvert Z - Z_{NS}\rvert > 5\ R_s$
R-6	Tail	Plasma sheet	3%	$L > 15$, $X < -30\ R_S$, $\lvert Z - Z_{NS}\rvert < 5\ R_S$
Aur.	Auroral	Regions	~75 h	$\lvert\lambda\rvert > 70°$, $R < 5\ R_S$
SKR	SKR generation	Regions	~4 h	$\lvert\lambda\rvert > 70°$, $R < 5\ R_s$, 9 h < L.T. < 14 h
OUTSIDE	MAGNETOSPHERE		47%	
MSH	Magnetosheath		36%	Between magnetopause and shock
SW	Solar	Wind	11%	Outside the planetary shock

of the nominal tour time (extending over 44 months) is spent inside our 'model' magnetosphere, and 47% outside of it, including 36% in the magnetosheath and 11% in the free solar wind. The magnetosphere itself, for the purpose of mission planning, has been divided into 8 different domains. Domains R-0 to R-2 correspond to closed-field-lines, approximately symmetric regions around Saturn's magnetic dipole axis. Regions R-0 and R-1 correspond approximately to the inner torus, and R-2 to the extended plasma sheet. Domain R-3, which excludes the magnetotail, corresponds to the outer magnetosphere. The boundary between the outer magnetosphere and the magnetotail has been defined as a plane orthogonal to the Sun-Saturn axis passing through the tail hinge point, located 30 R_S from Saturn in its equatorial plane in the midnight meridian. Located on the nightside of this boundary, the magnetotail is finally divided into its lobes (domain R-5) and its plasma sheet, which has been given an arbitrary extension of 5 R_S in either direction along the Z axis from the Z value of the hinge point. Finally, the auroral field lines domain has been defined as the regions of magnetic latitude larger than 70°, and closer than 5 R_S to the planet's center. This very schematic magnetospheric geometry was defined by the MAPS working group to assist in the evaluation of

TABLE IX
Exploration of the main magnetospheric regions during the CASSINI nominal Tour

Time in tour (Months)	Geometric Configuration	Magnetospheric regions More particularly explored
SOI	Passage above and through ring plane	Inner most magnetosphere, magnetically connected to the main rings
0–6	First orbits: Low inclination, high apoapsis	Dawnside equatorial magnetosphere
6–10	Medium inclination orbits dawn side	Middle and low latitude dawnside magnetosphere
10–14	Equatorial orbits. Rotation towards the nightside	Equatorial dawnside to nightside magnetosphere
14–22	Elongated orbits with Apoapsis on the nightside	Encounters with the tail plasma sheet
23–25	High inclination orbits	SKR generation regions and auroral zones
25–32	180° transfer from nightside to afternoon	Afternoon midlatitude magnetosphere
32–37	Low inclination orbits, apoapsis in the afternoon	Low latitude afternoon magnetosphere
37–44	High inclination orbits with apoapsis near noon	Nightside auroral zones

the candidate tours, and in order to check how and whether they fulfilled the MAPS tour requirements deduced from the different science objectives.

The presently selected tour, T 18.5, does a reasonably good job of satisfying most of these requirements, making it possible to explore the magnetosphere as a whole, as well as most of its key regions. Table IX proposes a segmentation of this tour into different periods corresponding to different properties of geographical coverage of the magnetosphere. Time is counted in months from SOI, and limited to the nominal tour duration. The variations in orbit configuration (central column) make it possible to successively explore the different regions indicated in the right-hand-side column of the table. In addition to the partial coverage of the middle and low latitude magnetosphere, which is achieved reasonably well by the progressive clock-wise rotation of the orbit orientation around Saturn, a few segments of the tour, corresponding to short explorations of very specific regions of high interest, need to be specifically pointed out. They are:

– the Saturn Orbit Insertion sequence (SOI), which will be our unique opportunity to explore the region of the inner magnetosphere which is magnetically connected to the rings system, and to measure Saturn's magnetic field very close to the planet;

– the segment between 14 and 22 months, which includes all the encounters with the tail plasma sheet;
– the short segment between 23 and 25 months, which includes the first period of encounters with the auroral field lines, and probably the only opportunities to cross or come close to the SKR generation regions;
– and, finally, a second period of high-inclination orbits, near the end of the mission, which will be the best opportunity to explore the nightside auroral zones.

Due to the high apoapsis of most of the orbits, the tour also offers many opportunities to explore the magnetopause and study its dynamics under the effect of variations in solar wind and/or in the magnetosphere. Figure 32, using the model magnetopause surface of Maurice and Engle (1995) shows the locations of the nominal inbound and outbound crossings for the dawn and dusk halves of the surface. As one can see, there will be essentially near-equatorial crossings on the dawn side, but a broader latitudinal exploration of the magnetopause on the dusk side and near noon.

As explained in section 3.2.4, the few hours spent inside the auroral zones and the SKR generation regions during the whole tour will be of outstanding interest for MAPS objectives. Figure 33 shows the locations of the footprint of the spacecraft, projected along Saturn's magnetic field lines, during these short encounters with the auroral regions. One sees that, in the presently planned tour, field lines will be explored up to invariant latitudes of nearly 85 degrees. The local time coverage, though not complete, is reasonable as a consequence of the two different encounter periods (see Table IX). It is absolutely essential to preserve the relatively good quality of this encounter geometry through all possible adjustments of the tour.

4.2. Contributions of MAPS instruments to the different science areas

The second key element in the MAPS investigation strategy is the combined operation of an outstanding suite of instruments. The instrument suite of interest to MAPS, which is summarized in Table X, allows the measurements of the electric and magnetic field (via RPWS and MAG), the plasma distribution functions of ions and electrons (via MIMI and CAPS) over a broad range of energies and consequently the flow velocities of each ion component, the dynamic spectra of plasma waves and radio emissions (RPWS), and even an energetic neutral atom (ENA) imaging capability which will provide global pictures of the plasma reservoirs in the inner magnetosphere and of the Titan/magnetosphere interaction, the INCA sensor of the MIMI investigation. In addition, the orbiter carries an ion and neutral mass spectrometer (INMS) and a radio science subsystem (RSS); the RSS will provide information on the ionospheres of Saturn and Titan while the INMS instrument will be mainly used to study the structure and composition of Titan's interaction with Saturn's magnetosphere. The Cosmic Dust Analyzer (CDA) will

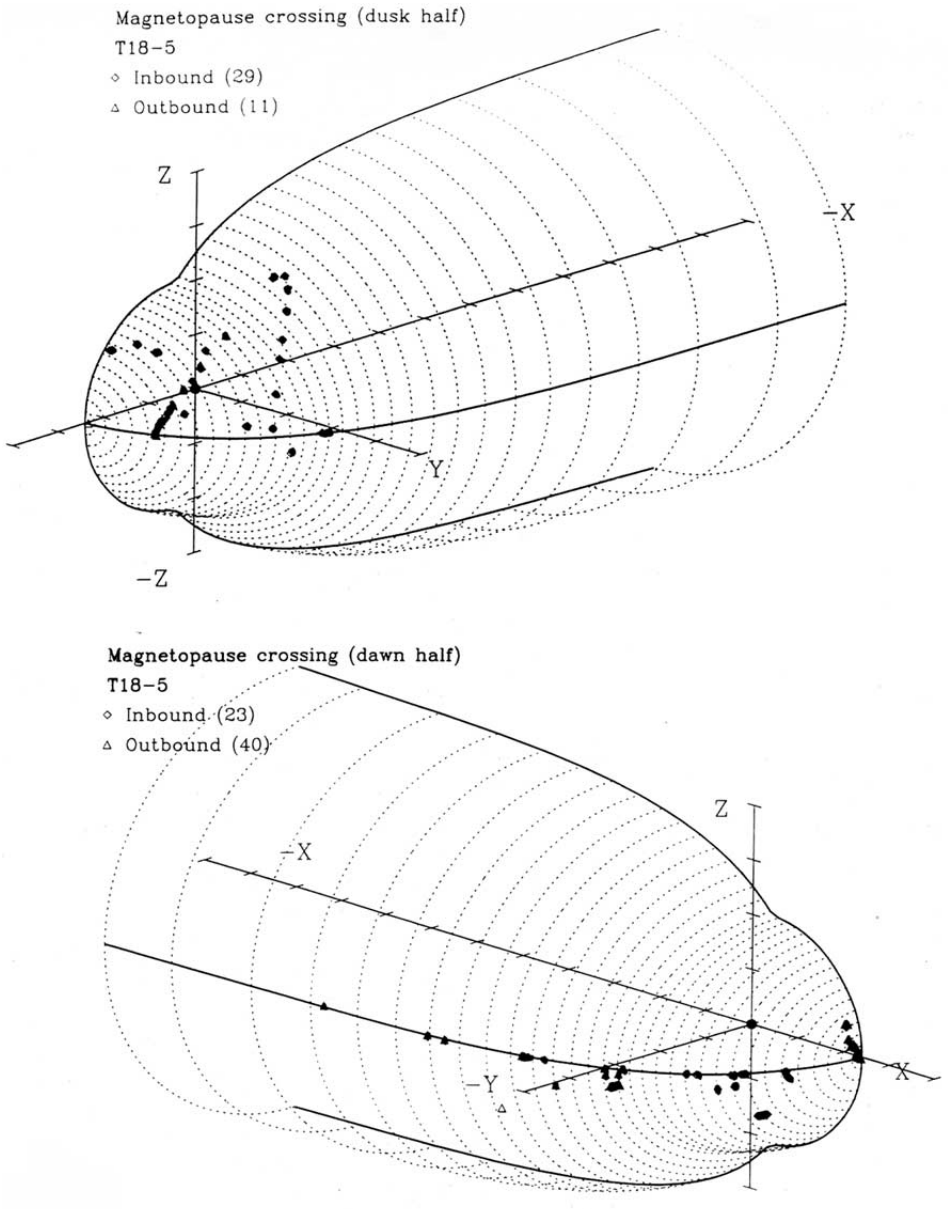

Figure 32. Distribution of nominal magnetopause crossings along the T 18.5 tour on the dawn (upper panel) and dusk (lower panel) halves of the magnetopause, calculated using the model magnetopause of Maurice and Engle (1995) for a magnetopause 'nose' distance of 23 R_S along the *X* axis.

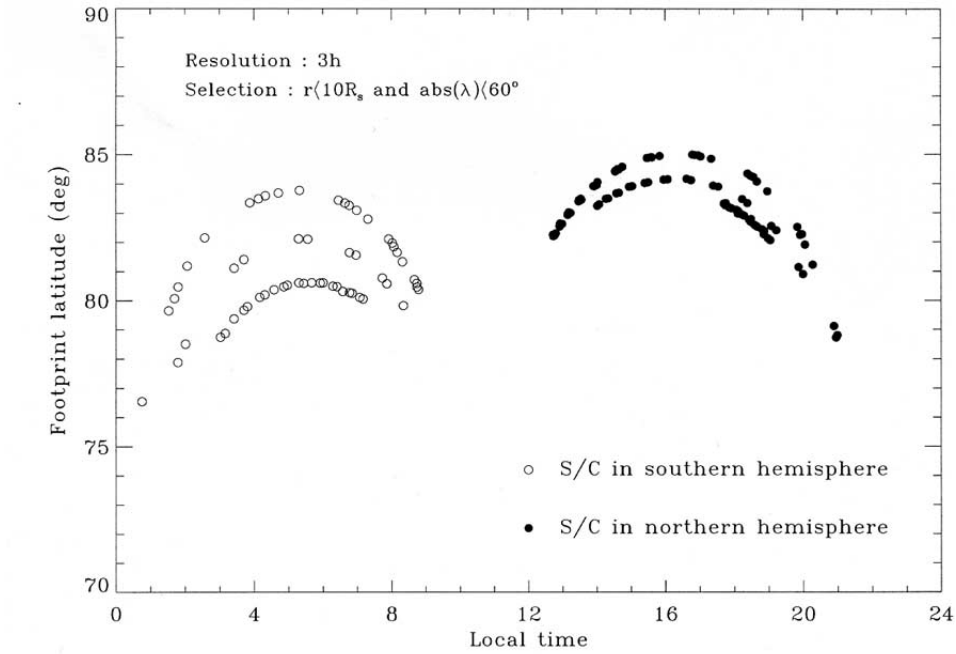

Figure 33. Representation of the magnetic projections onto Saturn's ionosphere of the sections of the CASSINI orbiter trajectory in the presently nominal tour (T 18.5) which passes inside the auroral and SKR generation regions, as defined in Table X.

provide direct observations of particulate matter in the Saturnian system (CDA), and the Ultraviolet Imaging Spectrograph (UVIS) will be a key instrument to study the upper atmospheres of Titan and Saturn, the neutral gas tori, airglow and auroral emissions. Detailed descriptions of each of these investigations are found in the corresponding articles of this issue.

One of the important characteristics of this instrument suite for MAPS is its ability to measure the three components of the electric and magnetic fields over a broad frequency range, as shown in Figure 34. Thanks to some overlap between the MAG instrument and the RPWS search coils, the magnetic field can be measured over a frequency range from quasi-static to 12 kHz. The electric field measurements are made over a frequency range from 1 Hz to 16 MHz. This will allow the studies of the electromagnetic field with CASSINI to cover a broad range of interests, from the study of Saturn's internal structure through the monitoring of the d.c. component of the magnetic field near the planet, to the analysis of SKR emissions, and through the detailed study of the different electrostatic and electromagnetic emissions generated in Saturn's magnetosphere.

TABLE X
Cassini Science Investigations directly related to MAPS

CAPS	Cassini Plasma Spectrometer (D. T. Young)	Measures composition, density, velocity and temperature of ions and electrons
CDA	Cosmic Dust Analyzer (E. Grün)	Measures flux, velocity, charge, mass and composition of dust and ice particles from 10^{-16} to 10^{-6} g
INMS	Ion and Neutral Mass Spectrometer (J. H. Waite)	Measures neutral species and low-energy ions
MAG	Dual Technique Magnetometer (D. Southwood)	Measures the direction and strength of magnetic field
MIMI	Magnetospheric Imaging Instrument (S. M. Krimigis)	Images Saturn's magnetosphere using energetic neutral atoms plus measures the composition, charge state and energy distribution of energetic ions and electrons
RPWS	Radio and Plasma Wave Science (D. A. Gurnett)	Measures wave emissions plus electron density and temperature
RSS	Radio Science Subsystem (A. J. Kliore)	Measures the density of Saturn's ionosphere
UVIS	Ultraviolet Imaging Spectrograph (L. W. Esposito)	Measures ultraviolet emissions to determine sources of plasma in Saturn's magnetosphere

The remarkable MAPS capability of the mission can also be appreciated through the energy and direction-of-arrival coverage of the different types of particles encountered in the Saturnian environment along the CASSINI orbit provided by the particle instruments. CASSINI will indeed offer a very broad access to the three types of particles of interest, electrons, ions and neutrals, with the capability of separating ions and neutrals of different masses and even, in the case of the IMS sensor of CAPS, some access to the identification of the different chemical species. In addition, the RPWS Langmuir probe will provide electron density and temperatures of ionospheric plasmas and should work reasonably well near the icy satellites as well as the inner plasma sheet. The RPWS sounder should also provide an independent electron density measurement.

Cassini will also have access to the dust component of Saturn's environment, not only through the CDA, but also through RPWS. While the RPWS measurements do not include composition and can only crudely determine mass, they use the entire spacecraft as a target and should be able to do a reasonable job of measuring the dust flux of micron-sized and larger particles, regardless of spacecraft orientation.

The energy coverage of the CASSINI particle instruments can be seen in Figure 35. Thanks to some overlap of their energy range, the particle instruments provide a continuous coverage from about 0.010 eV to about 18 MeV (ions),

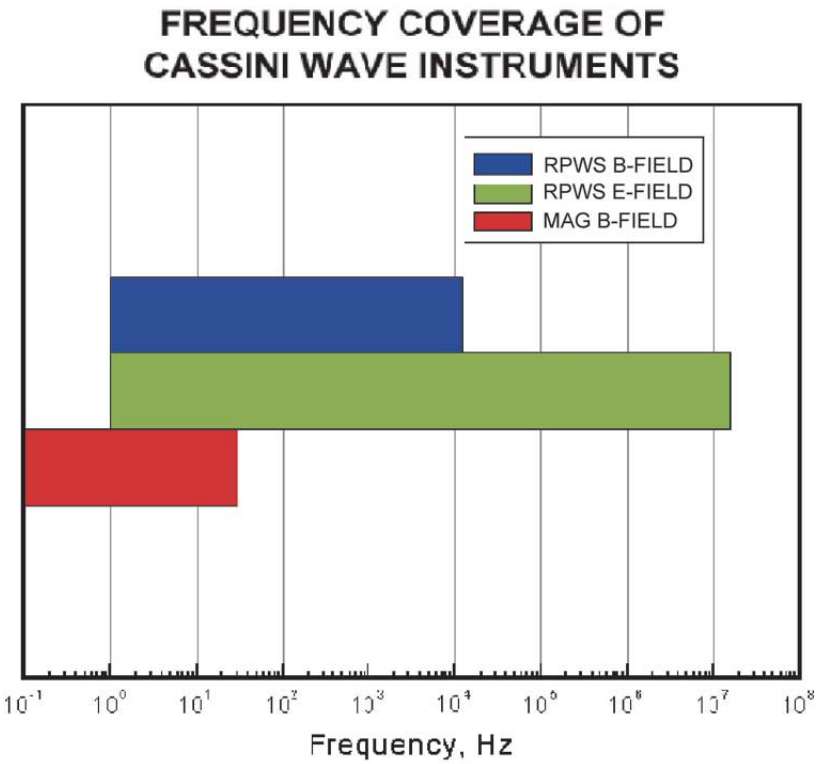

Figure 34. Frequency range of the Cassini wave instruments.

10 MeV (electrons) and 3 MeV (neutrals). They will thus allow the study of a very broad range of particle populations and their dynamics.

These instruments also have remarkable capabilities in terms of coverage of the velocity space of each particle species, by a combination of the 1-D or 2-D fields of views of the different sensors in velocity space with the additional orientation flexibility provided by turntables or actuators attached to the particle instruments.

The field of view (FOV) of the CAPS, INMS, MIMI and UVIS experiments is shown in Figure 36. The CAPS sensors (IMS, IBS and ELS) are mounted on a turntable, which through a windshield-wiper type motion around the spacecraft Z-axis allows the instruments to enlarge their FOV in the azimuthal direction. The MIMI LEMMS sensor is also mounted on a turntable, which provides a continuous rotation around the spacecraft Y-axis, allowing thus a complete coverage in elevation.

The FOVs shown in Figure 36 take into account the turntable rotations. As can be seen, the particle instruments onboard Cassini provide a good coverage of velocity space. When the spacecraft is in a spin mode, then the azimuthal coverage becomes complete (360°) over one spacecraft rotation (23 minutes), thus allowing

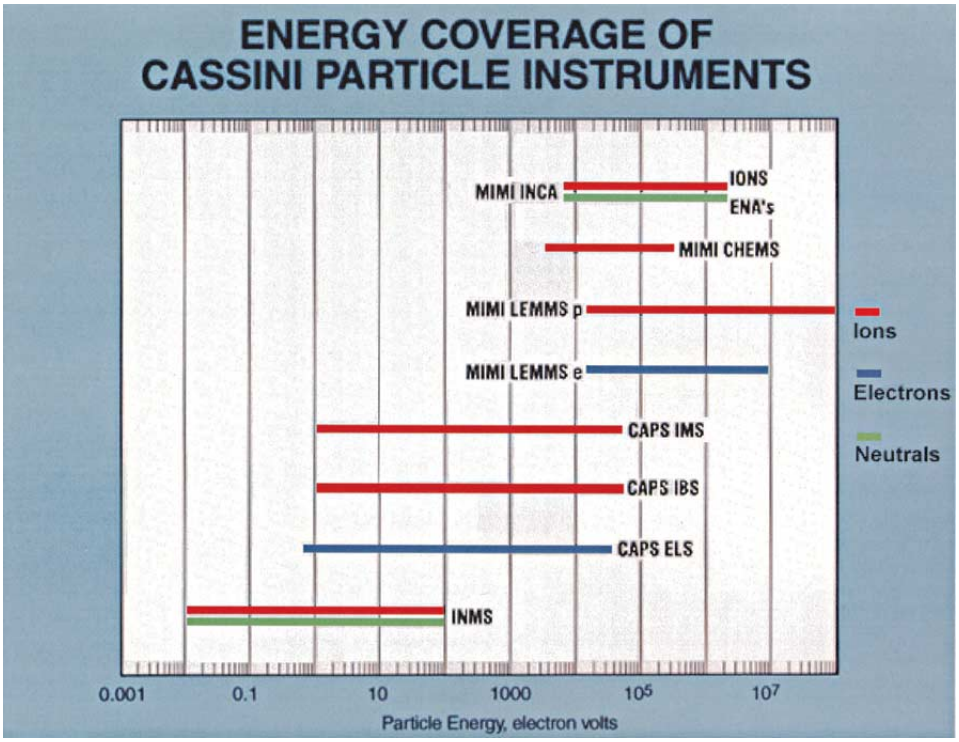

Figure 35. Energy range of the Cassini particle instruments for the different particles detected (ions, electrons, neutrals).

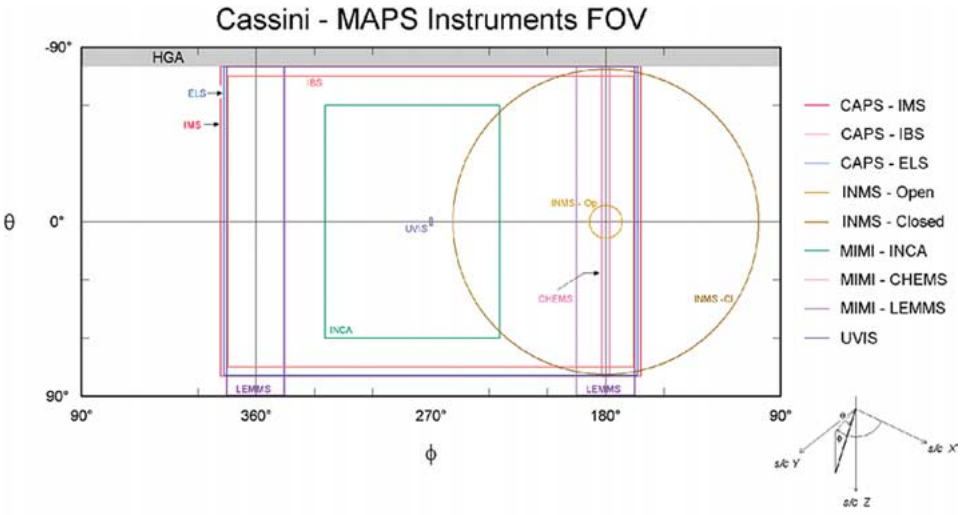

Figure 36. FOV (Field of View) of the CAPS, INMS, MIMI and UVIS experiments, with respect to the spacecraft body-built coordinate system. HGA corresponds to the High Gain Antenna.

TABLE XI
The combination of local measurements and remote sensing in MAPS Science Investigations

	Local measurements	Remote sensing
Plasma populations	CAPS, MIMI, INMS	MIMI
Fields and waves	MAG, RPWS	RPWS
Dust/Plasma interactions	CDA, CAPS, MIMI	
Neutral atmos./clouds	INMS, UVIS	UVIS
Ionospheres	INMS	RSS
Auroral emissions		RPWS, UVIS, VIMS, ISS
Ring/Plasma interactions		ISS, MIMI

one to retrieve the 3-D distribution functions of each particle species, averaged over this time interval, when temporal/spatial conditions in the medium allow.

Taken together, one of the remarkable properties of the MAPS instrument suite is that it combines local measurements along the orbit, providing a detailed but local analysis of the medium encountered, with remote sensing observations of the regions or components of key interest. As an illustration of this point, Table XI shows, for some of the most important topics of MAPS science, which instruments contribute to the local measurements or to the remote sensing measurements. It is quite remarkable that many of them, such as RPWS and MIMI for instance, contribute to both aspects.

5. Conclusions

Magnetospheric and plasma science in the Saturn system offers the unique opportunity to explore in depth particularly interesting examples of two types of magnetospheres: the 'induced' magnetosphere generated by the interaction of Titan with the surrounding plasma flow, and Saturn's 'intrinsic' magnetosphere, the magnetic cavity generated by Saturn's magnetic field interaction with the solar wind flow. This in-depth exploration of these two objects, conducted with the help of the most advanced and diverse package of instruments for the analysis of plasmas, energetic particles and fields ever flown to a planet, will make it possible to address and solve a series of key scientific questions concerning the interaction of these two magnetospheres with their environment.

During the more than 44 fly-bys of Titan planned over the duration of the mission, the key scientific questions will address two main topics:

5.1. TITAN'S IONOSPHERE

- What is the average morphology of Titan's ionosphere and how is it determined by its coupling with Titan's neutral atmosphere and with magnetospheric particles and fields?
- What is the variability of this ionosphere, and to what extent is it controlled by magnetospheric effects (importance and variability of energetic charged particles as plasma sources, of its magnetization by the surrounding plasma flow, etc.)?
- How important are the different escape processes from Titan's upper atmosphere and ionosphere, in the neutral or ionized phases, in the balance of magnetospheric plasma sources and for the long-term evolution of Titan's upper atmosphere?

5.2. TITAN/MAGNETOSPHERE INTERACTIONS

- What is the basic geometry of the interaction of Titan's atmosphere with Saturn's magnetized plasma flow?
- How does it vary with changing conditions in the upstream flow characteristics and with the geometry of local ionization sources?
- Is there a detectable intrinsic magnetic field at Titan, and if so what constraints does it provide on its internal structure?

Thanks to its broad coverage of the main magnetospheric regions, the 4-year tour of the Saturnian system will make it possible to study a magnetosphere which is in strong interaction with all other components of Saturn's environment. The analysis of the broad diversity of these interaction processes will be one of the main themes of MAPS science during the Cassini mission. We have shown in this article how it can be naturally divided into several interaction domains, which roughly coincide with different regions of the Saturnian system, and what are the key scientific questions related to these interaction domains:

5.3. RINGS/PLASMA/IONOSPHERE COUPLING

- What is the net exchange of plasma, neutral species and dust particles between the rings, Saturn's ionosphere and its inner plasmasphere, and what effect does this exchange play in the maintenance of the ionosphere and the evolution of the rings?
- What are the mechanisms responsible for the formation of spokes on Saturn's main rings?

5.4. MAGNETOSPHERE/ICY SATELLITES INTERACTIONS

- Can we determine the surface composition of the icy satellites during close CASSINI fly-bys from CAPS and MIMI data?
- What are the modes of interaction between Saturn's magnetospheric plasma flow and the icy satellites, and how do they depend on the net contribution to ion pick-up, the internal structure and conductivity, and possibly the state of magnetization of these satellites?

5.5. MAGNETOSPHERIC INTERACTIONS WITH THE INNER NEUTRAL GAS TORUS AND THE E RING

- Can we quantitatively understand the observed distribution of neutral and ion species in the inner torus from the balance of plasma generation, loss and radial transport?
- Does it provides constraints on poorly known quantities, such as the sputtering rates of water products from the icy satellites surfaces and from the E ring, or the key reaction rates along the chemical and photochemical paths?

5.6. COUPLING OF THE OUTER MAGNETOSPHERE TO SATURN'S UPPER ATMOSPHERE AND ASSOCIATED AURORAL PROCESSES

- What is the detailed spatial distribution of auroral UV, IR and radio emissions, and their temporal variability at the different scales and what does it tell us about their possible control by external (solar wind) and internal (storms and substorms) processes?
- What are the dominant ionosphere/magnetosphere coupling and particle acceleration mechanisms along auroral field lines?
- What role does the auroral upper atmosphere play in the regulation of magnetospheric plasma flows and the coupling of Saturn's environment to the solar wind?
- What are the effects of auroral particle, momentum and energy deposition on the energy balance, dynamics and chemical composition of Saturn's upper atmosphere?

5.7. COUPLING WITH THE SOLAR WIND AND THE HYDROGEN TORUS IN THE OUTER MAGNETOSPHERE

- What is the importance of ion pick-up from the hydrogen torus as an internal source of magnetospheric plasma, and how does it operate at the microscopic and macroscopic scales?
- How does ion pick-up compete with the other sources of plasma and momentum, namely the solar wind, Saturn's ionosphere and planetary rotation, to determine the overall configuration of plasma distribution, composition

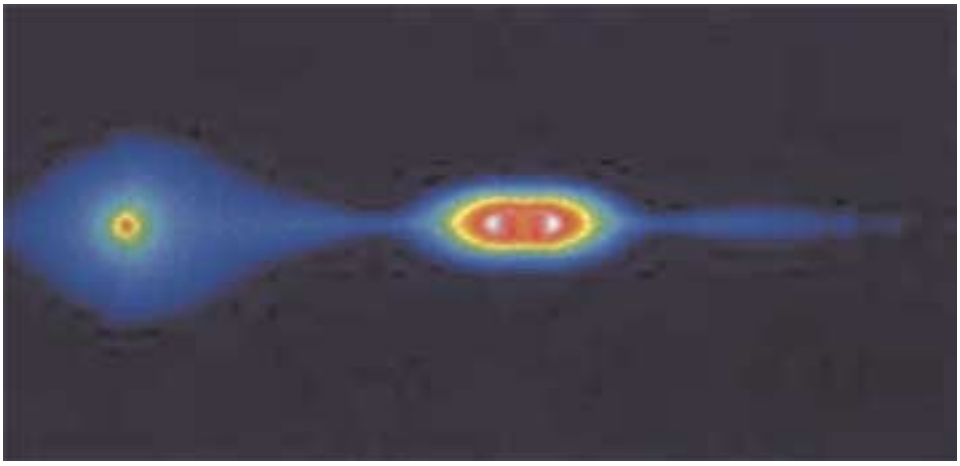

Figure 37. A synthetic image of the Saturn-Titan system as viewed by the MIMI/INCA energetic neutral atom imager. One can see Saturn at the center, and Titan with its neutral atom torus on the left-hand side.

and flow in the outer magnetosphere? How does this configuration vary with changing solar wind conditions?

At the time of writing this article, the CASSINI spacecraft is flying past Jupiter towards Saturn, after its successful encounters with Venus and our Earth. All teams are now focusing their efforts on our joint goal, namely to plan and achieve a very successful mission, which will unravel some of the most fascinating mysteries of Saturn. As we fly towards Jupiter, to encounter it and then make our final turn toward Saturn, no doubt each of us dreams of the time, a few years down the road, when Saturn, Titan and their gas and plasma environments are going to appear more and more distinctly in our imagers. Figure 37, a synthetic view of the Saturn-Titan system as it will be seen by the MIMI/INCA imager, gives us a first idea of what we expect to see when we finally reach the spacecraft's destination. Then the time will come to start to explore, discover and understand new and exciting phenomena. We hope that this article will have convinced the reader that Magnetospheric and Plasma Science, in strong interaction with all other disciplines, is going to play a major role in this exciting scientific endeavor.

Appendix A

Models of Saturn's magnetic field and associated boundaries

The magnetic field at Saturn (B), as for all planetary magnetospheres, is the sum of contributions from various sources, foremost among them being the internal contribution (B_p) to the planetary field, whose intensity at Saturn is sufficient to hold off the solar wind pressure. The total field B is the sum of B_p and additional

TABLE XII
Main characteristics of Saturn magnetic field models

Model reference	Main characteristics
Field models	
Acuña and Ness (1980)	Dipole representation of internal field
Z3 (Connerney *et al.*, 1982)	Higher-order representation of internal field from Voyager data
$P_{11}84$ (Davis and Smith, 1986)	Higher-order representation of internal field from Pioneer 11 data
SPV model (Davis and Smith, 1990)	Combines data sources and features of Z_3 and $P_{11}84$ models
SPV-R (Ladreiter *et al.*, unpublished)	Incorporates constraints on surface field from SKR data into a modified SPV model
Connerney *et al.* (1981, 1983)	Ring current model
Mauk *et al.* (1985)	Analytical representation of the shape of magnetic field lines near the equator
Maurice and Engle (1995)	Contribution of magnetopause currents to the field
Behannon *et al.* (1981)	Only existing model of the magnetotail contribution to the field. Uses a set of current loops
Boundary models	
Slavin *et al.* (1983)	Simplified analytical representation of magnetopause and bow shock shapes from all Pioneer and Voyager MP crossings
Maurice and Engle (1995)	Provides the magnetopause shape and contribution to the magnetospheric field
Maurice *et al.* (1996)	Analytical representation of the Maurice and Engle magnetopause model
Mauk *et al.* (1992)	Representation of the shape of the distant tail and of the intensity of the lobe field

contributions of Saturn's equatorial ring current (B_{RC}), magnetopause (B_{MP}) and magnetotail currents (B_t), and possibly more localized currents due to satellite and/or neutral cloud interactions with the magnetosphere (B_l):

$$B = B_P + B_{RC} + B_{MP} + B_t + B_l$$

Table XII summarizes the existing models of these different terms and their main characteristics, as well as the models of the magnetopause and planetary shock.

The internal contribution, B_P, to the Saturnian magnetic field may be approximated by a dipolar field of moment $\sim 0.21\ G \times R_S^3$ aligned within $\sim 1^\circ$ of Saturn's

rotation axis (Acuña and Ness, 1980; Ness *et al.*, 1981, 1982). The polarity of Saturn's dipole, like Jupiter's, is opposite to that of Earth. The most remarkable aspect of Saturn's planetary field is the close alignment of Saturn's magnetic and rotation axes.

Higher order models of B_P have been developed at Saturn, using the traditional spherical expansion of a scalar potential V from which the planetary field is obtained, via $B_P = \nabla V$. The scalar potential can be written as a sum of Legendre functions with Schmidt coefficients. There has been several approaches to derive a set of Schmidt coefficients for the internal field:

(1) The Z_3 internal field model of Connerney *et al.* (1982) based on Voyager data.
(2) The $P_{11}84$ internal field model of Davis and Smith (1986) based on Pioneer 11 data.
(3) The SPV internal field model by Davis and Smith (1990) which combines the data from all three encounters and the features of the Z_3 and $P_{11}84$ models.
(4) The SPV-R model by Ladreiter *et al.* (private communication) which includes the first terms of the SPV model but uses as an additional source of information the constraint on the surface magnetic field intensity derived from the high-frequency cut-off of the SKR radio emission (see sections 2.3 and 3.6).

While models 1, 2 and 3 only include the axially symmetric dipole, quadrupole, and octupole terms, model 4 is variable with longitude.

The ring current contribution, B_{RC}, results from the combination of the magnetization current and of the azimuthal gradient and curvature drifts of trapped particles, which produces a net azimuthal current. This net current also corresponds to the pressure gradient part of the magnetization current. Two models representing the ring current (1) or including its effects on the total field (2) have been developed:

(1) In the ring current model proposed by Connerney *et al.* (1981b, 1983), the ring current is an annular disk extending from 8 R_S to 15.5 R_S in Saturn's equatorial plane. The current is assumed to be distributed uniformly in z throughout the total disk thickness of 6 R_S, and decreases with radial distances from Saturn as $J\varphi = I_o/\rho$, where $I_o = 2.9\ (10^6)$ A/R_S, and ρ is the radial distance to Saturn's center in Saturn radii. The total integrated ring current is $\sim 10^7$A, only a few percent of the total current of the Jovian magnetodisk.
(2) Mauk *et al.* (1985) have developed a procedure to calculate the local shape of field lines encountered near Saturn's magnetic equator. These authors have derived an analytical form of each field line: the radial distance to the planet is a polynomial (degree 4) expansion of the magnetic latitude. This model already includes the planetary field B_P, and covers the region from ~ 7 R_S to ~ 16 R_S within ± 2 R_S of the equator.

The magnetopause contribution, B_{MP}, to the total field, is produced by the currents flowing on the magnetopause surface, which contribute to the pressure balance between the magnetospheric plasmas and field and the shocked solar wind. It

varies strongly with the magnetopause distance to the planet, R_{sub}, and the latitude of the sun in the Saturn reference frame.

Maurice and Engle (1995) have developed a model of the solar wind interaction with Saturn's magnetosphere, based on a numerical method developed by Mead and Beard (1964). They have been able to compute simultaneously the shape and size of the magnetopause, illustrated in this article by Figures 2 and 32, and the additional contribution to the total field (B_{MP}) from the surface currents. Inside the magnetosphere, $B_{MP} = -\nabla\phi^{MP}$.

The contribution, B_T, from the magnetotail was modeled by Behannon *et al.* (1983). Saturn's magnetic tail is a very complex region. Its magnetic field geometry is not symmetric around the planet except for $\lambda = 0$. The stretching of the field lines along the tail direction can be attributed to cross-tail currents, which have to close on the magnetopause surface. The closure of the field lines in the tail is very sensitive to the detailed current distribution. However, as there was no traversal of the tail current sheet at Saturn, models of Saturn's magnetic tail are necessarily speculative.

B_t is expected to become significant beyond $\sim 10\ R_S$. Saturn's tail presumably extends to a large distance from Saturn in the down-stream solar wind direction ($x < -100\ R_S$). Since cross-tail currents are driven by the solar wind, Saturn's tail field is essentially aligned along the Sun-Saturn axis, while other internal contributions (B_P, B_{RC}) are symmetric with respect to the equatorial plane. A hinge of the tail field must result, with a hinge point located near $x = -30\ R_S$ down the tail. In the model by Behannon *et al.* (1981), illustrated in Figure 13, the authors incorporate cross-tail currents which extend from $-16\ R_S$ to $-100\ R_S$ along the Sun-Saturn line and close onto the magnetopause. B_t is computed by summation of the field due to a system of individual closed current loops. Individual loops are spaced at 1 R_S-intervals and carry an eastward current. The current has a $1/\sqrt{\rho}$ dependence, decreasing outward from ~ 5 A/km at $-16\ R_S$. The average distant tail lobe field is ~ 3nT.

Models of the main magnetic boundaries of the magnetosphere.

The magnetopause shape, which results from the pressure balance between the magnetosphere and the shocked solar wind, has been modeled in three studies.

(1) Slavin *et al.* (1983) have fitted all Voyager and Pioneer magnetopause crossings (i.e. when $\lambda \sim 0°$), scaled to a common mean dynamic pressure of the solar wind, to a unique second order curve. They have used a magnetopause shape which is given by $r = L/(1 + \varepsilon \cos\theta)$ where ε is the conic eccentricity, L the semi-latus rectum. A third parameter, x_0, is the position of the conic focus point along the *x-axis*. Polar coordinates (r, θ) are determined from the point x_0. They have found $x_0 = 5\ R_S$, $\varepsilon = 1.09$ and $L = 30.8\ R_S$, which corresponds to $R_{sub} = 19.75\ R_S$. This model is valid for $x > -20\ R_S$.

(2) As already mentioned, Maurice and Engle (1995) have calculated the shape of Saturn's magnetopause consistently with the B_{MP} contribution. Later, Maurice *et al.*, (1996) have derived an analytical parameterization of this surface for R_{sub}

values between 17 R_S and 45 R_S, and possible λ between 0° and +/−26.7°. This model is valid for $x > -30\ R_S$ only.

(3) Macek *et al.* (1992) have computed the external shape of Saturn's distant magnetotail, using pressure equilibrium equations and conservation of momentum. Between $x = -100\ R_S$ and $x \sim -4500\ R_S$, their model provides the main features of the Saturnian magnetotail: elliptic dimensions in the y and z directions, and magnetic field intensity in the lobes, as functions of downstream distance.

The bow shock, upstream of Saturn's magnetosphere, is a transition layer within which a portion of the plasma flow energy is converted to internal energy, turbulence, and waves. Bow shock crossings are usually identified unambiguously from particle and field measurements.

Slavin *et al.* (1983) have fitted all Voyager and Pioneer bow shock crossings (i.e., when $\lambda = 0°$), scaled to a common mean dynamic pressure of the solar wind (see also Slavin and Holzer (1981)). They used the same parametric shape as for the magnetopause, and found in their fitting procedure $x_0 = 6\ R_S$, $\varepsilon = 1.71$ and $L = 55.4\ R_S$, when the magnetopause is scaled at $R_{SUB} = 19.75\ R_S$. The Slavin *et al.* (1983) model is the only existing representation of the bow shock.

References

Acuña, M. H. and Ness, N. F.: 1980, The magnetic field of Saturn: Pioneer 11 observations, *Science* **207**, 444.

Atreya, S. K.: 1986, *Atmospheres and ionospheres of the outer planets and their satellites*, Springer-Verlag, Berlin.

Atreya, S. K., Waite, Jr., J. H., Donahue, T. M., Nagy, A. F., and McConnell, J. C.: 1984, in T. Gehrels and M. S. Matthews (eds.), Theory, measurements, and models of the upper atmosphere and ionosphere of Saturn, in 'Saturn', Univ. of Ariz. Press, Tucson, pp. 239–277.

Bagenal, F.: 1992, Giant planet magnetospheres, *Ann. Rev. Earth & Planet. Sci.* **20**, 289.

Banaszkewicz, M., Lara, L. M., Rodrigo, R., Lopez-Moreno, J. J., and Molina-Cuberos, G. J.: 1999, The upper atmosphere and ionosphere of Titan: A coupled model, *Adv. Space Res.* **26**, 1547–1550.

Barbosa, D. D.: 1992, Theory and observations of electromagnetic ion cyclotron waves in Saturn's inner magnetosphere, *J. Geophys. Res.* **98**, 9345.

Barbosa, D. D.: 1990, Radial diffusion of low-energy plasma ions in Saturn's magnetosphere, *J. Geophys. Res.* **95**, 17167–17777.

Barbosa, D. D. and Kurth, W. S.: 1993, On the Generation of Plasma Waves in Saturn's Inner Magnetosphere, *J. Geophys. Res.* **98**, 9351.

Behannon, R. P., Lepping, P., and Ness, N. F.: 1983, Structure and dynamics of Saturn's outer magnetosphere and boundary regions, *J. Geophys. Res.* **88**, 8791.

Behannon, R. P., Connerney, J. E. P., and Ness, N. F.: 1991, Saturn's magnetic tail: structure and dynamics, *Nature* **292**, 753.

Bird, M. K., Dutta-Roy, R., Asmar, S. W., and Rebold, T. A.: 1997, Possible detection of Titan's ionosphere from Voyager 1 radio occutation observations, *Icarus* **130**, 426.

Brecht, S. H., Luhmann, J. G., Larson, D. J.: 2000, Simulation of the Saturnian magnetospheric interaction with Titan, *J. Geophys. Res.* **105**, 13119–13130.

Bridge, H. S., Bagenal, F., Belcher, J. W., Lazarus, A. J., Mc Nutt, R. L., Sullivan, J. D., Gazis, P. R., Hartle, R. E., Ogilvie, K. W., Scudder, J. D., Sittler, E. C., Eviatar, A., Siscoe, G. L., Goertz, C. K., and Vasyliunas, V. M.: 1982, Plasma observations near Saturn: Initial results from Voyager 2, *Science* **215**, 563.

Broadfoot, A. L. *et al.*: 1981, Extreme ultraviolet observations from Voyager 1 encounter with Saturn, *Science* **212**, 206–211.

Carlson, R. W., Johnson, R. E., Anderson, M. S.: 1999, Sulfuric acid on Europa and the radiolytic sulfur cycle, DPS abstract.

Connerney, J. E. P. and Waite, Jr., J. H.: 1984. New model of Saturn's ionosphere with an influx of water from the rings, *Nature* **312**, 136.

Connerney, J. E. P, Ness, N. F., and Acuña, M. H.: 1982, Zonal harmonic model of Saturn's magnetic field from Voyager 1 and 2 observations, *Nature* **297**, 44.

Connerney, J. E. P., Acuña, M. H., and Ness, N. F.: 1983, Currents in Saturn's magnetosphere, *J. Geophys. Res.*, **88**, 8779–8789.

Connerney, J. E. P., Acuña, M. H. and Ness, N. F.: 1981, Saturn's ring current and inner magnetosphere, *Nature* **292**, 724.

Cravens, T. E., Keller, C. N. and Gan, L.: 1992, The ionosphere of Titan and its interaction with Saturnian magnetospheric electrons, in *Proceedings of Symposium on Titan*, Toulouse, France, Sept. 1991, ESA SP-338, p. 273.

Cravens, T. E., Lindgren, C.J. and Ledvina, S.A.: 1998, A two-dimensional multifluid MHD model of Titan's plasma environment, *Planet. Space Sci.* **46**, 1193–1206.

Davis, Jr., L. and Smith, E. J.: 1990, A model of Saturn's magnetic field based on all available data, *J. Geophys. Res.* **95**, 15257.

Davis, Jr., L. and Smith, E. J.: 1986, New models of Saturn's magnetic field using Pioneer 11 vector helium magnetometer data, *J. Geophys. Res.* **91**, 1373.

Demars, H.G.: 1995, A generalized transport model of plasma flow between Saturn's ionosphere and inner magnetosphere, *J. Geophys. Res.* **100**, 23533.

Dougherty, M. K.: 1999, Detached high density plasma regions in Saturn's magnetosphere, private communication.

Eviatar, A., Siscoe, G. L., Scudder, J. D., Sittler, E. C., and Sullivan, J. D.: 1982, The plumes of Titan, *J. Geophys. Res.* **87**, 8091–8103.

Eviatar, A., McNutt, Jr, R. L., Siscoe, G. L., and Sullivan, J. D.: 1983, Heavy ions in the outer kronian magnetosphere, *J. Geophys. Res.* **88**, 823–831.

Eviatar, A.: 1982, The plumes of Titan, *J. Geophys. Res.* **87**, 8091.

Eviatar, A. and Richardson, J. D.: 1992, Water-group plasma in the magnetosphere of Saturn, *Ann. Geophys*., **8**, 725, 1990.

Eviatar, A., and J.D. Richardson, Thermal plasma in the inner kronian magnetosphere, *Ann. Geophys.* **10**, 511–518.

Festou, M. F. and Shemansky, D.: 2000, private communication.

Fox, J. L. and Yelle, R. V.: 1997, A new model of the ionosphere of Titan, *Geophys. Res. Lett.* **24**, 2179.

Franck, L. A., Bureck, B. G., Ackerson, K. L., Wolfe, J. H., and Mihalov, J. D.: 1980, Plasma in Saturn's magnetosphere, *J. Geophys. Res.* **85**, 5695–5708.

Galand, M., Lilensten, J., Toublanc, D. and Maurice, S.: 1999, The ionosphere of Titan: Ideal diurnal and nocturnal cases, Icarus, **140**, 92–105.

Galopeau, P. and Zarka, P.: 1992, Reply to the comment by J. E. P. Connerney and M. D. Desch on 'Evidence of Saturn's magnetic field anomaly from SKR high-frequency limit', *J. Geophys. Res.*, **97**, 12291–12297.

Galopeau, P., Zarka, P. and Le Quéau, D.: 1995, Source location of SKR: The Kelvin-Helmholtz instability hypothesis, *J. Geophys. Res.* **100**, 26397–26410.

Galopeau, P., Zarka, P. and Le Quéau, D.: 1989, Theoretical model of Saturn's kilometric radiation spectrum, *J. Geophys. Res.* **94**, 8739–8755.

Gan, L., Keller, C. N. and Cravens, T. E.: 1992, Electrons in the ionosphere of Titan, *J. Geophys. Res.* **97**, 12137.

Gan-Baruch, Z., Eviatar, A., Richardson, J. D., and McNutt, Jr., R. L.: 1994, Plasma observations near the ring plane of Saturn, *J. Geophys. Res.* **99**, 11063.

Geballe, T. R., Jagod, M.-F. and Oka, T.: 1993, Detection of H_3^+ infrared emission lines in Saturn, *Astrophys. J.* **408**, L109.

Gérard, J. C., Dols, V., Grodent, D., Waite, J. H., Gladstone, G. R., and Prangé, R.: 1995, Simultaneous observations of the Saturnian aurora and polar haze, with the HST/FOC, *Geophys. Res. Lett.* **22**, 2685.

Goertz, C. K.: 1983, Detached plasma in Saturn's front side magnetosphere, *Geophys. Res. Lett.* **10**, 455–458.

Goertz, C. K. and Morfill, G.: 1983, A model for the formation of spokes in Saturn's ring, *Icarus* **53**, 219–229.

Gombosi, T. I., DeZeeuw, D. L., Häberli, R. M., and Powell, K. G.: 1996, Three-dimensional multiscale MHD model of cometary plasma environments, *J. Geophys. Res.* **101**(A7), 15233–15253.

Gombosi, T.I., DeZeeuw, D. L., Groth, C. P. T., and Powell, K. G.: 2000, Magnetospheric configuration for Parker-spiral IMF conditions: Results of a 3D AMR MHD simulation, *Adv. Space Res.* **26(1)**, 139–149.

Gombosi, T.I., DeZeeuw, D. L., Groth, C. P. T., Hansen, K. C., Kabin, K., and Powell, K. G.: 2000, in R. Fujii, M. Hesse, R. Lysak, and S. Ohtani (eds.), MHD simulations of current systems in planetary magnetospheres: Mercury and Saturn, in *Magnetospheric Current Systems*, AGU monograph, **118**, 363–370.

Gurnett, D. A., Kurth, W. S. and Scarf, F. L.: 1981a, Plasma Waves near Saturn: Initial Results from Voyager 1, *Science* **212**, 235.

Gurnett, D. A., Kurth, W. S. and Scarf, F. L.: 1981, Narrowband Electromagnetic Emissions from Saturn's Magnetosphere, *Natur*e, **292**, 733.

Gurnett, D. A., Scarf, F. L. and Kurth, W. S.: 1982, The structure of Titan's wake from plasma wave observations, *J. Geophys. Res.* **87**, 1395–1403.

Gurnett, D. A., Kurth, W. S., Roux, A., Bolton, S. J., and Kennel, C. F.: 1996, Evidence for a magnetosphere at Ganymede from plasma wave observations by the Galileo spacecraft, *Nature* **382**, 535–537.

Hall, D. T., Feldman, P. D., Holberg, J. B., and McGrath, M. A.: 1996, Fluorescent hydroxyl emissions from Saturn's ring atmosphere, *Science* **272**, 516–518.

Hamilton, D. P. and Burns, J. A.: 1994: Origin of Saturn's E ring: Self sustained, naturally, *Science* **264**, 550–553.

Hartle, R. E., Sittler, Jr, E. C., Ogilvie, K. W., Scudder, J. D., Lazarus, A. J. and Atreya, S. K.: 1982, Titan's ion exosphere observed from Voyager 1, *J. Geophys. Res.* **87**, 1383–1394.

Hartle, R. E. *et al.*: 1983, Titan's ion exosphere observed from Voyager 1, *J. Geophys. Res.* **87**, 1383.

Hansen, K. C., Gombosi, T. I., DeZeeuw, D. L., Groth, C. P. T., and Powell, K. G.: 1999, A 3D global MHD simulation of Saturn's magnetosphere, *Adv. Space Res.* **26**, 1681–1690.

Hunten, D. M., Tomasko, M. G., Flasar, F. M., Samuelson, R. E., Strobel, D. F., and Stevenson, D. J.: 1984, Titan , in *Saturn*, edited by T. Gehrels and M. S. Matthews, University of Arizona Press, Tucson, pp. 671–759.

Ip, W. H.: 1983, Equatorial confinement of thermal plasma near the rings of Saturn, *Nature* **302**, 599–600.

Ip, W. H.: 1990, Titan's upper ionosphere, *Astophys. J.* **362**, 354–363.

Ip, W. H.: 1992, Plasma interaction of Titan with the Saturnian magnetosphere: A review of a critical issue, Proceedings of the Symposium on Titan, ESA SP-338, pp. 243–253.

Ip, W. H.: 1995, The exospheric systems of Saturn's rings, *Icarus* **115**, 295–303.
Ip, W. H. and Mendis, D. A.: 1983, On the equatorial transport of Saturn's ionosphere as given by a dust-ring current system, *Geophys. Res. Lett.* **10**, 207.
Johnson, R. E. and Sittler, Jr., E. C.: 1990, Sputter-produced plasma as a measure of satellite surface composition: The Cassini mission, *Geophys. Res. Lett.* **17**, 1629.
Johnson, R. E.: 1990, Energetic charged particle interactions with atmospheres and surfaces, in Physics and Chemistry in Space, vol. 19, Planetology, Springer-Verlag, New-York, 232 pp.
Johnson, R. E., Pospieszalska, M. K., Sittler Jr., E. C., Cheng, A. F., Lanzerotti, L. J., and Sieveka, E. M.: 1989, The neutral cloud and heavy ion inner torus at Saturn, *Icarus* **77**, 311–329.
Jurac, S., Johnson, R. E., Richardson, J. D., and Paranicas, C.: 2001a Satellite sputtering in Saturn's magnetosphere, *Planet. Space Sci.* **49**, 319.
Jurac, S., Johnson, R. E. and Richardson, J. D.: 2001b, Saturn's E Ring and Production of the Neutral Torus, *Icarus* **149**, 384.
Jurac, S., McGrath, M. A., Johnson, R. E., Richardson, J. D., Vasyliunas, V. M., Eviator, A.: 2002, Saturn: search for a missing water source, *Geophys. Res. Lett.*, submitted.
Kabin *et al.*: 1999, Interaction of the Saturnian magnetosphere with Titan: Results of a three-dimensional MHD simulation, *J. Geophys. Res.* **104**, 2451.
Kabin, K., Gombosi, T. I., De Zeeuw, D. L., Powell, K. G., and Israelevich, P. L.: 1999, Interaction of the Saturnian magnetosphere with Titan: Results of a three-dimensional MHD simulation, *J. Geophys. Res.* **104**(A2), 2451–2458.
Kaiser, M. L, Desch, M. D. and Connerney, J. E.P.: 1984, *J. Geophys. Res.* **89**, 2371.
Kaiser, M. L., Desch, M. D., Kurth, W. S., Lecacheux, A., Genova, F., Pedersen, B. M., and Evans, D. R.: 1984, in T. Gehrels and M. S. Matthews (eds.), Saturn as a radio source, in 'Saturn', Univ. of Ariz. Press, Tucson, pp. 378–415.
Keller, C. N., Cravens, T. E. and Gan, L.: 1992, A model of the ionosphere of Titan, *J. Geophys. Res.* **97**, 117.
Keller, C. N., Cravens, T. E. and Gan, L.: 1994a, One-dimensional multispecies magnetohydrodynamic models of the ramside ionosphere of Titan, *J. Geophys. Res.* **99**, 6511.
Keller, C. N., Cravens, T. E. and Gan, L.: 1994b, One dimensional multispecies hydrodynamic models of the wakeside ionosphere of Titan, *J. Geophys. Res.* **99**, 6527.
Keller, C. N., Anicich, V. G. and Cravens, T. E.: 1998, Model of Titan's ionosphere with detailed hydrocarbon ion chemistry, *Planet. Space Sci.* **46**, 1157.
Kivelson, M. G. and Russell, C. T.: 1983, The interaction of flowing plasmas with planetary ionospheres: A Titan-Venus comparison, *J. Geophys. Res* **88**, 49–57.
Kivelson, M. G., Khurana, K. K., Russell, C. T., Walker, R. J., Warnecke, J., Coroniti, F. V., Polanskey, C., Southwood, D. J., and Schubert, G.: 1996, Discovery of Ganymede's magnetic field by the Galileo spacecraft, *Nature* **384**, 537.
Kliore, A. J. *et al.*: 1980, Structure of the ionosphere and atmosphere of Saturn from Pioneer 11 Saturn radio occultation, *J. Geophys. Res.* **85**, 5857.
Kliore, A. J., Hindon, D. P., Flasar, F. M., Nagy, A. F., and Cravens, T. E.: 1997, The ionosphere of Europa from Galileo radio observations, *Science* **277**, 355.
Krimigis, S. M., Carbary, J. F., Keath, E. P., Armstrong, T. P., Lanzerotti, L. J. and Gloeckler, G.: 1983, General characteristics of hot plasma and energetic particles in the Saturnian magnetosphere: results from the Voyager spacecraft, *J. Geophys. Res.* **88**, 8871–8892.
Krimigis, S. M., Armstrong, T. P., Axford, W. I., Bostrom, C. O., Gloeckler, G., Keath, E. P., Lanzerotti, L. J., Carbary, J. F., Hamilton, D. C., and Roelof, E. C.: 1981, Low-energy charged particles in Saturn's magnetosphere: Results from Voyager 1, *Science* **212**, 225.
Kurth, W. S., Scarf, F. L., Gurnett, D. A. and Barbosa, D. D.: 1983, A Survey of Electrostatic Waves in Saturn's Magnetosphere, *J. Geophys. Res.* **88**, 8959.
Kurth, W. S. and Gurnett, D. A.: 1991, Plasma Waves in Planetary Magnetospheres, *J. Geophys. Res.* **96**, 18,977.

Ladreiter, H. P., Galopeau, P. H. M. and Zarka, P.: 1994, The magnetic field anomaly of Saturn, International Symposium On 'Magnetospheres Of Outer Planets', Graz, Austria, 8/1994.

Lazarus, A. J. and McNutt, Jr., R. L.: 1983, Low-energy plasma ion observations in Saturn's magnetosphere, *J. Geophys. Res.* **88**, 8831.

Lecacheux, A., Galopeau, P. and Aubier, M.: 1997, in H. O. Rucker, S. J. Bauer and A. Lecacheux (eds.), Revisiting Saturnian kilometric radiation with Ulysses, in "Planetary Radio Emissions IV", Austrian Acad. Sci. press, Vienna, pp. 313–325.

Ledvina, S.A. and Cravens, T. E.: 1998, A three-dimensional MHD model of plasma flow around Titan, *Planet. Space Sci.* **46**, 1175.

Lepping, R. P., Burlaga, L. F. and Klein, L. W.: 1981, Surface waves on Saturn's magnetopause, *Nature* **292**, 750–753.

Luhmann, J. G., Russell, C. T., Schwingenschuh, K., and Yeroshenko, Ye.: 1991, A comparison of induced magnetotails of planetary bodies: Venus, Mars, Titan, *J. Geophys. Res.* **96**, 11,199–11,208.

Ma, T. Z., Gurnett, D. A. and Goertz, C. K.: 1987 Interpretation of electrostatic noise observed by Voyager 1 in Titan's wake, *J. Geophys. Res.* **92**, 8595.

Macek, W. M., Kurth, W. S., Lepping, R. P., and Sibeck, D. G.: 1992, Distant magnetotails of outer magnetic planets, *Adv. Space Res.* **12**(8), 47.

Majeed, T. and McConnell, J. C.: 1991, The upper ionosphere of Jupiter and Saturn, *Planet. Space Sci.* **39**, 1715.

Majeed, T. and McConnell, J. C.: 1996, Voyager electron density measurements on Saturn: Analysis with a time dependent ionospheric model, *J. Geophys. Res.* **101**, 7589.

Mauk, B. H, Krimigis, S. M., Mitchell, D. G., Roelof, E. C., Keath, E. P. and Dandouras, J.: 1998, Imaging Saturn's dust rings using energetic neutral atoms, *Planet. Space Sci.* **46**(9/10), 1349–1362.

Mauk, B. H., Krimigis, S. M. and Lepping, R. P.: 1985, Particle and field stress balance within a planetary magnetosphere, *J. Geophys. Res.* **90**, 8253.

Maurice, S., Blanc, M., Prangé, R., and Sittler, Jr, E. C.: 1997, The magnetic-field-aligned polarization electric field and its effects on particle distribution in the magnetospheres of Jupiter and Saturn, *Planet. Space Sci.* **45**(11), 1449–1465.

Maurice, S. and Engle, I. M.: 1995, Idealized Saturn magnetosphere shape and field, *J. Geophys. Res.* **100**, 17143.

Maurice, S., Engle, I. M., Blanc, M. and Skubis, M.: 1996, The geometry of Saturn's magnetopause model, *J. Geophys. Res.* **101**, 27053.

Maurice, S., Sittler, E. C., Cooper, J. F., Mauk, B. H., Blanc, M., and Selesnick, R. S.: 1996, Comprehensive analysis of electron observations at Saturn: Voyager 1 and 2, *J. Geophys. Res.* **101**, 15211–15232.

McKibben, R. B. and Simpson, J. A.: 1980, Charged particle diffusion and acceleration in Saturn's radiation belts, *J. Geophys. Res.* **85**, 5773–5783.

McCord, T. M. *et al.*: 1999, Hydrated salt minerals on Europa's surface from the Galileo near-infrared mapping spectrometer (NIMS) investigation, *J. Geophys. Res.* **104**, 11827.

Mc Elroy, M. B.: 1973, The ionospheres of the major planets, *Space Sci. Rev.* **14**, 460.

McLennan, C. G., Lanzerotti, L. J., Krimigis, S. M., Lepping, R. P., and Ness, N. F.: 1982, Effects of Titan on trapped particles in Saturn's magnetosphere, *J. Geophys. Res.* **87**, 1411–1418.

Nagy, A. F., Barakat, A. R. and Schunk, R. W.: 1986, is Jupiter's ionosphere a significant plasma source for its magnetosphere ? *J. Geophys. Res.* **91**, 351.

Nagy, A. F., Cravens, T. E. and Waite, Jr., J. H.: 1995, All ionospheres are not alike: Reports from other planets, *Rev. Geophys., Suppl.*, US Natl. Report to IUGG 1991–1995, pp. 525–533.

Nagy, A. F. *et al.*: 2001, The interaction between the magnetosphere of Saturn and Titan's ionosphere, *J. Geophys. Res.* **106**, 6151–6160.

Nagy, A. F. and Cravens, T. E.: 1998, Titan's ionosphere: A review, *Planet. Space Sci.* **46**, 1149.

Ness, G. D., Acuña, M. H., Lepping, R. P., Connerney, J. E. P., Behannon, K. W., Burlaga, L. F., and Neubauer, F. M.: 1981, Magnetic field studies by Voyager 1: Preliminary results at Saturn, *Science* **212**, 211.

Ness, G. D., Acuña, M. H., Lepping, R. P., Connerney, J. E. P., Behannon, K. W., Burlaga, L. F., and Neubauer, F. M.: 1982, Magnetic field studies by Voyager 2: Preliminary results at Saturn, *Science* **215**, 558.

Ness, N. F., Acuna, M. H., Behannon, K. W. and Neubauer, F. M.: 1982, The induced magnetosphere of Titan, *J. Geophys. Res.* **87**, 1369–1381.

Neubauer, F.: 1998, The sub-Alfvenic interaction of the Galilean satellites with the Jovian magnetosphere, *J. Geophys. Res* **103**, 19843–19866.

Neubauer, F. M., Gurnett, D. A., Scudder, J. D., and Hartle, R. E.: 1984, in T. Gehrels and M. S. Matthews (eds.), Titan's magnetospheric interaction, in 'Saturn', Univ. of Ariz. Press, Tucson, pp. 760–787.

Northrop, T. G. and Birmingham, T. J.: 1990, Plasma drag on a dust grain due to coulomb collisions, *Planet. Space Sci.* **38**(3), 319–326.

Paranicas, C., Cheng, A. F., Mauk, B. H., Keath, E. P., and Krimigis, S. M.: 1997, Evidence of a source of energetic ions at Saturn, *J. Geophys. Res.* **102**, 17459–17466.

Pospieszalska, M. and Johnson, R. E.: 1989, Plasma ion bombardment profiles: Europa and Dione, *Icarus* **78**, 1.

Powell, K. G., Roe, P. L., Linde, T. J., Gombosi, T. I., and DeZeeuw, D. L.: 1999, A solution-adaptive upwind scheme for ideal magnetohydrodynamics, *J. Comput. Phys.*, bf 154, 284–309.

Randall, B. A.: 1994, Energetic electrons in the magnetosphere of Saturn, *J. Geophys. Res.* **99**, 87771.

Richardson, J. D., Eviatar, A. and Siscoe, G. L.: 1986, Satellite tori at Saturn, *J. Geophys. Res.* **91**, 8749–8755.

Richardson, J. D., Eviatar, A., McGrath, M. A., and Vasyliunas, V. M.: 1998, OH in Saturn's magnetosphere: Observations and implications, *J. Geophys. Res.* **103**, 20245–20555.

Richardson, J. D.: 1995, An extended plasma model for Saturn, *Geophys. Res. Lett.* **22**, 1177-1180.

Richardson, J. D., Sittler, Jr, E. C.: 1990, A plasma density model for Saturn based on Voyager observations, *J. Geophys. Res.* **95**, 12019–12031.

Richardson, J. D.: 1986, Thermal ions at Saturn: plasma parameters and implications, *J. Geophys. Res.* **91**, 1381–1389.

Richardson, J. D.: 1998, Thermal plasma and neutral gas in Saturn's magnetosphere, *Rev. Geophys*., **36**(4), 501-524.

Roboz, A. and Nagy, A.F.: 1994, The energetics of Titan's ionosphere, *J. Geophys. Res.* **99**, 2087.

Sandel, B.R. *et al.*: 1982, Extreme ultraviolet observations from Voyager 2 encounter with Saturn, *Science* **215**, 548–553.

Saur, J., Neubauer, F. M., Strobel, D. F. and Summers, M. E.: 1999, Three-dimensional plasma simulation of Io's interaction with the Io plasma torus: Asymmetric plasma flow, *J. Geophys. Res.* **104**, 25105–25126.

Saur, J., Strobel, D. F., Neubauer, F. M.: 1998, Interaction of the jovian magnetosphere with Europa: Constraints on the neutral atmosphere, *J. Geophys. Res.* **103**, 19947.

Scarf, F. L., Gurnett, D. A., Kurth, W. S. and Poynter, R. L.: 1982, Voyager-2 Plasma Wave Observations at Saturn, *Science* **215**, 587.

Scarf, F. L., Frank, L. A., Gurnett, D. A., Lanzerotti, L. J., Lazarus, A. and Sittler, Jr., E. C.: 1984, in T. Gehrels and M. S. Matthews (eds.), Measurements of plasma, plasma waves, and suprathermal charged particles in Saturn's inner magnetosphere, in 'Saturn', Univ. of Ariz. Press, Tucson, pp. 318–353.

Schardt, A. W and McDonald, F. B.: 1983, The flux and source of energetic protons in Saturn's inner magnetosphere, *J. Geophys. Res.* **88**, 8923–8935.

Schardt, A. W., Kurth, W. S., Lepping, R. P. and McClennan, C. G.: 1985, Particle acceleration in Saturn's outer magnetosphere: In memoriam Alois Schardt, *J. Geophys. Res.* **90**, 8539–8542.

Schardt, A. W., Behannon, K. W., Lepping, R. P., Carbary, J. F., Eviatar, A., and Siscoe, G. L.: 1984, in T. Gehrels and M. S. Matthews (eds.), The outer magnetosphere in *Saturn*, University of Arizona Press, Tuscon, p. 416.

Shemansky, D. E. and Hall, D. T.: 1992, The distribution of atomic hydrogen in the magnetosphere of Saturn, *J. Geophys. Res.* **27**, 4143–4161.

Shemansky, D. E., Matheson, P., Hall, D. T., Hu, H.-Y., and Tripp, T. M.: 1993, Detection of the hydroxyl radical in the Saturn magnetosphere, *Nature* **363**, 329–331.

Shi, M., Baragiola, A., Grosjean, D. E., Johnson, R. E., Jurac, S., and Schou, J.: 1995, Sputtering of water ice surfaces and the production of extended neutral atmospheres, *J. Geophys. Res.* **100**, 26387–26395.

Simpson, J. A., Bastian, T. S., Chenette, D. L., McKibben, R. B., and Pyle, K. R.: 1980, The trapped radiations of Saturn and their absorption by satellites and rings, *J. Geophys. Res.* **85**, 5731.

Sittler Jr, E. C., Ogilvie, K. W. and Scudder, J. D.: 1983, Survey of low energy electrons in Saturn's magnetosphere: Voyagers 1 and 2, *J. Geophys. Res.* **88**, 8847.

Slavin, J. A., Smith, E. J., Gazis, P. R. and Mihalov, J. D.: 1983, A Pioneer-Voyager study of the solar wind interaction with Saturn, *Geophys. Res. Lett.* **10**, 9.

Smith, E. J. and Tsurutani, B. T.: 1983, Saturn's magnetosphere: Observations of ion cyclotron waves near the Dione L shell, *J. Geophys. Res.* **88**, 7831.

Southwood, D. J., Dougherty, M. K., Leamon, R. J., and Haynes, P. L.: 1995, Origin and dynamics of field nulls detected in giant planet magnetospheres, *Adv. Space Res.* **16**, 4177.

Tagger, M., Henriksen, R. N. and Pellat, R.: 1991, On the nature of the spokes in Saturn's rings, *Icarus* **91**, 297–314.

Trauger, J. T. *et al.*: 1998, Saturn's hydrogen aurora: WFPC2 imaging from the HST, *J. Geophys. Res.* **103**, 20237.

Tsintikidis, D., Kurth, W. S., Gurnett, D. A., and Barbosa, D. D.: 1995, A Study of Dust in the Vicinity of Dione Using the Voyager 1 Plasma Wave Instrument, *J. Geophys. Res.* **100**, 1811.

Van Allen, J. A., Randall, B. A. and Thomsen, M. F.: 1980, Sources and Sinks of energetic electrons and protons in Saturn's magnetosphere, *J. Geophys. Res.* **85**, 5679–5684.

Vasyliunas, V. M.: 1995, in A. J. Dessler (ed.) *Physics of the Jovian Magnetosphere*, Cambridge University Press, Cambridge, p. 395.

Wagener, R. and Caldwell, J. J.: 1986, IUE observations of Saturn's rings, Proc. Joint NASA/ESA/SERC Conference on new insights in Astrophysics, ESA SP-269.

Waite, Jr., J. H. and Cravens, T. E.: 1987, Current review of the Jupiter, Saturn, and Uranus ionospheres, *Adv. Space Res.* **7**(12), 119.

Wilson, G. R. and Waite, Jr., J. H.: 1989, Kinetic modeling of the Saturn ring-ionosphere plasma environment, *J. Geophys. Res.* **94**, 17286.

Wilson, G. R.: 1991, The plasma environment, charge state, and currents of Saturn's C and D rings, *J. Geophys. Res.* **96**, 9689–9701.

Wolf, D. and Neubauer, F. M.: 1982, Titan's highly variable plasma environment, *J. Geophys. Res.* **87**, 881–885.

Zarka, P.: 1992, in H. O. Rucker *et al.* (eds.), Remote probing of auroral plasmas, in 'Planetary Radio Emissions III', Austrian Acad. Sci. Press, Vienna, pp. 351–369.

Zarka, P.: 1998, Auroral radio emissions at the outer planets: Observations and theories, *J. Geophys. Res.*, **103**, 20159–20194.